

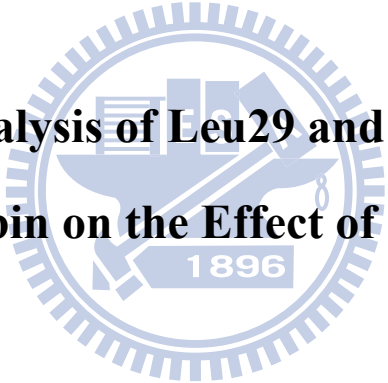
國立交通大學

生物資訊研究所

碩士論文

Leu29 與 His93 位置之飽和定點突變抹香鯨肌紅蛋白對其
過氧化能力之影響

**Mutational Analysis of Leu29 and His93 from Sperm
Whale Myoglobin on the Effect of Peroxidase Activity**



研究生： 吳育勳

指導教授： 吳東昆 博士

中華民國九十八年七月

**Leu29 與 His93 位置之飽和定點突變抹香鯨肌紅蛋
白對其過氧化能力之影響**

**Mutational Analysis of Leu29 and His93 from Sperm
Whale Myoglobin on the Effect of Peroxidase Activity**

研究生：吳育勳

Student: Yu-Hsun Wu

指導教授：吳東昆 博士

Advisor: Dr. Tung-Kung Wu



A Thesis

Submitted to Department of Bioinformatics
College of Science
National Chiao Tung University
in partial Fulfillment of the Requirements
for the Degree of
Master
in
Bioinformatics
July, 2009
Hsinchu, Taiwan, Republic of China
中華民國九十八年七月

Leu29 與 His93 位置之飽和定點突變抹香鯨肌紅蛋白對其過氧化能力之影響

研究生：吳育勳

指導教授：吳東昆 博士

國立交通大學 生物資訊研究所碩士班

摘要

肌紅蛋白(myoglobin)為一種血基質蛋白(heme-protein)，在脊椎動物體內具有儲存及攜帶氧氣的功能。本論文研究主要是將不具酵素活性的肌紅蛋白利用飽和定點突變成 H93X；及將具有過氧化酵素 (peroxidase) 活性的突變 H64D/V68L/I107M 肌紅蛋白，再 Leu29 位置利用飽和突變技術改變 L29X/H64D/V68L/I107M 這個推測可改變活性的胺基酸，以進一步分析比較這些突變蛋白的過氧化酵素能力。將其與過氧化氫和 2,2'-azinobis(3-ethylbenzothiazoline-6-sulfonic acid),ABTS,反應後利用 UV-Vis 分光光譜儀偵測並分析其一個電子傳遞的過氧化酵素活性與機制。發現四突變的過氧化氫催化能力不比三突變的活性差，但是對 ABTS 的催化活性不到三突變的一半，可得知 Leu-29 這位置對於 ABTS 進入反應中心有非常重要的調控機制。而 His-93 的突變幾乎沒有活性，證明過氧化催化能力，主要取決於反應的環境，與鐵金屬的原子軌域影響較小。

Multiple Sites Mutational Analysis of Sperm Whale Myoglobin on the Effect of Peroxidase Activity

Student: Yu-Hsun Wu

Advisor: Dr. Tung-Kung Wu

Institute of Bioinformatics and Systems Biology

National Chiao Tung University

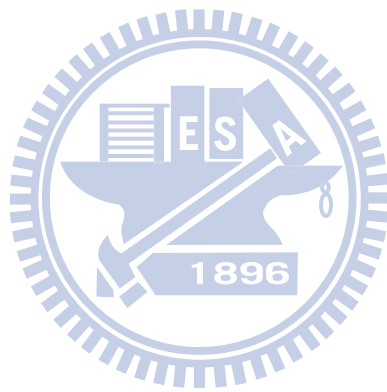
Abstract

Myoglobin (Mb) is a heme-protein, functioning as oxygen carrier in vertebrates. In previous study, Mb^{H64D/V68L/I107M} had been engineered into an enzyme with peroxidase activity. We further investigated the L29X/H64D/V68L/I107M and site-saturated H93X mutational effects on peroxidase activity. A well established peroxidase activity with one-electron oxidation reacted with 2'-azinobis (3-ethylbenzothiazoline-6-sulfonic acid) (ABTS) was observed by the UV/Vis spectrophotometer and demonstrated its capability in electron transfer reaction. When ABTS was used as substrate, the results showed that the activity of quadruple mutants was less than triple mutant, indicating the important role of Leu-29 in maintaining peroxidase function, especially the catalysis of ABTS. The catalyses of H₂O₂ of Mb^{L29I/H64D/V68L/I107M}, Mb^{L29F/H64D/V68L/I107M}, and Mb^{L29M/H64D/V68L/I107M} were as good as that of triple mutants. The H93X mutants exhibited no activity, indicating that the peroxidase activity was related with the environment.

Contents

1. Introduction	
1-1 Myoglobin	1
1-2 Heme proteins.....	2
1-3 Peroxidase.....	4
1-4 Mutated Myoglobin	6
1-5 Peroxidase Cycle of Mutated Mb	10
1-6 Enzyme Kinetics.....	11
1-7 Research Goal.....	14
2 Materials and Methods.....	21
2-1 Materials	21
2-1-1 Chemicals	21
2-1-2 Buffers and Reagents	23
2-1-3 Equipments.....	25
2-1-4 Bacterial strains, vectors, animal, and cell.....	25
2-2 Method.....	26
2-2-1 Molecular modeling	26
2-2-2 Preparation of Myoglobin Variants	26
2-2-3 Preparation of Clones	31
2-2-4 Preparation of SDS-polyacrylamide gel electrophoresis (SDS-PAGE)	31
2-2-5 Protein detection.....	32
2-2-6 Crude Extract.....	34
2-2-7 Expression of Apo-Mb	35
2-2-8 Crude extract of inclusion body	35
2-2-9 Denature and refolding of inclusion body.....	36
2-2-10 Purification of Apo-Mb	36
2-2-11 Reconstitution of Apo-Mb with heme	37
2-2-12 Analysis of Peroxidase Activity	38
3 Results and Discussion	39
3-1 All clones	39
3-2 Protein detection.....	41
3-3 Activity Test of Crude Extract	42
3-4 Purification of mutated Mbs	46
3-5 Reconstitution of mutated Mbs.....	48
3-6 Enzyme kinetics measurements.....	50
4 Conclusion and Future Perspective.....	58

5 References.....62
6 Appendix.....64



Figures

Figure 1. The structure of Myoglobin	1
Figure 2. The structure of heme.....	2
Figure 3. The functions of heme protein	3
Figure 4. The proposed mechanism of compound I formation. The distal histidine first functions as a general base, and then the protonated imidazole serves as a general acid to cleave the O-O bond. ⁴	5
Figure 5. Comparison of reaction cycles of peroxidase and cytochrome P450. Compound I, a ferryl porphyrin radical cation, is a critical catalytic species for both hemoenzymes ⁴	6
Figure 6. X-ray crystal structures of oxy forms of cytochrome c peroxidase mutant (W191F CcP) and myoglobin (Mb). ⁴	7
Figure 7. The Asp-64 effect of resting state ⁹	8
Figure 8. Using known changes in valency of the heme iron, one can the derive functional cycle ¹²	10
Figure 9. Chemical formulae of ABTS and its oxidation products ¹⁴	11
Figure 10. Michaelis-Meten plot	13
Figure 11. Lineweaver-Burk plot.....	14
Figure 12. MbCO structure showing juxtaposition of Val 68 on the bound CO, and the steric interactions path through Leu69 to Val17, at the AB corner. ¹⁷	18
Figure 13. The distance of Mb ^{WT} crystal structure (PDB: 104M)(white one) and molecule modeling of Mb ^{V17W} (yellow one)	19
Figure 14. Illustration of the Phe 43 and 46 displacements, and the connecting CD loop ¹⁷	20

Figure 15. Amino acid residues mutation in sperm whale Mb.	20
Figure 16. Western blotting experiments for clone expression	42
Figure 17. Comparisons of (a) wavelength scan and (b) peroxidase activity of crude extract from Mb ^{H64D/V68L/I107M} clone (red) and BL-21 without insert (black)	44
Figure 18. (a) The peroxidase activity of Mb ^{L29X/H64D/V68L/I107M} clones. (b) The activity of H93X clones. (c) The peroxidase activity of V17W, F43Y, and F46Y clones.....	46
Figure 19. 20% SDS-PAGE analysis of purified mutated apoMb. (a) Lane M : marker, lane 1 : before adding IPTG, lane 2 : after IPTG induced, and lane 3 : purified 17kDa Mb. (b) Lane M : marker, lane 1 : Mb ^{WT} , lane 2 : Mb ^{H64D/V68L} , lane 3 : Mb ^{H64D/V68L/I107M} , lane 4 : Mb ^{V17W} , lane 5 : Mb ^{L29C/H64D/V68L/I107M} , lane 6 : Mb ^{L29F/H64D/V68L/I107M} , lane 7 : Mb ^{L29I/H64D/V68L/I107M} , and lane 8 : Mb ^{L29M/H64D/V68L/I107M}	48
Figure 20. The UV-visible spectra of reconstituted Mb ^{H64D/V68L/I107M} and Apo-Mb ^{H64D/V68L/I107M} in 100 mM potassium phosphate buffer at pH 7.0	49
Figure 21. The absorbance change at 730 nm for Mb ^{H64D/V68L/I107M} , Apo-Mb ^{H64D/V68L/I107M} , and heme in 100 mM potassium phosphate buffer at pH 7.0.....	50
Figure 22. General reaction cycles of heme proteins with peroxide ⁹	53
Figure 23. The catalytic efficiency of ABTS	55
Figure 24. The catalytic efficiency of H ₂ O ₂	55
Figure 25. The shortest distance of Leu-68 and Val-68 to iron atom by crystal of Mb ^{V68L} (PDB: 1MLQ) and Mb ^{WT} (PDB: 104M).....	57
Figure 26. Stereoview of the CPO active site ²⁶	60

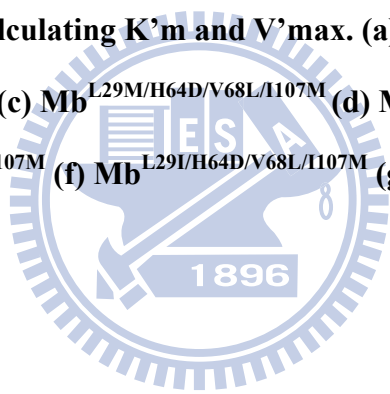
Figure 27. The Soret band of L29X/H64D/V68L/I107M clones65

Figure 28. The Soret band of H93X clones67

Figure 29. The Soret band of V17W, F43Y, and F46Y clones68

Figure 30. The Michaelies-Menten plot of mutant myoglobin catalyzing different concentration of ABTS, and the Lineweaver-Burk plot of mutant myoglobin for calculating K'm and V'max. (a) Mb^{H64D/V68L} (b) Mb^{H64D/V68L/I107M} (c) Mb^{L29M/H64D/V68L/I107M} (d) Mb^{L29C/H64D/V68L/I107M} (e) Mb^{L29F/H64D/V68L/I107M} (f) Mb^{L29I/H64D/V68L/I107M} (g) Mb^{V17W} 75

Figure 31. The Michaelies-Menten plot of mutant myoglobin catalyzing different concentration of H₂O₂, and the Lineweaver-Burk plot of mutant myoglobin for calculating K'm and V'max. (a) Mb^{H64D/V68L} (b) Mb^{H64D/V68L/I107M} (c) Mb^{L29M/H64D/V68L/I107M} (d) Mb^{L29C/H64D/V68L/I107M} (e) Mb^{L29F/H64D/V68L/I107M} (f) Mb^{L29I/H64D/V68L/I107M} (g) Mb^{V17W}82



Scheme and Table

Scheme 1. Experimental procedures-1	26
Scheme 2. Experimental procedures-2	34
Scheme 3. Experimental procedures-3	35
Scheme 4. Experimental procedures-4	37
Scheme 5. Experimental procedures-5	38
Scheme 6. Heme dependence of tryptophan oxidation⁹	49
Scheme 7. The rates of the slow kinetic processes were made based on a simple reaction scheme. ¹⁰	52
Table 1. The residues and distances away from iron atom of the wild type of sperm Mb.	17
Table 2. The His-93 mutants and distances away from iron atom	17
Table 3. Primer design for site-saturated mutagenesis	27
Table 4. QuikChange Site-Directed Mutagenesis Kit PCR composition	29
Table 5. QuikChange Site-Directed Mutagenesis Kit program	29
Table 6. QuikChange Site-Directed Mutagenesis Kit PCR products digestion ...	30
Table 7. 20% separating gel and 4% stacking gel of SDS-PAGE	32
Table 8. List of all clones.	40
Table 9. Kinetic data of ABTS by mutated Mb	54
Table 10. Kinetic data of H₂O₂ by mutated Mb	54
Table 11. Possibly homologous residues of Mb and CPO	61

1. Introduction:

1-1 Myoglobin

Myoglobin (Mb) was the first breakthrough towards understanding the three-dimensional structure of a globular protein by using x-ray diffraction studies developed by John Kendrew in the 1960s.¹ Mb is a single-chain globular protein (44 x 44 x 25 Å) made up 153 amino acids. The molecular weight is approximately 16,700 Daltons. It is composed of eight alpha helices (75 percent), named A-H, and it has a hydrophobic core (Fig.1). Mb is a relatively small oxygen-carrying pigment of muscle cells, and it is particularly abundant in the muscles of diving mammals such as the sperm whale. It contains a heme (iron-containing porphyrin) prosthetic group in its center, around which the remaining apo-protein folds. The same heme group is found in hemoglobin (Hb), the oxygen-binding protein of erythrocytes, and is responsible for the deep red-brown color of both Mb and Hb.²

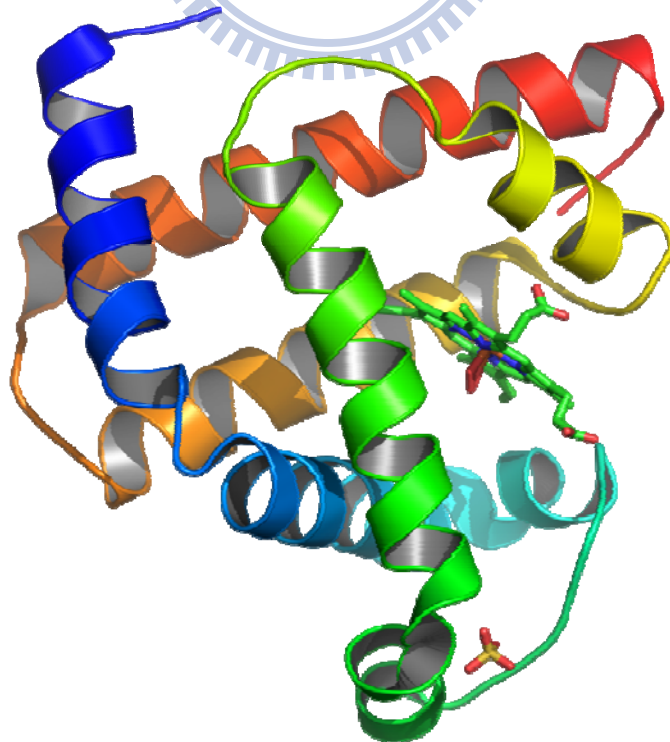


Figure. 1 The structure of Myoglobin

The flat heme group rests in a crevice, or pocket, within the myoglobin molecule.³(Fig. 2) The iron atom is at the center of the heme group, a large heterocyclic organic ring known as a porphyrin, has two bonding (coordination) positions perpendicular to the heme plane. One of these is bound to the R group of the Histidine residue at position 93 in sperm whale Mb; the other is the site at which an O₂ molecule binds. Within this pocket, the accessibility of the heme group to solvent is highly restricted. Free heme groups in an oxygenated solution are rapidly oxidized from the ferrous form, which is active in the reversible binding of O₂, to the ferric form that does not bind O₂.

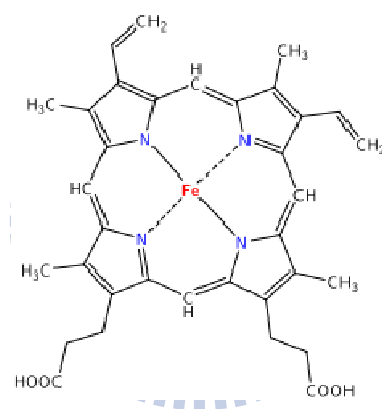


Figure 2. The structure of heme

1-2 Heme proteins

The four principal biological functions of heme proteins are the transport of oxygen (e.g., hemoglobin, Mb), the transport of electrons (e.g., cytochrome b5), the catalysis of redox reactions (e.g., horseradish peroxidase, cytochrome P450, catalase), and the sensing of oxygen, carbon monoxide (e.g., FixL, CoxA) or nitric oxide⁴ (Fig. 3). A common strategy used for structure-function studies of a particular enzyme involve substitution of amino acid residues followed by investigations into the effect(s) caused by those substitution(s) on the catalytic activity⁴. The electron carrier

hemoproteins have two strong axial ligands. The coordination site on the distal side of the heme pocket is either vacant or occupied by a water molecule, which is easily exchanged for other ligands such as an oxygen molecule. A histidine residue on the proximal side serves as one of the axial ligands, and the distal histidine stabilizes binding of O₂ through a hydrogen-bonding interaction. The heme in FixL, an oxygen-sensing hemoprotein, appears to have one accessible coordination site, as observed in globins. CoxA from *Rhodospirillum rubrum*, which regulates the expression of *coo* operons with carbon monoxide as an effector, is another sensor hemoprotein that plays a role in homeostasis. Despite the differences in functions, all of these proteins have an iron protoporphyrin IX (heme) as a prosthetic group. The amino acid residues surrounding the prosthetic group appear to control the intrinsic functions of the heme.

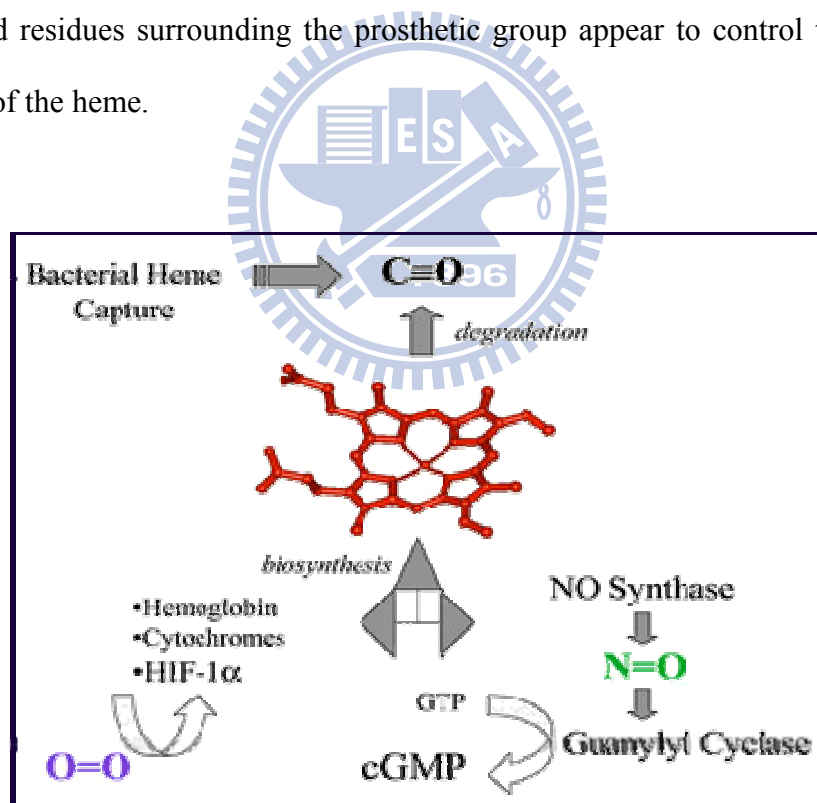


Figure 3. The functions of heme protein

1-3 Peroxidase

Horseradish peroxidase (HRP) is a common peroxidase enzyme. Generally speaking, peroxidases react with H_2O_2 to produce a species known as compound I, an oxoferryl ($\text{O}=\text{Fe}^{\text{IV}}$) species paired with a porphyrin radical cation⁴. On the basis of such evidence, Michaelis and Menten showed that such relationships could be explained by the assumption that an intermediate compound of enzyme and substrate was formed: $\text{E} + \text{S} \rightarrow \text{ES} \rightarrow \text{E} + \text{P}$ ⁵. During compound I formation (Fig. 4), the distal histidine first serves as a general base to allow the binding of H_2O_2 to the iron embedded in the heme. The protonated distal histidine then transfers the proton to the single protonated oxygen atom of the bound HO_2^- . Heterolytic O-O bond cleavage results in the release of a water molecule. The positively charged distal arginine also contributes to this process in polarization of the O-O bond. The combination of catalytic functions in the distal histidine and arginine residues has been described as the “pull effect”. On the other hand, the cytochrome P450 monooxygenases bind O_2 instead of H_2O_2 and require the input of two electrons for the formation of a putative hydroperoxide bound to the iron. Heterolytic O-O bond cleavage generates a highly reactive catalytic species equivalent to compound I. The cytochrome P450 monooxygenase reaction cycle differs from that of the peroxidases in that the oxo-ferryl oxygen atom is transferred to the substrates.⁴

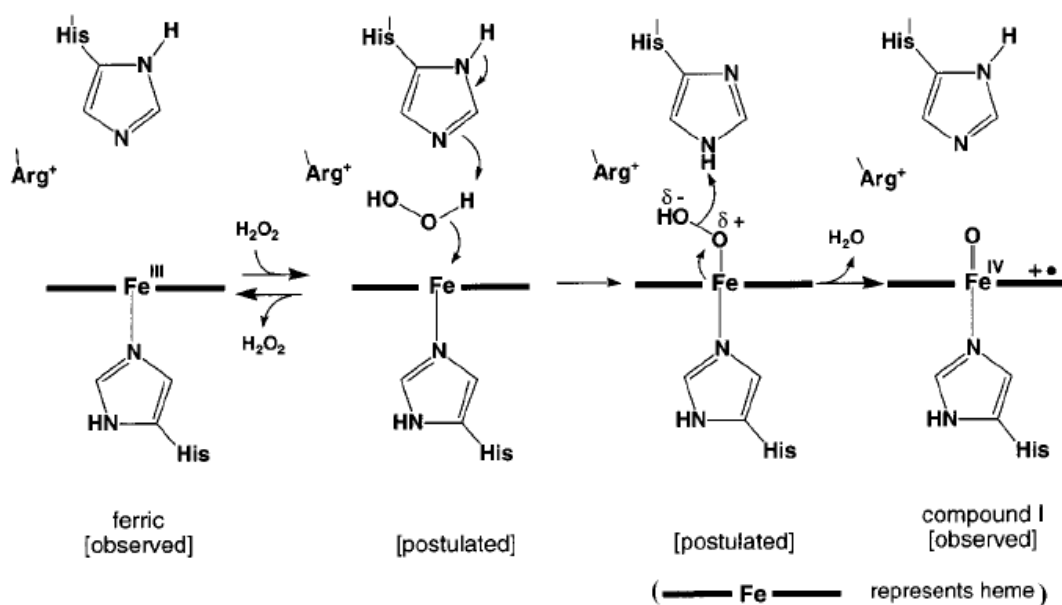


Figure 4. The proposed mechanism of compound I formation. The distal histidine first functions as a general base, and then the protonated imidazole serves as a general acid to cleave the O-O bond. ⁴

Figure 5 illustrates the overlapping nature of the various types of reactive intermediates involved in peroxidase and monooxygenase chemistry. Structural features of the cytochrome P450s include a cysteine thiolate ligand, the absence of obvious catalytic functional residues in the distal heme pocket, and the presence of a water shuttle pathway from the exterior of the protein to the distal heme pocket. The catalytic efficiency of the cytochrome P450s has long been attributed to O-O bond cleavage induced by strong electron donation of the thiolate ligand. It called “push effect”. The transition from compound I to compound II is a reduction process: $\text{Compound I} + \text{AH}_2 \rightarrow \text{Compound II} + \text{AH}$, and the transition from compound II to ferric enzyme is a reduction process: $\text{Compound II} + \text{AH}_2 \rightarrow \text{ferric enzyme} + \text{AH}$.⁶

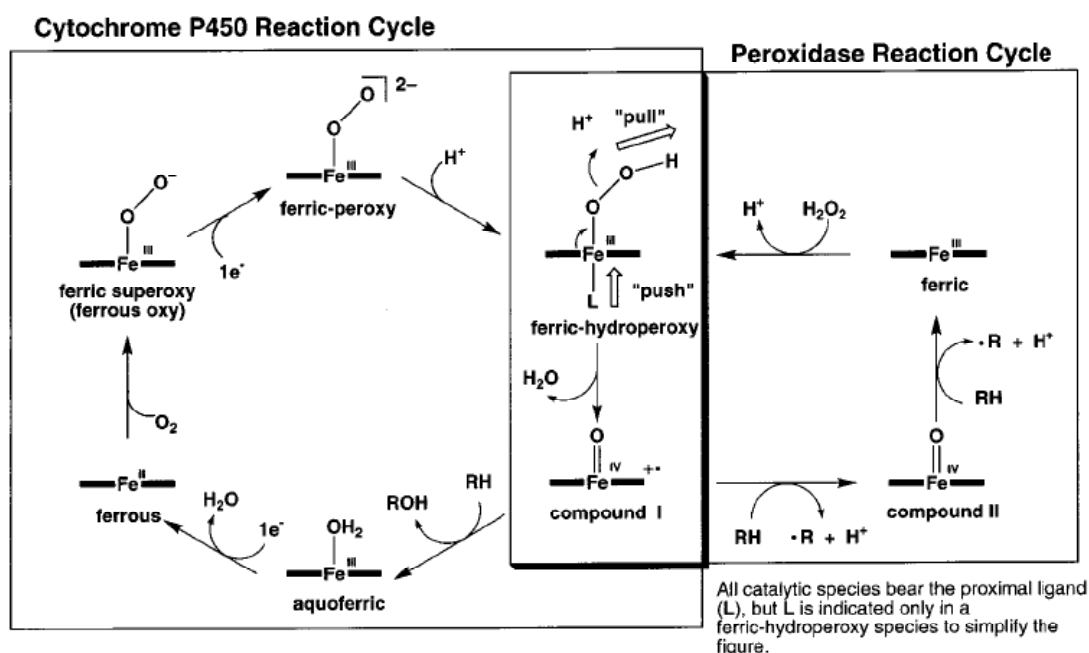


Figure 5. Comparison of reaction cycles of peroxidase and cytochrome P450. Compound I, a ferryl porphyrin radical cation, is a critical catalytic species for both hemoenzymes⁴.

1-4 Mutated Myoglobin

Ozaki *et al.* have attempted to convert a non-enzymatic heme protein, (i.e., Mb) into a heme enzyme (i.e., peroxidase). This strategy provided valuable insight into the general structural requirements for the activation of H₂O₂⁴.

They proved that the distal histidine of sperm whale Mb (i.e., His-64) is a critical residue for activating H₂O₂ and for destabilizing a ferryl porphyrin radical cation, compound I. However, compound I could not be produced in the wild type Mb⁷. After comparing the crystals of Mb and W191F Cytochrome C Peroxidase(CcP), the distances between N_ε of the distal histidine and the oxygen atoms of oxy-Mb were determined to be 2.7 Å for the terminal oxygen atom (O₁) and 3.0 Å for the oxygen atom bound to the iron (O₂), while the values for oxy-W191F CcP were 3.0 and 3.9 Å, respectively.(Fig. 6) It is expected that when CcP reacts with H₂O₂, the protonated imidazole forms a hydrogen bond only with the terminal oxygen atom (O₁) during initiation of heterolysis of the O-O bond. On the other hand, in the reaction of Mb

with H_2O_2 , both oxygen atoms would be positioned to accept a proton from N_ϵ of the distal histidine. It is considered that this arrangement is responsible for the poor reactivity of Mb with H_2O_2 ⁴. Replacement of His-64 with a hydrophobic amino acid such as Ala significantly decreases the reactivity of H_2O_2 .^{7,8} Moreover, Pfister *et al.* set forth the following conclusion⁹. A water molecule may provide the sixth ligand and result in a less reactive ferric state (Fig. 7). Compound I has been successfully observed for the distal histidine deletion mutants. This result was obtained by Alayash *et al.*¹⁰. In contrast, compound I of the wild type Mb was not detected with H_2O_2 because of its simultaneous decay to compound II (i.e., a ferryl species).

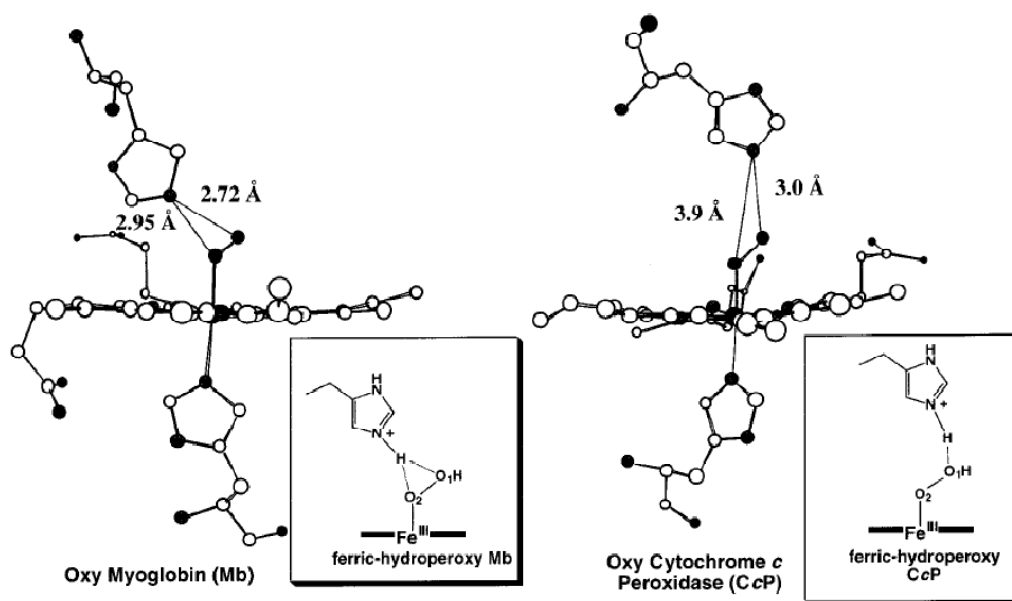


Figure 6. X-ray crystal structures of oxy forms of cytochrome c peroxidase mutant (W191F CcP) and myoglobin (Mb).⁴

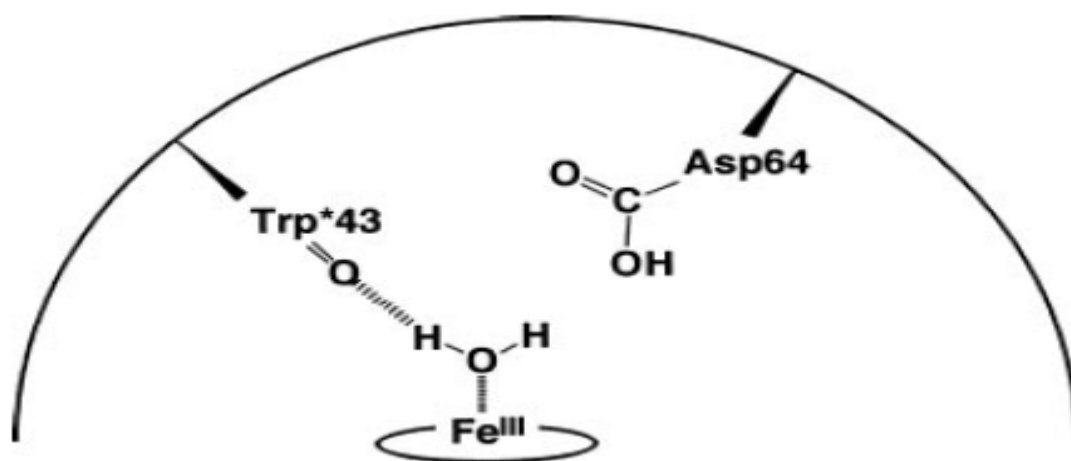


Figure 7. The Asp-64 effect of resting state⁹

Interestingly, the substitution of His-64 with a negatively charged aspartate residue accelerated the reaction with H_2O_2 and improved peroxidase (i.e., one-electron oxidation) and peroxygenase activity (i.e., two-electron oxidation associated with a ferryl oxygen transfer) (Fig. 8). Additional H-bonding may also be provided by Asp-64. Among the distal histidine deletion mutants, Mb^{H64D} is the best enzyme engineered to date for oxidation in the presence of H_2O_2 . Ozaki *et al.* found that the distal histidine of Mb can be replaced with Asp to mimic chloroperoxidase (CPO), in which Glu-183 and His-105 function cooperatively as catalytically important amino acids in compound I formation (Fig. 9). This process may be mediated by similar mechanisms to peroxidase activity.

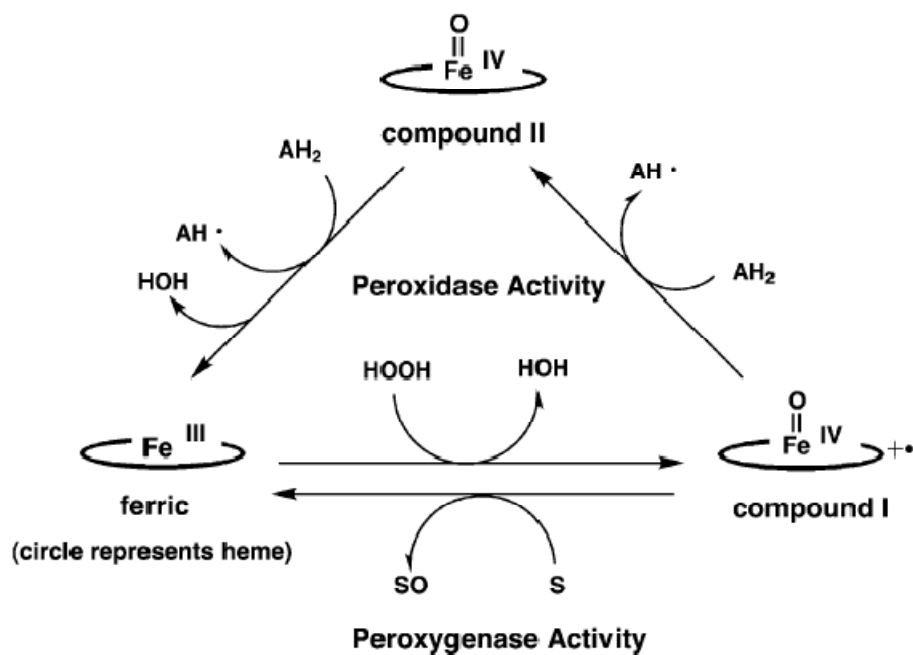


Figure 8. Peroxidase and peroxygenase reaction cycle.⁴

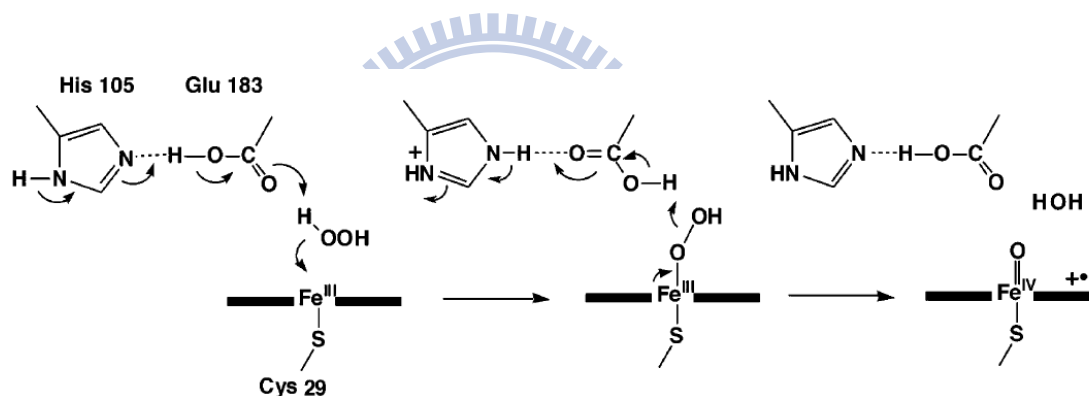


Figure 9. Possible Functions of Chloroperoxidase (CPO) Glu-183 in Compound I Formation¹¹

Previously mutagenesis of Val-68 in Mb^{H64D} was carried out to improve the enantioselectivity since residue 68 as well as residue 64 (i.e., His-64 and Val-68 in wild-type Mb) is known to influence the association and dissociation rate constants for ligand binding (e.g., O₂ and CO). The replacements of Val-68 with Leu in Mb^{H64D} successfully improved the peroxidase activity and enhanced the peroxygenase activity.

1-5 Peroxidase Cycle of Mutated Mb

In its natural state, the ferrous-dioxygen, iron(II), bond in Mb plays a vital role in their physiological functions. However, the iron of heme on the peroxidase cycle begins from ferric, iron(III). There are two ways by which iron(II) is led to iron(III). First, during reversible oxygen binding, the oxygenated form of myoglobin or hemoglobin is oxidized easily to the ferric met form, subsequently causing the generation of the superoxide anion¹². Second, where equation 1 represents the primary formation of ferryl-Mb(IV) from deoxy-Mb(II), which is in equilibrium with MbO₂, a two-equivalent oxidation occurs with H₂O₂. Once the ferryl species is formed, it rapidly reacts with another deoxy-Mb so as to yield 2 units of metMb.¹³ After leading iron(II) to iron(III), the Mb mutants initiate the peroxidase cycle. Mb mutants react with H₂O₂ to give a two-electron oxidized heme (compound I), which is normally a ferryl porphyrin cation radical (Fe^{IV}=O Por^{•+}) followed by the addition of a reduced 2,2'-azino-bis(3-ethylbenzthiazoline-6-sulphonic acid) (ABTS) and the loss of one-electronequivalent-oxidized ABTS to yield compound II. Further addition of ABTS and release of the ABTS radical then regenerates iron(III) (Fig. 8)^{11,14}.

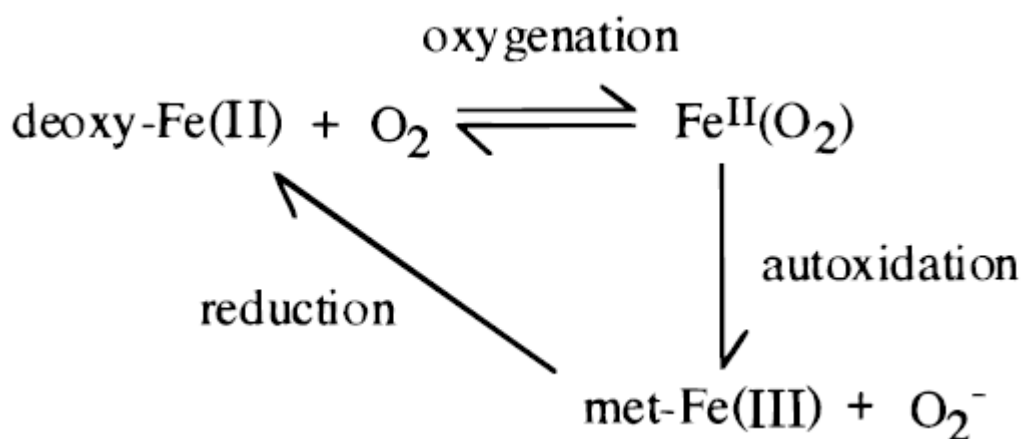
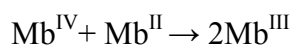


Figure 8. Using known changes in valency of the heme iron, one can the derive functional cycle¹².



Equation 1 The metMb formation by ferryl-Mb(IV)¹³

ABTS is commonly used as a substrate of H₂O₂ for the peroxidase enzyme. The absorbance change at 405 nm and 730 nm ($\epsilon = 1.4 \times 10^4 \text{ M}^{-1} \text{ cm}^{-1}$) can be easily analyzed with a spectrophotometer.

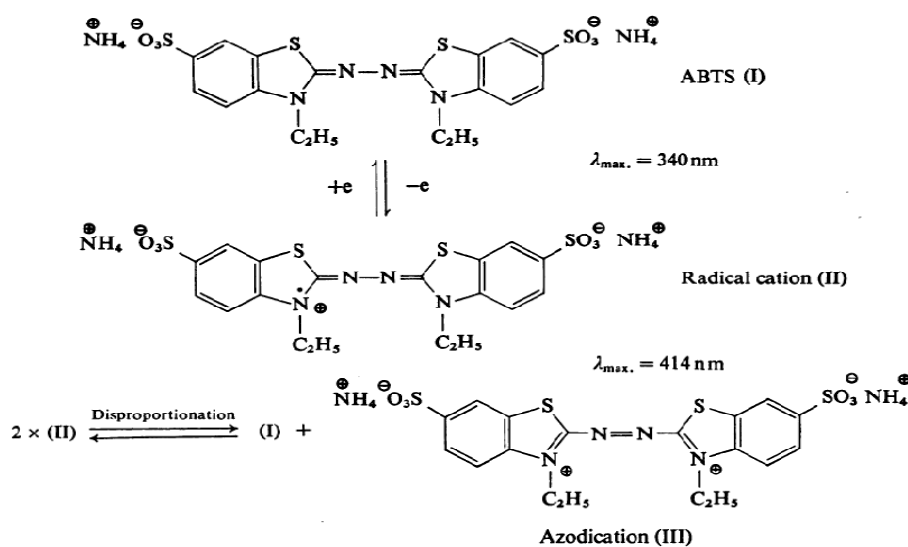


Figure 9. Chemical formulae of ABTS and its oxidation products¹⁴

1-6 Enzyme Kinetics

The central approach used for studying the mechanism of an enzyme-catalyzed reaction is to determine the rate of the reaction. Enzyme kinetics is the study of the chemical reactions that are catalyzed by enzymes, with a particular focus on their reaction rates.

Because enzymes are not consumed by the reactions they catalyze, enzyme assays usually trace concentration changes of either substrates or products to obtain accurate measurements of the reaction. Spectrophotometric assays are the most

convenient measurements.

A key factor affecting the rate of a reaction catalyzed by an enzyme is the concentration of the substrate [S]. One simplified approach in kinetics experiments is to measure the initial rate, designated V_0 . As enzyme-catalyzed reactions are saturable, their rate of catalysis does not show a linear response to increasing substrate concentrations. If the initial rate of the reaction is measured over a range of [S], the V_0 increases as [S] increases (as shown on the right). However, as [S] gets higher, the enzyme becomes saturated with substrate and the rate reaches the enzyme's maximum rate, V_{\max} .

The Michaelis-Menten kinetic model of a single-substrate reaction and a single intermediate complex is shown Figure 10. $E + S \xrightleftharpoons[k_{-1}]{k_1} ES \xrightarrow{k_2} E + P$ Some enzymes, that have more than one substrate, do not fit this single-substrate mechanism. Peroxidase is an example of this; as the enzyme reacts with a first H_2O_2 substrate molecule, it becomes compound I and is then reduced by a second molecule of substrate. Although a single substrate is involved, the existence of a modified enzyme intermediate means that the mechanism of peroxidase is actually a *ping-pong* mechanism. Pseudo single-substrate reactions and multi-substrate reactions are thus grouped as single-substrate reaction. An initial bimolecular reaction occurs between the enzyme E and substrate S leading to the formation of the enzyme-substrate complex ES. Typically, one rate-determining enzymatic step allows this reaction to be modeled as a single catalytic step with an apparent unimolecular rate constant, k_{cat} . $ES \xrightarrow{k_{\text{cat}}} E + P$ If the reaction pathway proceeds over one or several intermediates, k_{cat} will be a function of several elementary rate constants; whereas in the simplest case of a single elementary reaction k_{cat} will be identical to the elementary unimolecular rate constant k_2 . The apparent unimolecular k_{cat} rate constant is also

known as the *turnover number* and denotes the maximum number of enzymatic reactions able to be catalyzed per second. The Michaelis–Menten equation quantitatively describes how the V_0 depends on the position of the substrate-binding equilibrium and the rate constant k_2 . $K_M = K_2 + K_{-1} / K_1 \approx K_D$, $V_{\max} = k_{cat} [E]_{tot}$,

$$V_0 = V_{\max} [S] / (K_M + [S])^{3,15}$$

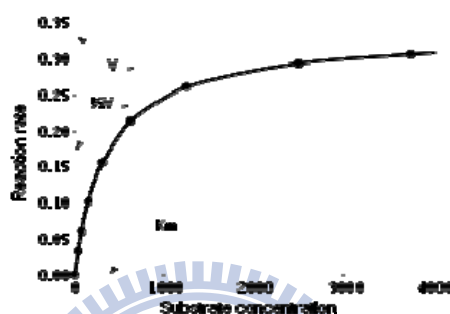


Figure 10. Michaelis-Menten plot

The plot of v versus $[S]$ depicted above is not linear; although initially linear at low $[S]$, it begins to plateau saturation of enzyme at high $[S]$. Prior to the modern era of computationally derived nonlinear curve-fitting, this nonlinearity could make it difficult to estimate K_m and V_{\max} accurately. Therefore, several researchers developed linearizations of the Michaelis-Menten equation, such as the Lineweaver–Burk plot. This linear type of representation continues to be useful for initial visualization of the data, but should not be used to determine kinetic parameters. As computer software is now readily available more accurate determination by nonlinear regression methods can be easily achieved. The Lineweaver–Burk plot, or double reciprocal plot is a common way of illustrating kinetic data and is produced by taking the reciprocal of both sides of the Michaelis–Menten equation. As shown on the right, the linear form of the Michaelis–Menten equation produces a straight line via the equation $y = ax + b$ where the y -intercept is equivalent to $1/V_{\max}$ and the x -intercept of the graph

represents $-1/K_m$. (Fig. 11) $\frac{1}{V} = \frac{K_m}{V_{\max}} [S] + \frac{1}{V_{\max}}$ ^{3,15}

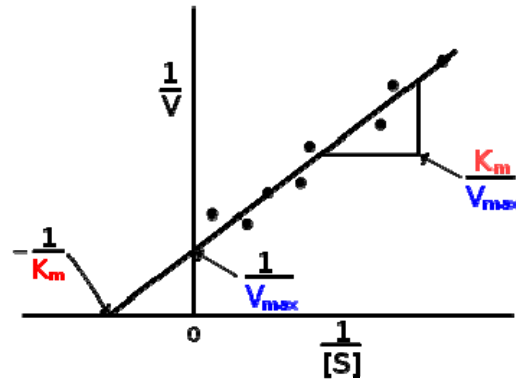


Figure 11. Lineweaver-Burk plot

1-7 Research Goal

The non-enzymatic myoglobin was functionally converted into a heme enzyme with peroxidase activity. In a previous study, an Mb^{H64D/V68L/I107M} enzyme with peroxidase activity had been engineered. This mutant version of myoglobin was capable of over-expression and, hence, purification. The activity of Mb^{H64D/V68L/I107M} was determined to be approximately 30% of H₂O₂ and 60% of ABTS better than that of Mb^{H64D/V68L} ¹⁶.

The Ile-107 was located 6.8Å away from the iron of heme. When the Ile-107 was replaced with Met, the peroxidase activity of mutated Mb was further improved. The distance between each residue and the center of heme has been summarized in Table 1. The Leu-29 was located 7.64Å away from the iron of heme. Alayash *et al.* determined that the Leu-29 affected the binding activity of O₂ with heme¹⁰. We believe this residue may have an important role in mediating peroxidase activity. To examine this hypothesis, we engineered the Leu-29 to construct Mb^{L29X/H64D/V68L/I107M}.

Residue number	Residue name	Nearly atom	Distance	Residue number	Residue name	Nearly atom	Distance	Residue number	Residue name	Nearly atom	Distance
1	Val	CG1	-25.02	52	Glu	OE2	20.47	103	Tyr	OH	-12.87
2	Leu	CD1	-21.05	53	Ala	CB	23.68	104	Leu	CD2	-6.54
3	Ser	OG	-28.16	54	Glu	OE1	21.17	105	Glu	OE2	-17.46
4	Glu	OE2	-27.26	55	Met	CE	16.06	106	Phe	CD2	12.84
5	Gly	CA	-28.67	56	Lys	NZ	21.25	107	Ile	CD1	6.76
6	Glu	OE2	-26.5	57	Ala	CB	21.56	108	Ser	OG	-11.7
7	Trp	CH2	-18.96	58	Ser	OG	15.55	109	Glu	OE2	17.08
8	Gln	NE2	29.89	59	Glu	OE2	18.92	110	Ala	CB	12.8
9	Leu	CD2	27.28	60	Asp	OD2	12.73	111	Ile	CD1	10.53
10	Val	CG1	18.79	61	Leu	CD1	10.79	112	Ile	CD1	17.33
11	Leu	CD2	19.64	62	Lys	NZ	19.57	113	His	NE2	20.89
12	His	ND1	27.01	63	Lys	NZ	15.55	114	Val	CG2	16.19
13	Val	CG2	20.39	64	His	CD2	8.48	115	Leu	CD2	17.25
14	Trp	CH2	13.11	65	Gly	CA	9.56	116	His	NE2	25.89
15	Ala	CB	22.86	66	Val	CG1	13.08	117	Ser	OG	21.27
16	Lys	NZ	27.49	67	Thr	CG2	7.15	118	Arg	NH2	19.52
17	Val	CG1	15.96	68	Val	CG2	4.99	119	His	NE2	20.7
18	Glu	OE2	16.25	69	Leu	CD2	10.32	120	Pro	CD	26.38
19	Ala	CB	22.75	70	Thr	OG1	12.44	121	Gly	CA	29.08
20	Asp	OD1	19.63	71	Ala	CB	7.89	122	Asp	OD2	27.24
21	Val	CG1	13.9	72	Leu	CD1	10.4	123	Phe	CZ	20.28
22	Ala	CB	16.56	73	Gly	CA	13.49	124	Gly	CA	27.54
23	Gly	CA	17.5	74	Ala	CB	13.52	125	Ala	CB	28.7

24	His	ND1	17.93	75	Ile	CD1	-10.1	126	Asp	OD1	28.5
25	Gly	CA	12.16	76	Leu	CD2	-15.02	127	Ala	CB	24.54
26	Gln	OE1	17.37	77	Lys	NZ	18.69	128	Gln	OE1	23.08
27	Asp	OD1	17.94	78	Lys	NZ	-20.08	129	Gly	CA	23.7
28	Ile	CG2	10.73	79	Lys	NZ	-25.64	130	Ala	CB	23.2
29	Leu	CD2	7.64	80	Gly	CA	-19.4	131	Met	CE	17.6
30	Ile	CG1	15.2	81	His	ND1	-22.87	132	Asn	OD1	18.66
31	Arg	NH1	18.98	82	His	ND1	-15.76	133	Lys	NZ	-26.19
32	Leu	CD2	8.35	83	Glu	OE1	-20	134	Ala	CB	-17.52
33	Phe	CZ	9.33	84	Ala	CB	-17.44	135	Leu	CD1	14.03
34	Lys	NZ	21.19	85	Glu	OE2	-16.73	136	Glu	OE2	-19.09
35	Ser	OG	17.21	86	Leu	CD1	-12.72	137	Leu	CD1	-18.88
36	His	NE2	15.61	87	Lys	NZ	-17.63	138	Phe	CZ	-8.17
37	Pro	CG	17.72	88	Pro	CB	-11.24	139	Arg	NH2	-14.07
38	Glu	OE1	15.62	89	Leu	CD1	-6.2	140	Lys	NZ	-21.4
39	Thr	CG2	10.72	90	Ala	CB	-10.76	141	Asp	OD2	-17.03
40	Leu	CD1	12.3	91	Gln	NE2	-13.71	142	Ile	CD1	-9.6
41	Glu	OE1	16.17	92	Ser	OG	-6.79	143	Ala	CB	-15.44
42	Lys	NZ	-11.36	93	His	NE2	-2.18	144	Ala	CB	-18.04
43	Phe	CZ	5.25	94	Ala	CB	-11.24	145	Lys	NZ	-16.77
44	Asp	OD2	13.14	95	Thr	OG1	-12.5	146	Tyr	OH	-8.47
45	Arg	NH1	10.88	96	Lys	NZ	-10.07	147	Lys	NZ	-23.24
46	Phe	CE2	8.94	97	His	NE2	-5.69	148	Glu	OE1	-19.11
47	Lys	NZ	13.86	98	Lys	NZ	-14.52	149	Leu	CD1	-14.36
48	His	ND1	16.68	99	Ile	CD1	-6.47	150	Gly	CA	-18.92

49	Leu	CD1	14.93	100	Pro	CD	-10.07	151	Tyr	OH	-15.42
50	Lys	NZ	24.72	101	Ile	CD1	-11.69	152	Gln	OE1	-16.45
51	Thr	OG1	22.52	102	Lys	NZ	-18.05	153	Gly	CA	-16.09

Table 1. The residues and distances away from iron atom of the wild type of sperm Mb.

When CO binds and later leaves the heme, the distance between the His-93 and the iron of heme becomes longer and shorter respectively. His-93, which binds the heme directly, could affect the position of iron¹⁷. We performed the molecular modeling of H93X, first. Next, we identified some mutants close to the heme that may affect the steric and electric orbital existence of iron (Table 2). We then engineered the His93 to construct Mb^{H93X}.

Mutant	Distance(Å)	Atom	Mutant	Distance(Å)	Atom
H93H	2.08	NE2	H93I	6.32	CG2
H93A	6.62	CB	H93N	5.66	ND2
H93F	2.19	CZ	H93W	5.54	CH2
H93E	2.79	OE2	H93V	6.37	CG1
H93D	6.91	OD1	H93T	5.7	OG1
H93C	6.02	CB	H93S	7.54	OG
H93G	7.22	O	H93R	2.19	NH2
H93M	4.12	CE	H93Q	2.47	NE2
H93L	5.42	CD2	H93P	6.85	CG
H93K	2.39	NZ	H93Y	2.74	OH

Table 2. The His-93 mutants and distances away from iron atom

Alayash *et al.* additionally found that Mb^{V68L} exhibited peroxidase activity¹⁰. The Val17 in helix A, which acts as a steric interaction path by which Leu-69 is to Val-68 at helix E (Fig. 12), is changed to Trp for different size¹⁷. We expect the Val68 will close the iron atom if we change the size of amino residue 17. We compared the distance of Val17 to Leu69 and Trp17 to Leu69. The distance of V17W was determined to be shorter than that of the wild type(Fig. 13), similar to Val-68 → Leu. We then performed molecular modeling of V17W.

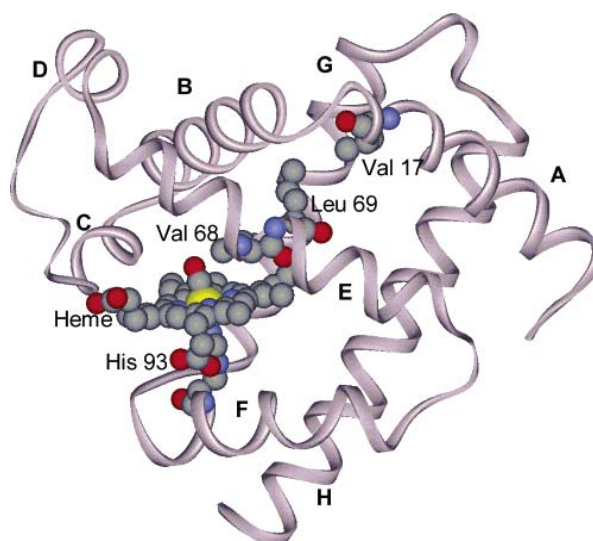


Figure 12. MbCO structure showing juxtaposition of Val 68 on the bound CO, and the steric interactions path through Leu69 to Val17, at the AB corner.¹⁷

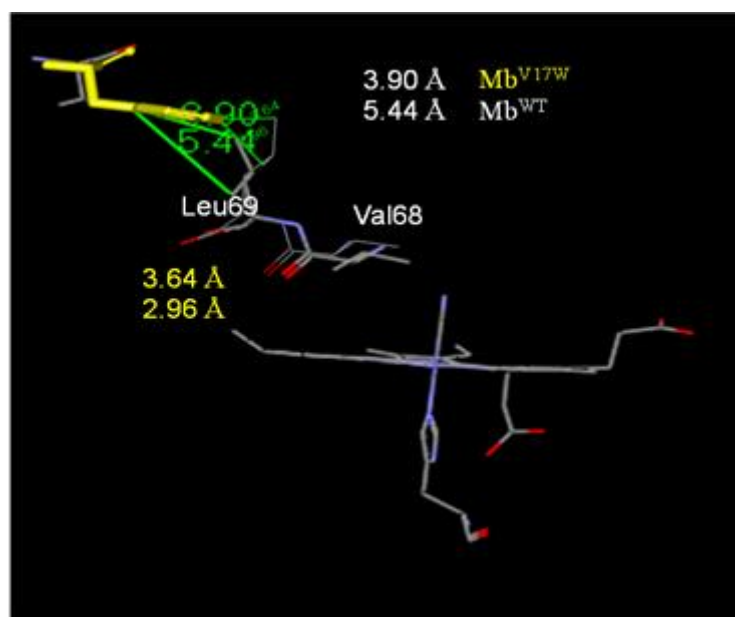


Figure 13. The distance of Mb^{WT} crystal structure (PDB: 104M)(white one) and molecule modeling of Mb^{V17W} (yellow one)

The physical mechanism involved non-bonded contact of the water molecule with the side chains of the CD loop residues Phe-43 and Phe-46, which moved out away when the H₂O molecule was introduced (Fig. 14)¹⁷. When Phe-43 and Phe-46 were replaced with Tyr, the protein character was transformed from hydrophobic to hydrophilic, and we expected enhancement of the H₂O₂ binding ability.

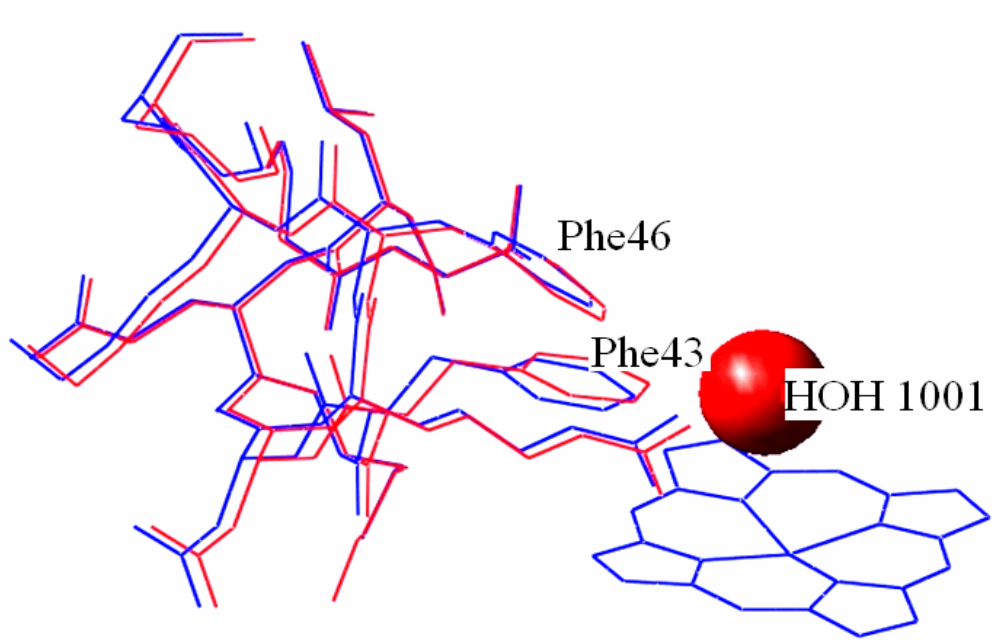


Figure 14. Illustration of the Phe 43 and 46 displacements, and the connecting CD loop¹⁷

We conjectured these mutants could affect the peroxidase activity of Mb so we summarized the relative positions of these mutants. (Fig. 15).

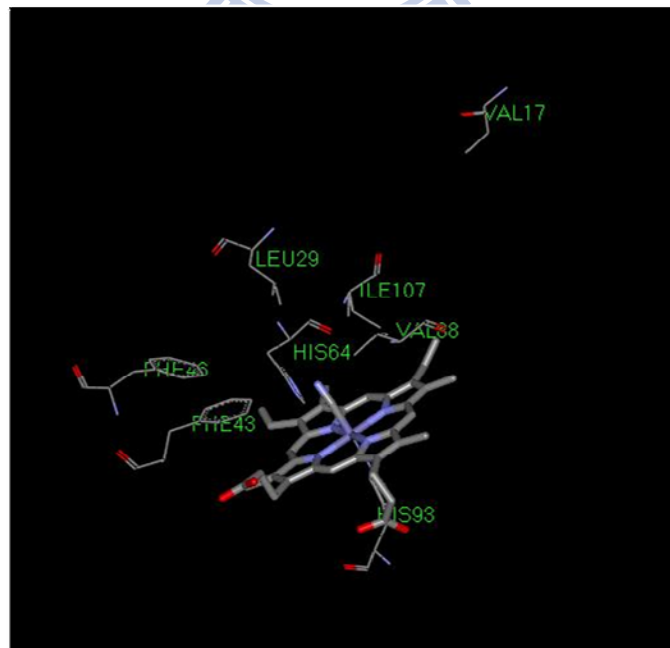


Figure 15. Amino acid residues mutation in sperm whale Mb.

2 Materials and Methods

2-1 Materials

2-1-1 Chemicals

Acetic acid (Merck)

40% Acrylamide (GE Healthcare)

Agarose (USB)

APS (GE Healthcare)

2,2'-azino-bis(3-ethylbenzothiazoline 6-sulfonic acid) (ABTS) (Sigma)

Bacto™ Agar (DIFCO)

Bromophenol blue (USB)

Citric acid (Sigma)

Coomassie® Brilliant blue R 250 (Merck)

Dimethyl sulfoxide (MP Biomedicals)

DEAE sepharose (Bio-Rad)

Dodecyl sulfate sodium salt (Merck)

dNTP Set, 100 mM Solutions (GE Healthcare)

Ethylenediamine-tetraacetic acid (Merck)

Glycerol (Merck)

Glycine (Merck)

Guanidine hydrochloride (Gdm-HCl) (Sigma)

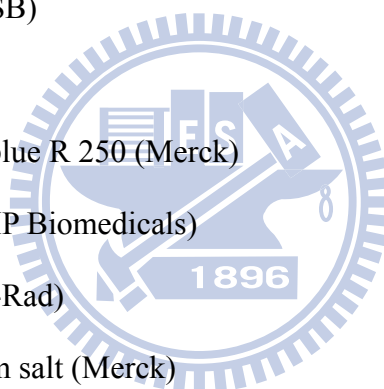
Hydrogen chloride (Merck)

IPTG (GeneMark, Taiwan)

Kanamycin sulfate (USB)

LB Broth, Miller (DIFCO)

2-mercaptoethanol (Merck)



Methanol (Merck)

N,N'-methylene-bis-acrylamide (Bis-Acrylamide)(Sigma)

Potassium chloride (Merck)

Potassium diphosphate (Merck)

Potassium phosphate (Merck)

Primers (Bio Basic Inc., Taiwan)

Restriction enzymes (New England Biolabs)

Sodium azide (Merck)

Sodium chloride (AMRESCO)

Sodium hydroxide (Merck)

Sodium diphosphate (Merck)

Sodium phosphate (Merck)

SYBR[®] Green I (Roche)

T4 DNA ligase (Promega)

TEMED (GE Healthcare)

Tris base (USB)

BCA Protein Assay Reagent and Albumin Standard (PIERCE)

BigDye[®] Terminator v3.1 Cycle Sequencing Kit (Applied Biosystems)

CNBr-activated Sepharose 4B(GE)

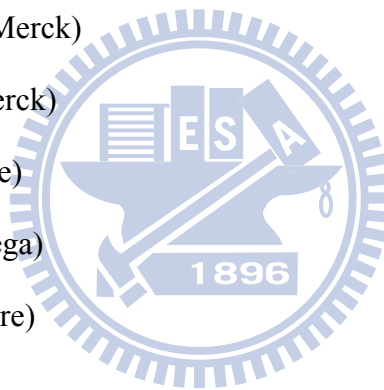
GFX[™] PCR DNA and Gel Band Purification Kit (GE Healthcare)

LMW-SDS Marker Kit (GE Healthcare)

Plasmid Miniprep Purification Kit (GeneMark)

rTth DNA polymerase, XL & XL Buffer II Pack (Applied Biosystems)

QuickChange Site-Directed Mutagenesis Kit (Stratagene)



2-1-2 Buffers and Reagents

50X TAE Buffer :

242 g Tris base, 57.1 mL acetic acid, 0.5 M EDTA in 1 L H₂O, [pH=8.5]

6X DNA loading dye:

0.25% bromophenol blue, 30% glycerol, stock at -20°C

30% Acrylamide Mix :

40% acrylamide 750 mL, 10 g bis-acrylamide in 1 L ddH₂O, stock at 4 °C in dark place

Separation Gel Buffer :

1 M Tris pH 8.8, stock at 4 °C

Stacking Buffer :

1 M Tris pH 6.8, stock at 4 °C

20% SDS :

20 g SDS, in 100 mL H₂O, stock at room temp.

10X Running Buffer :

144 g glycine, 30 g Tris-base, 10 g SDS, in 1 L H₂O, stock at 4 °C. dilute it to 1X

5X Sample Buffer :

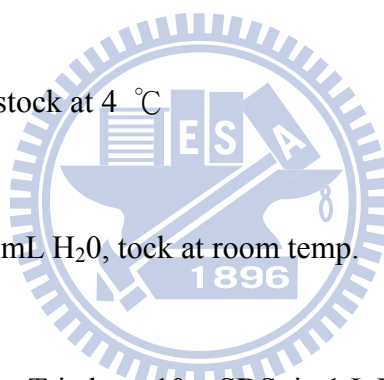
1 mL 1M Tris-HCl (pH 6.8), 0.8 mL glycerol, 1.6 mL 10% SDS, 0.4 mL 2-mercaptoethanol, 0.05% bromophenol blue, in 8 mL H₂O

0.1% Coomassie blue R-250 Stain Solution :

1 g Coomassie brilliant blue R-250, in 400 mL methanol, with 100 mL acetic acid, in 1 L H₂O

Destain Solution I :

400 mL methanol, 100 mL acetic acid, in 1 L H₂O



Destain Solution II :

50 mL methanol, 70 mL acetic acid, in 1 L H₂O

Lysis buffer :

Tris-HCl 100mM, KCl 100mM and EDTA 1mM, pH 8.0

Solubilization buffer

Tris-HCl 100 mM, pH 8.0, Gdm-HCl 8 M

Disruption buffer

Tris-HCl 100 mM, pH 8.0

Equilibration buffer :

Sodium phosphate 50 mM, pH 7.2

Luria-Bertani medium

10 g Bacto-Tryptone, 5 g yeast extract, 5 g NaCl, in 1 L H₂O

IPTG

IPTG (isopropyl β -D-thiogalactoside) solute in ddH₂O, filtered through a 0.22 μ m cellulose acetate filter, stock at -20 °C

Tetracycline

Tetracycline 20 mg/ml with Ethanol, -20 °C

LB-Tet medium

Agar 15 g/1L LB medium with 1 mL Tetracycline at 4 °C, in dark

Kanamycin (25 mg/mL)

250 mg kanamycin sulfate with 10 ml ddH₂O, filtered through a 0.22 μ m cellulose acetate filter, stock at -20 °C

LB-Kan medium

Agar 15 g/1L LB medium with 1 mL Kanamycin at 4 °C, in dark

2-1-3 Equipments

DC120 Kodak Electrophoresis Documentation and Analysis System 120(Kodak)

ABI PRISM[®] 3100 Genetic Analyzer (Applied Biosystems)

Orbital shaking incubator Model-S302R (Firstek Scientific)

Allegra[™] 21R Centrifuge (Beckman)

Avanti[®] J-E Centrifuge (Beckman)

Centrifuges 5415R (Eppendorf)

Spin Vacuum SPD-111V (SAVANT)

DU-7500 spectrophotometer (Beckman)

Amicon (Ultrafiltration System)

Packard (Fusion Universal Microplate Analyzer)

GeneAmp[®] PCR System 9700(Applied Biosystems)

Amersham Pharmacia

8453 UV-Visible Spectrophotometer (Agilent Technologies)

2-1-4 Bacterial strains, vectors, animal, and cell

Escherichia coli XL1-Blue (Stratagene)

Escherichia coli BL21(DE3) (Novagen)

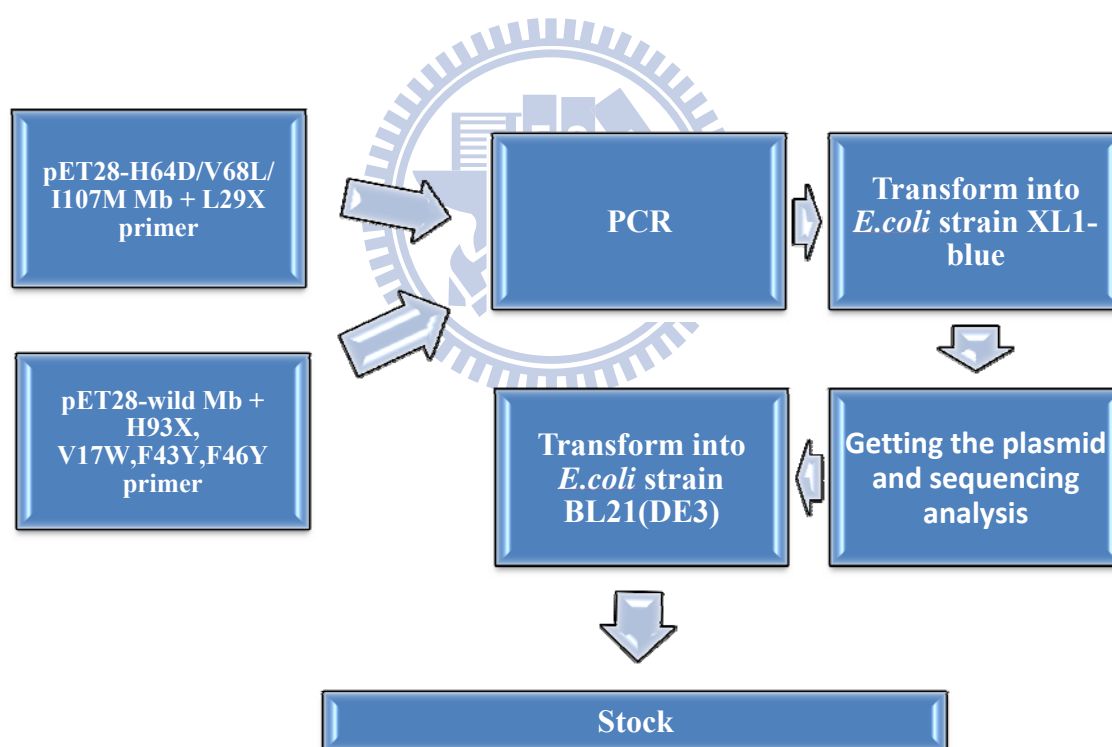
pET-28a(+) (Novagen)

2-2 Method

2-2-1 Molecular modeling

- Molecular-modeling studies were performed, using the DiscoveryStudio program with X-ray structure of wild type Mb as the template. We inputted mutant Mb and counted by the program. This software are provided by National Center for High-Performance Computing (NCHC) institution.

2-2-2 Preparation of Myoglobin Variants



Scheme 1. Experimental procedures-1

The sperm whale Mb mutants were constructed by cassette mutagenesis. The

sequence is from NCBI. The expression vector of wild-type sperm whale Mb was from Hung-Ming Lin.¹⁶ The cassette including silent *EcoR* V restriction site was inserted between the *BamH* I and *Nco* I sites. The expression was in *Escherichia coli* strain pET-28a(+).

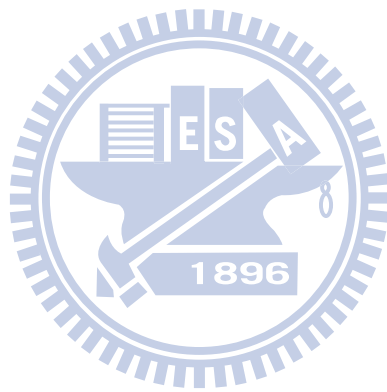
The mutations of Mb^{L29X/H64D/V68L/I107M}, Mb^{H93X}, Mb^{F43Y}, Mb^{F46Y}, and Mb^{V17W} were constructed by Site-Directed mutagenesis strategies.

(1) Primer design:

YHWu-Mb-L29X-1	<p>G Q D I X I L F K</p> <p>5' ggT Cag gAT ATC <u>NNN</u> ATT CgA CTg TTC 3'</p> <p><i>EcoR</i> V</p>
YHWu-Mb-H93X-1	<p>L A Q S X A T K I</p> <p>5' CTT gCg CAA TCg <u>NNN</u> gCT ACT AAA CAT 3'</p>
YHWu-Mb-V17W-1	<p>V W A K W E A D V</p> <p>5' gTT Tgg gCT AAA <u>Tgg</u> gAA gCT gAC gTC 3'</p>
YHWu-Mb-F43Y-1	<p>T L E K Y D R F K</p> <p>5' ACT CTg gA AAA <u>TAC</u> gAT CgT TTC AAA 3'</p>
YHWu-Mb-F46Y-1	<p>E K P D R Y K H L K</p> <p>5' gA AAA TTC gAT CgT <u>TAC</u> AAA CAT CTg AAA AC 3'</p>

Table 3. Primer design for site-saturated mutagenesis

The letters with gray background in the sequence line of primers show the target mutations, and “N” means A, T, C, G four bases, which are arranged in order to form 20 possible amino acids. The bolded letters indicate silent mutation for *EcoR* V mapping analysis and these constructions are marked with underline.



(2) QuikChange PCR:

Reagent	Volume(μ L)
Template	1
Primer 1 (10 μ M/ μ l)	1
Primer 2 (10 μ M/ μ l)	1
10X <i>Pfu</i> Buffer	5
dNTP (10 mM)	4
DDW	37
<i>Pfu</i> polymerase	1
Total reaction volume	50

Table 4. QuikChange Site-Directed Mutagenesis Kit PCR composition

segment	Cycles	Temperature	time
1	1	95 °C	2 min
2	18	95 °C	30 sec
		Primer $T_m - 5\sim 8$ °C	30 sec
		72 °C	12 min
3	1	72 °C	10 min
4	1	4 °C	∞

Table 5. QuikChange Site-Directed Mutagenesis Kit program

(3) *Dpn* I digest parental DNA template:

The digest reaction was incubated at 37 °C for 3 hours to digest the parental supercoiled DNA.

Reagent	Volume(μL)
PCR products	17
10X NEBuffer 4	1
DDW	1
<i>Dpn</i> I	1
Total reaction volume	20

Table 6. QuikChange Site-Directed Mutagenesis Kit PCR products digestion

(4) Transformation into XL1-Blue and enzyme mapping:

The digestion of QuikChange products were added into 100 μl *E.coli* XL1-Blue competent cells of each reaction and incubated on ice for 20 min. The cells were transformed by heatshock methods for 1 min at 42 °C, following 1 min on ice. Then, the cells were transferred to 1 ml LB medium immediately and shaken at 200 rpm for 1 hour at 37 °C incubator. After that, the cells were centrifuged at 8,000 rpm for 1 min and propagated on LB plate containing 25 μg/ml kanamycin. These plates were incubated at 37 °C overnight. Selected and cultured the transformed colonies in 3 ml LB medium containing 25 μg/ml kanamycin at 37 °C overnight. The plasmid DNAs were isolated by Plasmid Miniprep Purification Kit, according to the manufacturer instructions.

(5) Sequencing analysis of myoglobin mutants:

The exact amino acid substitution at Val17, Leu29, Phe43, Phe46, and His93 positions were determined by sequencing of the DNA using ABI PRISM 3100 auto-sequencer. Nucleotide sequencing was performed using the dideoxynucleotide chain-termination method with only one forward or reverse primers. Sequencing reactions were carried out with BigDye[®] Terminator v3.1 Cycle Sequencing Kit, according to manufacturer protocol. Each of the samples were performed with 1 μ l each forward or reverse primer, 2 μ l plasmid DNA, 3 μ l 5X sequencing buffer, 1 μ l premix and ddH₂O to get a final volume of 20 μ l. Each of reactions was performed on ABI PRISM[®] 3100 Genetic Analyzer, following the manufacture's guidelines.

2-2-3 Preparation of Clones

The plasmids after checked were added into 100 μ l *E.coli* BL21 (DE3) competent cells of each reaction mixture and incubated on ice for 20 min. The cells were transformed by heatshock methods for 1 min at 42 °C, following 1 min on ice. Then, the cells were propagated on LB plate containing 25 μ g/ml kanamycin with 40 μ l. These plates were incubated at 37 °C overnight. Injected the colonies and cultured in 1ml LB medium containing 25 μ g/ml kanamycin at 37 °C overnight. Taking one of the medium mixed the same volume of glycerol and stocked at -80 °C.

2-2-4 Preparation of SDS-polyacrylamide gel electrophoresis (SDS-PAGE)

The glass-plate sandwich of the electrophoresis apparatus was assembled according to manufacturer's instructions. The gel solution was prepared as follows:

Solution	Separating gel (20%)
ddH ₂ O	2 ml
30% acrylamide mix	6.6 ml
1.5 M Tris (pH 8.8)	2.5 ml
20% SDS	50 µl
10% ammonium persulfate	200 µl
TEMED	10 µl

Solution	Stacking gel (4%)
ddH ₂ O	3 ml
30% acrylamide mix	0.67 ml
1 M Tris (pH 6.8)	1.25 ml
20% SDS	50 µl
10% ammonium persulfate	50 µl
TEMED	10 µl

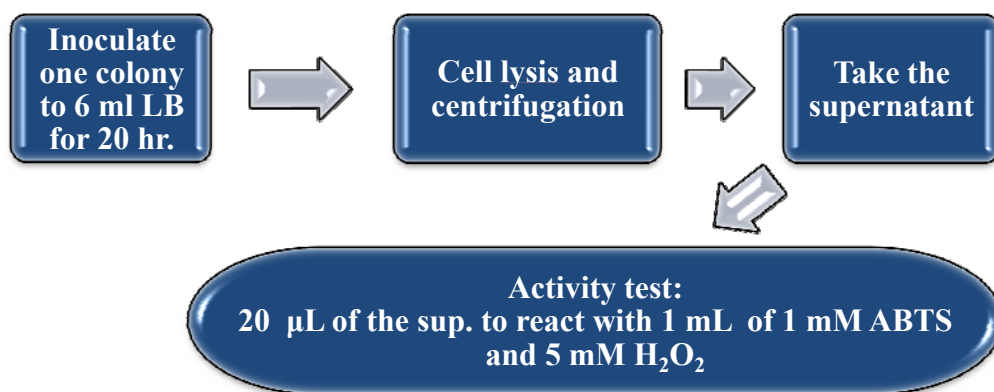
Table 7. 20% separating gel and 4% stacking gel of SDS-PAGE

2-2-5 Protein detection

For expression experiments, protein detection was completed with SDS-PAGE and Western blotting methods. All the clones were inoculated in 3 ml LB medium containing 25 µg/ml kanamycin at 37 °C overnight. The cells were centrifuged at 8,000 rpm for 1 min and re-suspended with 200 µl lysis buffer. After that, the solutions were immediately frozen in liquid nitrogen, then defrosted at 42 °C water

bath and repeated for several times. The solutions were centrifuged at 13,000 rpm for 1 min. The 20 μ l supernatant was mixed with 5X sample treatment buffer (125 mM Tris-HCl, pH 6.8, 2% SDS, 10% glycerol, 5% β -mercaptoethanol, and 0.05% bromophenol blue), and heated at 100 $^{\circ}$ C for 10 min. Electrophoresis was performed according to the manufacturer's instructions. After electrophoresis, the gel was soaked in Coomassie Blue R 250 staining solution for 20 min, and the gel was destained with the destaining solution I (40% methanol, 7% acetic acid) and II (5% methanol, 7% acetic acid) until the stained band was distinct against a clear background.

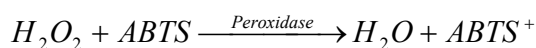
In Western blotting experiments, the supernatants were electrophoretically separated with SDS-PAGE and transferred onto polyvinylidene difluoride (PVDF) membranes. The PVDF membranes were washed by the PBS buffer (pH 7.6) containing 0.05% Tween 20 (PBST) for 10 min, and immunodetection was carried out by following the procedure for the ECL Western blotting system, using monoclonal antibody raised against the hemolysin (1:500) and anti-mouse immunoglobulin HRP-peroxidase conjugate (1:5000). Excess ligand was washed away with PBST for 30 min, and the detection of the proteins was performed according to the manufacturer's instructions (Amersham Pharmacia Biotech, Piscataway, NJ, USA). Membranes were exposed to Hyperfilm ECL (Amersham) for different times or until a suitable signal was obtained from the exposed films.



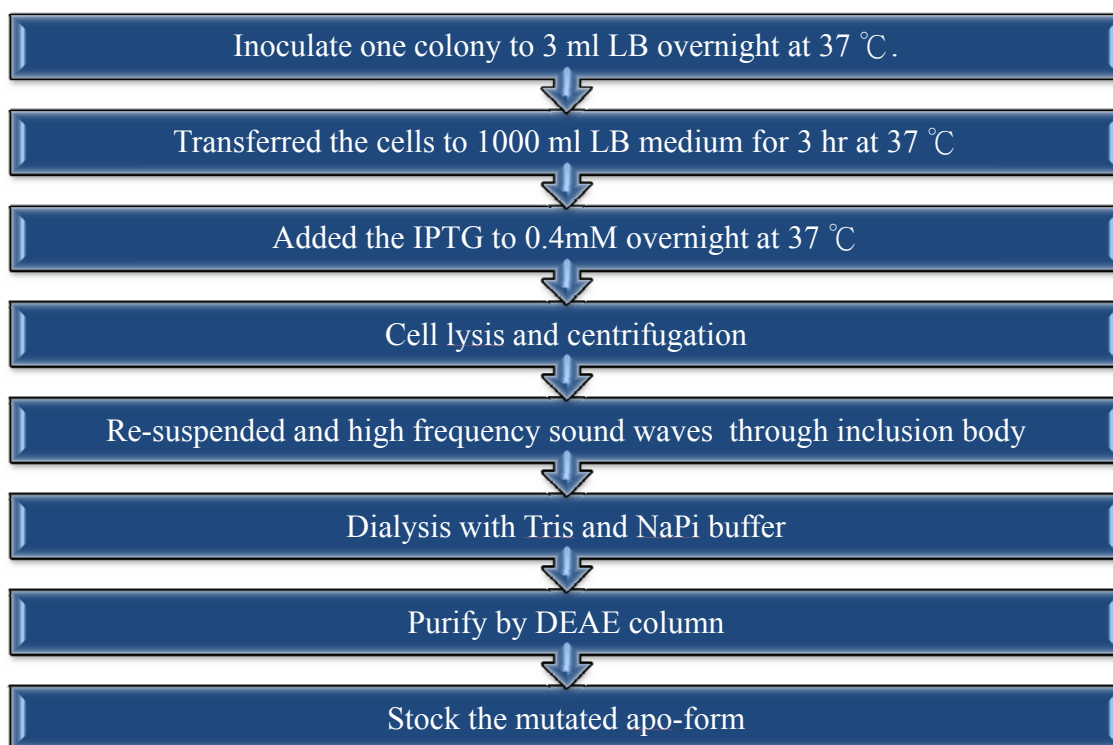
Scheme 2. Experimental procedures-2

2-2-6 Crude Extract

For high speed sieving the peroxidase activity of clones, all the clones were inoculated in 6 ml LB medium containing 25 µg/ml kanamycin at 37 °C more than 20 hours. The cells were centrifuged at 8,000 rpm for 1 min and re-suspended with 200 µl lysis buffer. After that, the solutions were quick-frozen in liquid nitrogen, then defrosted at 42 °C water bath to repeat for several times and centrifuged at 13,000 rpm for 1 min. The 10 µl supernatant was mixed with 1ml of 1 mM ABTS and 5 mM H₂O₂. The rate of the ABTS cation radical formation was monitored at 730 nm ($\epsilon_{730} = 1.4 \times 10^4 \text{ M}^{-1}\text{cm}^{-1}$) where the absorption of Mb was negligible so it can detect the difference at 730 nm in size.



Equation 2. Hydrogen peroxide reacts with ABTS



Scheme 3. Experimental procedures-3

2-2-7 Expression of Apo-Mb

The clones which had better peroxidase activity than others were chosen to incubate in 3ml LB medium containing 25 µg/ml kanamycin at 37 °C overnight, and the cells were transferred to 1000ml LB medium at 37 °C for 3 hours then induced with 0.4 mM of IPTG at 37 °C overnight. The cells were centrifuged at 8,000 rpm for 20 min and re-suspended with 20ml lysis buffer.

2-2-8 Crude extract of inclusion body

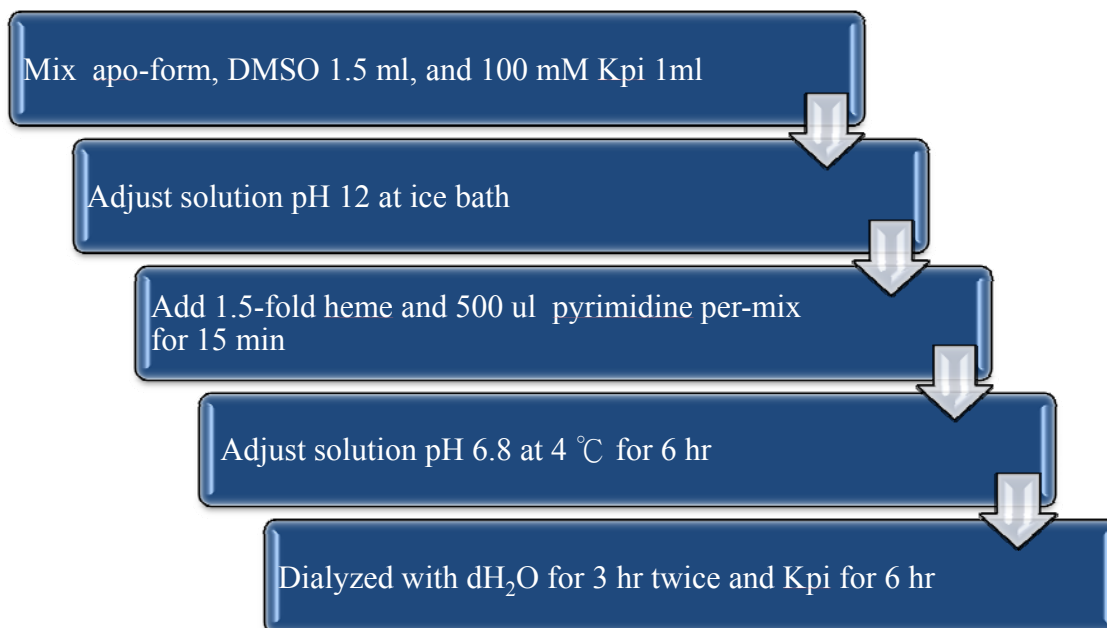
We used ultrasonicator to agitate and lyse cells. To prevent excessive heating, ultrasonic treatment was applied in multiple short bursts to a sample immersed in an ice bath. The sonication set with 30 % energy, pulsed 2 s, rest 1s, total 30 s, 6 cycles. The solution was centrifuged at 12,000 rpm for 30 min. The pellet was dissolved with 20 ml solubilization buffer.

2-2-9 Denature and refolding of inclusion body

We used ultrasonicator to scatter the inclusion body. To prevent excessive heating, ultrasonic treatment was applied in multiple short bursts to a sample immersed in an ice bath. The sonication set with 30% energy, pulsed 2 s, rest 1 s, total 30 s, 3 cycles. Disruption buffer was slowly added into the solution each time 10 ml, total 80 ml. The solution was dialyzed with 500 ml of Tris buffer twice each time for 2 hours, 2 L of Tris buffer overnight, and with 1 L of solubilization buffer twice each time for 2 hours, and 5 L of solubilization buffer overnight. The solution was centrifuged at 12,000 rpm for 30 min at 4 °C.

2-2-10 Purification of Apo-Mb

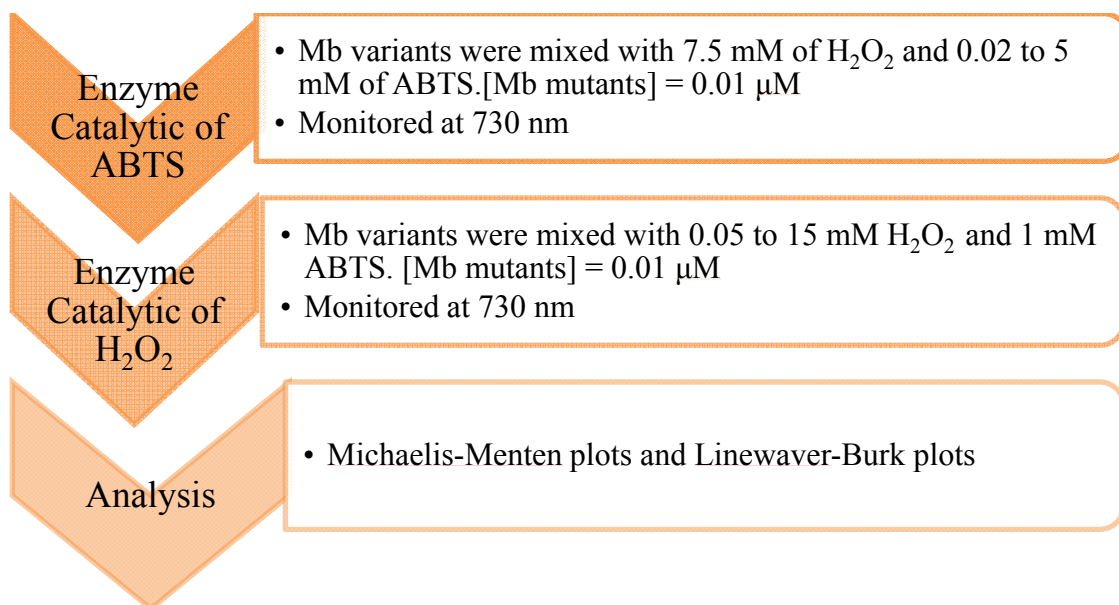
The supernatants added into DEAE column. The DEAE column was equilibrated with 5 bed volumes of 100 mM KPi buffer and the protein was recovered in the flow throughout. The CM column was equilibrated with 5 bed volumes of equilibration buffer but the protein was recovered with KPi buffer. The examination of expression yield and protein profile purification was performed by 20% SDS–polyacrylamide gel electrophoresis (SDS–PAGE).



Scheme 4. Experimental procedures-4

2-2-11 Reconstitution of Apo-Mb with heme

Reconstitution of heme into apo-Mb followed the modified method of Axup *et al.*(10) A 1.5-fold stoichiometric amount of heme in 100 mM KPi/pyrimidine (1/1, v/v, 500 μ l) solution was dropwisely added to an apo-Mb solution in 100 mM KPi/DMSO (4/1) buffer pH 12 (7.5 mL) cooled in an ice bath. After incubation for 15 min, the solution was adjusted to pH 6.8 and slowly stirred at 4°C for additional 6 hrs. The solution was transferred into a dialysis membrane against ddH₂O, with two times change of ddH₂O to remove organic solvent, followed by additional dialysis against 100 mM KPi buffer pH 6.8 for overnight. The solution was then filtrated with 0.45 μ m cellulose membrane before applied to a Sephadex G-25 column, equilibrated with 100 mM KPi buffer pH 6.8, and eluted with the same buffer at 4 °C. The protein band was collected and stored at -20 °C.



Scheme 5. Experimental procedures-5

2-2-12 Analysis of Peroxidase Activity

Activity for one-electron oxidation of ABTS was measured at room temperature in 100 mM potassium phosphate buffer (pH 7.0) on 8453 UV-Visible spectrophotometer. At least three experiments were performed for each experimental data point. The rate of the ABTS cation radical formation was monitored at 730 nm ($\epsilon_{730}=1.4 \times 10^4 \text{ M}^{-1} \text{ cm}^{-1}$) where the absorption of Mb was negligible. The reaction mixture contained ABTS (0.1-5 mM) and variable amounts of H₂O₂ (0.2-15 mM). The final concentration for Mb mutants was 0.01 μM.

3 Results and Discussion

3-1 All clones

The site directed mutagenesis strategy is a general method used in structural function studies for enzymes. In a previous study, Mb^{H64D/V68L/I107M} had been engineered to form an enzyme with peroxidase activity¹⁶. By using H₂O₂ and ABTS as substrates in a peroxidase activity assay, the activity of Mb^{H64D/V68L/I107M} was determined to be better than Mb^{H64D/V68L}. We further engineered the Leu-29 in Mb^{H64D/V68L/I107M} and His-93 in Mb^{WT} to construct Mb^{L29X/H64D/V68L/I107M} and Mb^{H93X} by site-saturated mutants. The X designation for each mutant represents the positions that were replaced with 19 amino acids. In addition, Val-17 was changed to Trp to construct Mb^{V17W} by site-directed mutagenesis. Phe-43 and Phe-46 were replaced with Tyr to construct Mb^{F43Y} and Mb^{F46Y}, respectively. The sequences of the above-mentioned clones were confirmed by DNA sequencing. The mutated plasmids were transformed into BL21(DE3) to facilitate protein expression. The results have been summarized in Table 8.

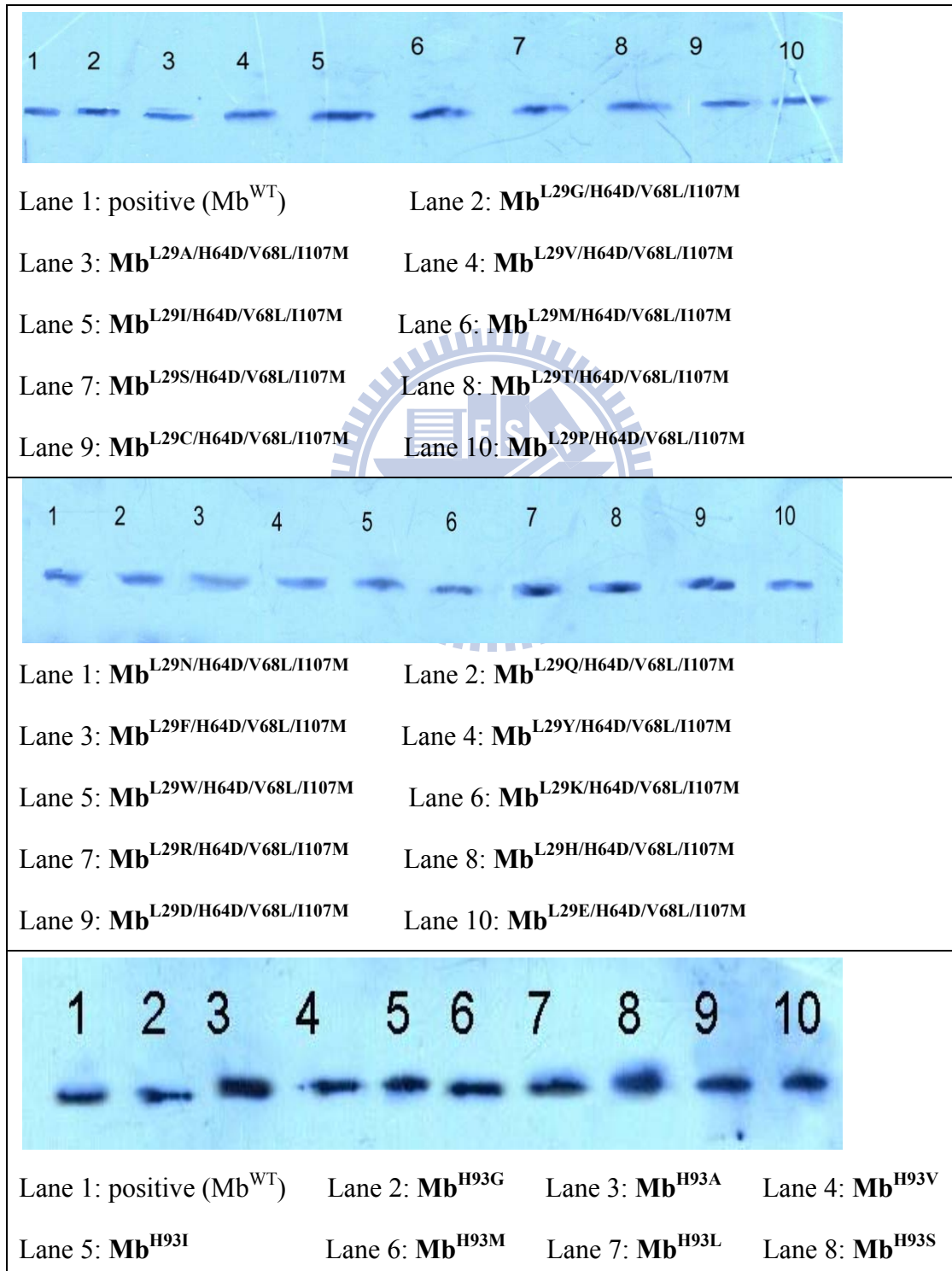
Mb	Sequence	Transform to BL21(DE3)	Mb ^{H64D/V68L/I107M}	sequence	Transform to BL21(DE3)
H93A(Ala)	V	V	L29A(Ala)	V	V
H93R(Arg)	V	V	L29R(Arg)	V	V
H93N(Asn)	V	V	L29N(Asn)	V	V
H93D(Asp)	V	V	L29D(Asp)	V	V
H93C(Cys)	V	V	L29C(Cys)	V	V

H93E(Glu)	V	V	L29E(Glu)	V	V
H93Q(Gln)	V	V	L29Q(Gln)	V	V
H93G(Gly)	V	V	L29G(Gly)	V	V
H93L(Lus)	V	V	L29H(His)	V	V
H93I(Ile)	V	V	L29I(Ile)	V	V
H93K(Lys)	V	V	L29K(Lys)	V	V
H93M(Met)	V	V	L29M(Met)	V	V
H93F(Phe)	V	V	L29F(Phe)	V	V
H93P(Pro)	V	V	L29P(Pro)	V	V
H93S(Ser)	V	V	L29S(Ser)	V	V
H93T(Thr)	V	V	L29T(Thr)	V	V
H93W(Trp)	V	V	L29W(Trp)	V	V
H93Y(Tyr)	V	V	L29Y(Tyr)	V	V
H93V(Val)	V	V	L29V(Val)	V	V
Mb	sequence	Transform to BL21(DE3)	Mb	sequence	Transform to BL21(DE3)
F43Y(Tyr)	V	V	V17W(Trp)	V	V
F46Y(Tyr)	V	V			

Table 8. List of all clones.

3-2 Protein detection

We incubated all clones in 6 ml LB medium at 37 °C for 20 hours and then lysed the cells. To confirm that our clones could express mutated Mbs efficiently in BL-21, the crude extracts were analyzed by Western blotting. The results revealed that all of our clones could express mutated Mbs efficiently (Fig. 16).



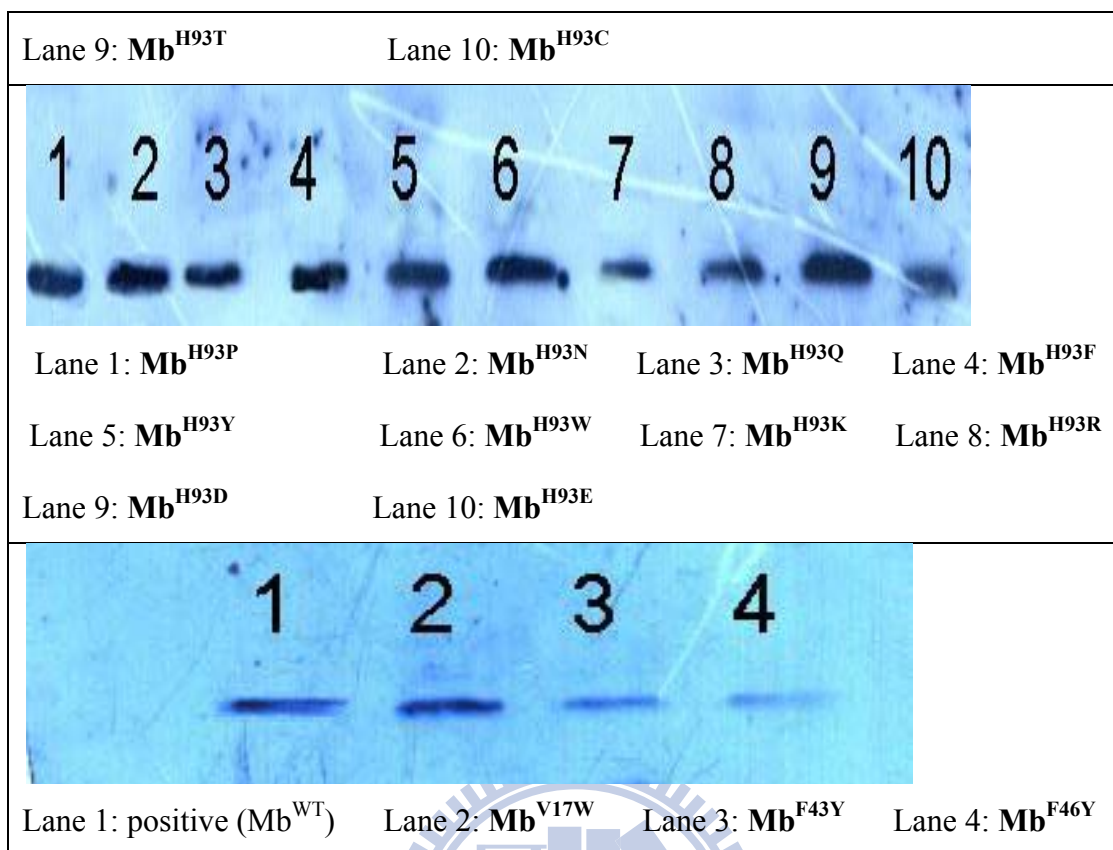


Figure 16. Western blotting experiments for clone expression

3-3 Activity Test of Crude Extract

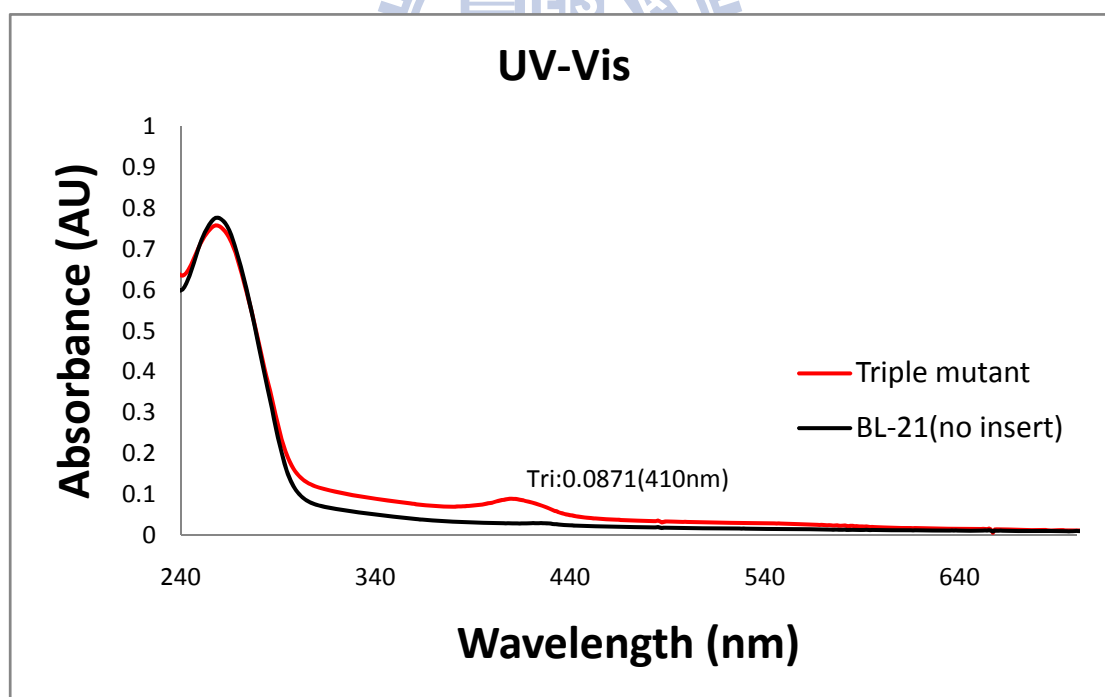
In order to prove that the mutated Mb clones can express and confer peroxidase activity, we analyzed the peroxidase activity between BL-21 clones with Mb^{H64D/V68L/I107M} insert and BL-21 clones without insert. We detected the Soret band of Mb. The characteristic Soret band of Mb is expected to be around 410 nm and is contributed by heme in Mb. The Soret band will shift in accordance with different pH values, different solutions, or different mutants.

First, we lysed the cells to obtain the crude extract. We then analyzed the difference in the UV-Vis spectrum. According to the absorbance pattern at 410nm, the results indicated that the Mb^{H64D/V68L/I107M} clone could express the mutated protein consistently. No absorbance was detected at 410nm for the BL-21 clone without insert

(Fig. 17-a).

Next, we attempted to confirm functional peroxidase activity. The activity was from the Mb^{H64D/V68L/I107M} which was expressed by the inserted clone. 20 µl of extract was allowed to react with 1 ml mixed solution of 1 mM of ABTS and 5 mM of H₂O₂. The absorbance change detected at 730 nm, ($\epsilon_{730} = 1.4 \times 10^4 \text{ M}^{-1} \text{ cm}^{-1}$) where the absorption of Mb was negligible, was recorded and compared. The results indicated; there was no absorbance change at 730 nm for the crude extract of BL-21 clone without insert. On the other hand, the absorbance change at 730 nm for the crude extract of Mb^{H64D/V68L/I107M} clone was increased gradually. It was confirmed that the peroxidase activity was from the Mb^{H64D/V68L/I107M}, and not from other proteins in the BL-21 cell (Fig. 17-b).

(a)



(b)

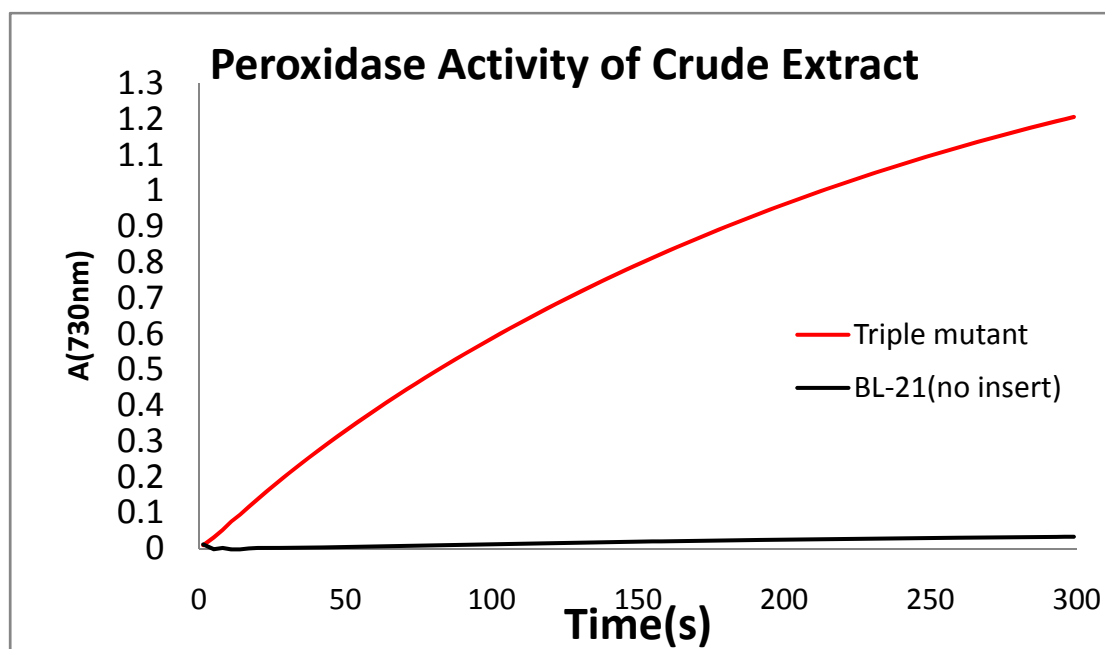
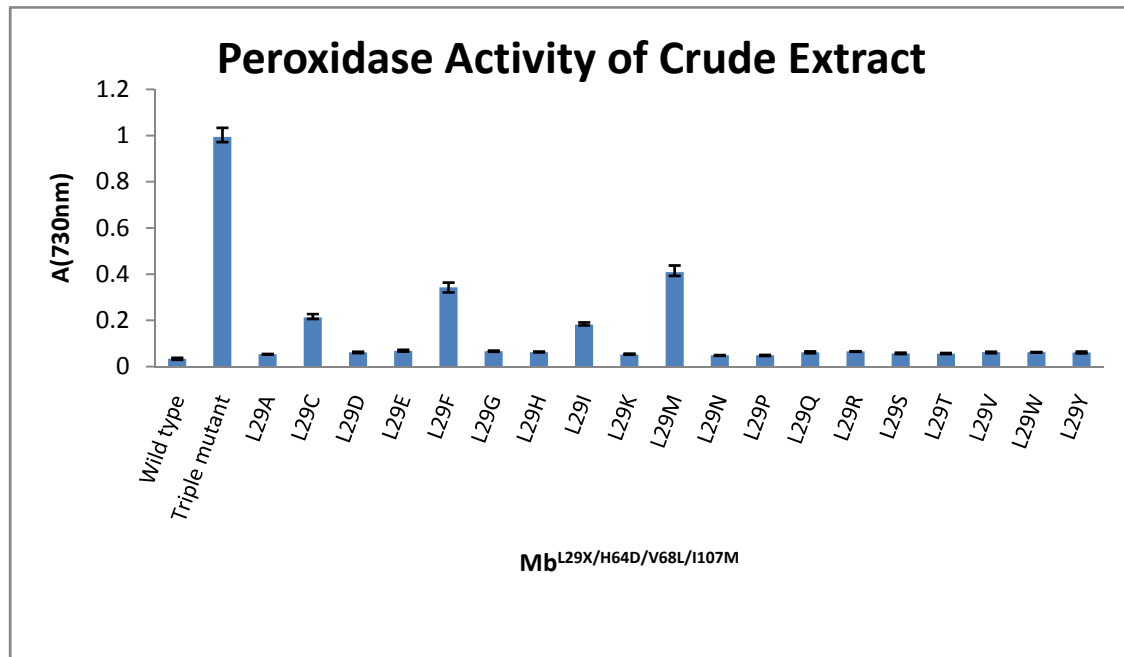


Figure 17. Comparisons of (a) wavelength scan and (b) peroxidase activity of crude extract from Mb^{H64D/V68L/I107M} clone (red) and BL-21 without insert (black)

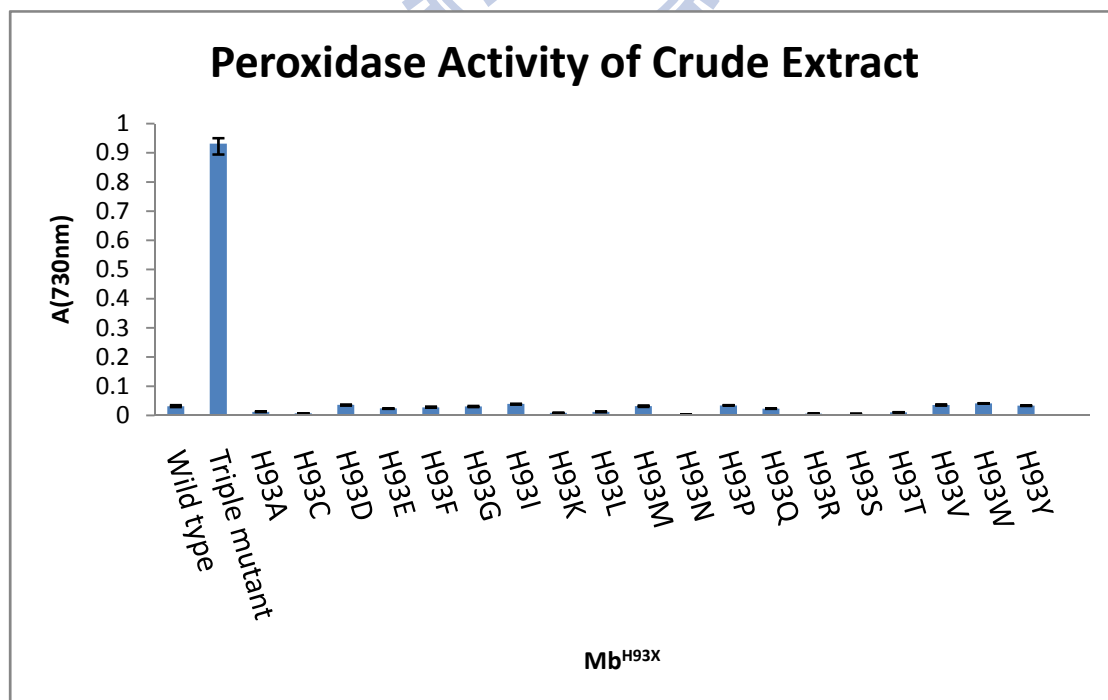
Also, the influence of Mb^{L29X/H64D/V68L/I107M}, Mb^{H93X}, Mb^{V17W}, Mb^{F43Y}, and Mb^{F46Y} on peroxidase activity was analyzed using the crude extracts. The concentrations of all crude extracts were normalized by the absorbance of Soret band (shown in Appendix Figs. 27, 28, and 29). All of the crude extract concentrations were adjusted to 0.058 μ M and mixed with 1 ml of 1 mM ABTS and 5 mM H₂O₂. The peroxidase activity of these crude proteins was analyzed spectrophotometrically at 25°C by using the H₂O₂-dependent oxidation of ABTS at 730 nm. Peroxidase activity results from Mb^{L29X/H64D/V68L/I107M}, Mb^{H93X}, Mb^{V17W}, Mb^{F43Y}, and Mb^{F46Y} have been shown in Figure 18, by using the triple mutant Mb^{H64D/V68L/I107M} as positive control and wild type Mb as negative control. In crude extract of Mb^{L29X/H64D/V68L/I107M}, each clone exhibited peroxidase activity but worse than that of Mb^{H64D/V68L/I107M} (Fig. 18-a). In crude extract of Mb^{H93X}, most did not have detectable peroxidase activity (Fig. 18-b). In crude extract of Mb^{V17W}, Mb^{F43Y}, and Mb^{F46Y}, only the Mb^{V17W} clone

showed activity (Fig. 18-c).

(a)



(b)



(c)

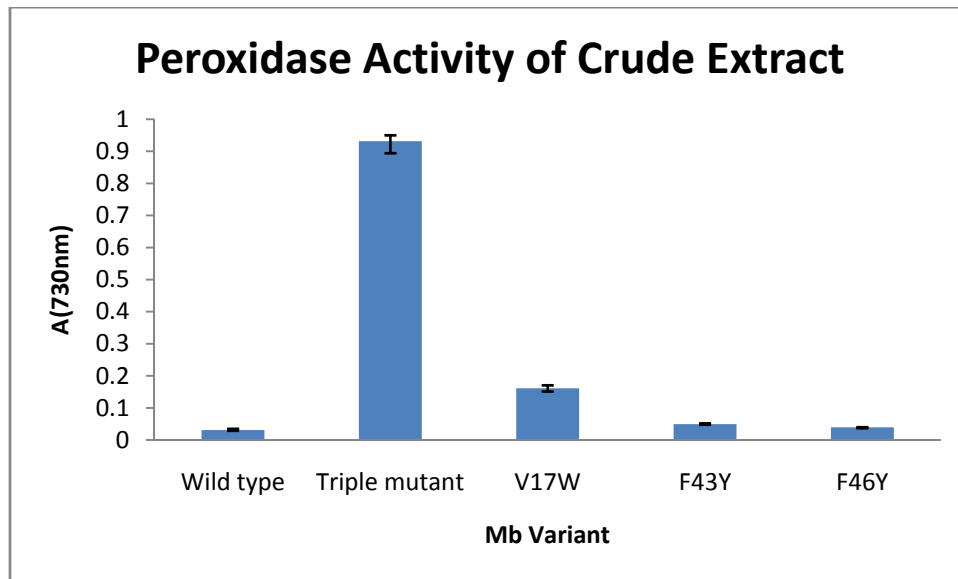


Figure 18. (a) The peroxidase activity of Mb^{L29X/H64D/V68L/I107M} clones. (b) The activity of H93X clones. (c) The peroxidase activity of V17W, F43Y, and F46Y clones.

Based on peroxidase activity results obtained using the crude cell extract, we further purified those clones with better activity. These were Mb^{L29C/H64D/V68L/I107M}, Mb^{L29F/H64D/V68L/I107M}, Mb^{L29I/H64D/V68L/I107M}, Mb^{L29M/H64D/V68L/I107M}, and Mb^{V17W}.

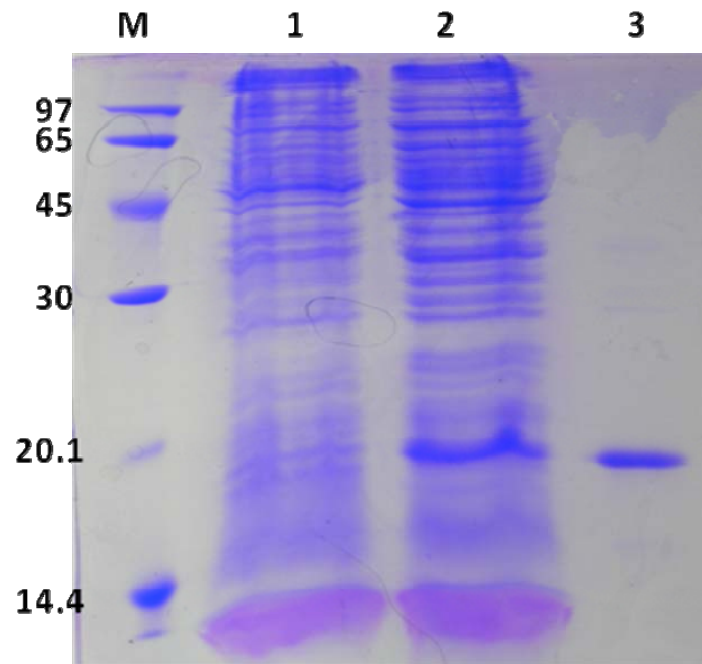
3-4 Purification of mutated Mbs

To produce highly pure and large amount of Mb variants, we deferred to the research of Ribeiro *et al.*¹⁸, which produces inclusion bodies. When we isolated the inclusion bodies, we were to remove the miscellaneous proteins easily.

First, we used IPTG to induce *Escheria coli.* to produce inclusion bodies of our variant Mbs. Then, we lysed the cells. There were many inclusion bodies in the crude extracts. The inclusion bodies were isolated via centrifugation. The inclusion body was expected to be in the pellet because of its high density, and the miscellaneous proteins, which were in the supernatant, were able to be efficiently removed. The inclusion bodies recovered were re-dissolved by Guanidine hydrochloride (Gdm-HCl). Upon removal of the Gdm-HCl by dialysis, Mbs would slowly refold to avoid

subsequent aggregation. Last, Mbs were purified by using DEAE column, and analyzed by 20% SDS-PAGE to confirm the purity of the extracted proteins. The results showed that these Mb variants were pure and expressed in large quantities. (Fig.19).

(a)



(b)

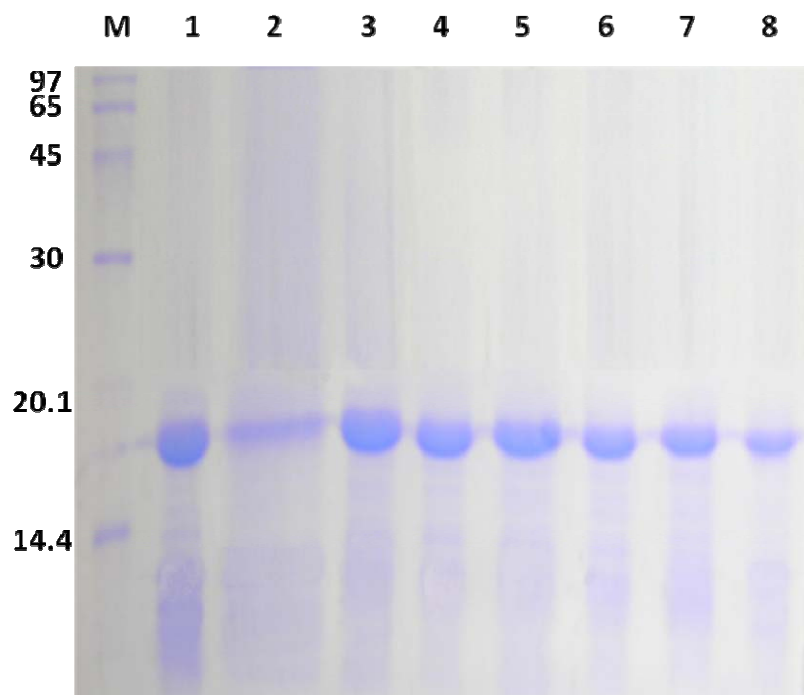
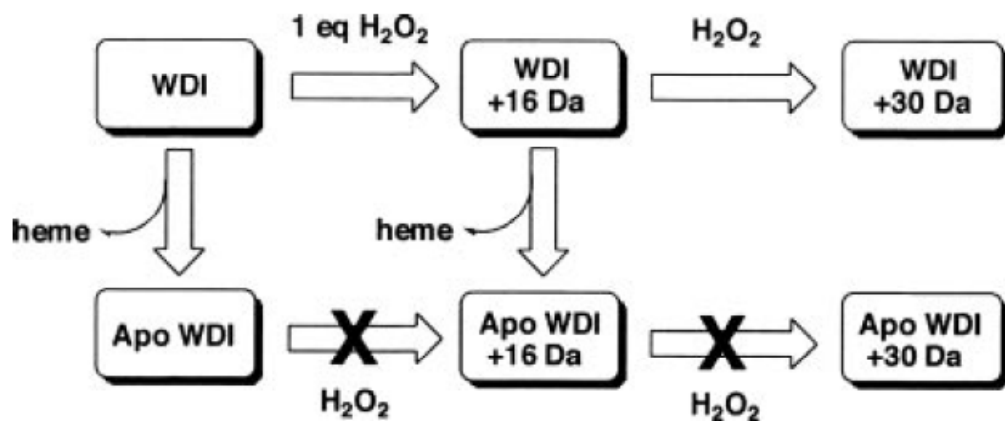


Figure 19. 20% SDS-PAGE analysis of purified mutated apoMb. (a) Lane M : marker, lane 1 : before adding IPTG, lane 2 : after IPTG induced, and lane 3 : purified 17kDa Mb. (b) Lane M : marker, lane 1 : Mb^{WT}, lane 2 : Mb^{H64D/V68L}, lane 3 : Mb^{H64D/V68L/I107M}, lane 4 : Mb^{V17W}, lane 5 : Mb^{L29C/H64D/V68L/I107M}, lane 6 : Mb^{L29F/H64D/V68L/I107M}, lane 7 : Mb^{L29I/H64D/V68L/I107M}, and lane 8 : Mb^{L29M/H64D/V68L/I107M}

3-5 Reconstitution of mutated Mbs

In the extreme high or low pH range, Mbs are unfolding and the heme can exist as monomer or dimer. For this reason, Mb and heme were mixed in pH 12 solution and slowly adjusted to pH 6.8, in hopes of improving cofactor reconstitution. At the same time, heme was dissolved in pyridine to prevent aggregation, and dimethyl sulfoxide (DMSO) was added to the protein solution to increase the protein solution's co-solubility. After the solution was completely adjusted to pH 6.8 and dialyzed, the heme that had not reconstituted with myoglobin was aggregated. We separated out that form of heme by passing through 0.45 μm filter and desalting column and discarded it.

To ensure the reconstituted Mbs had peroxidase activity, 10 μl of reconstituted Mb^{H64D/V68L/I107M}, apo-Mb^{H64D/V68L/I107M}, and heme only ([Mb]= 0.53 $\mu\text{g/ml}$ =0.031 μM =[heme]) (Fig. 20) were reacted with ABTS (1 mM) and H₂O₂ (5 mM). Only the reconstituted protein had peroxidase activity (Fig. 21). This result was in agreement with the results published by Pfister *et al.* (Scheme 5).



Scheme 6. Heme dependence of tryptophan oxidation⁹

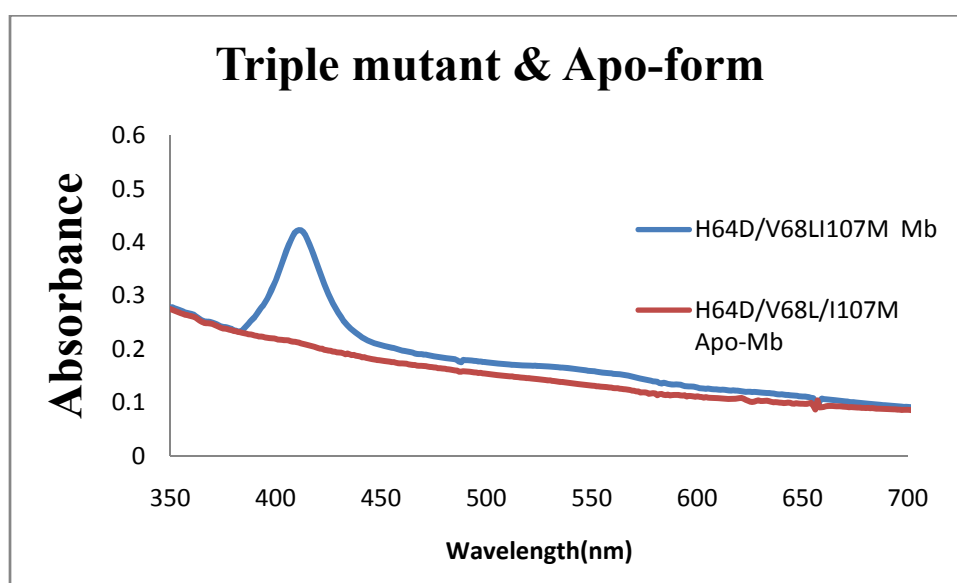


Figure 20. The UV-visible spectra of reconstituted Mb^{H64D/V68L/I107M} and Apo-Mb^{H64D/V68L/I107M} in 100 mM potassium phosphate buffer at pH 7.0

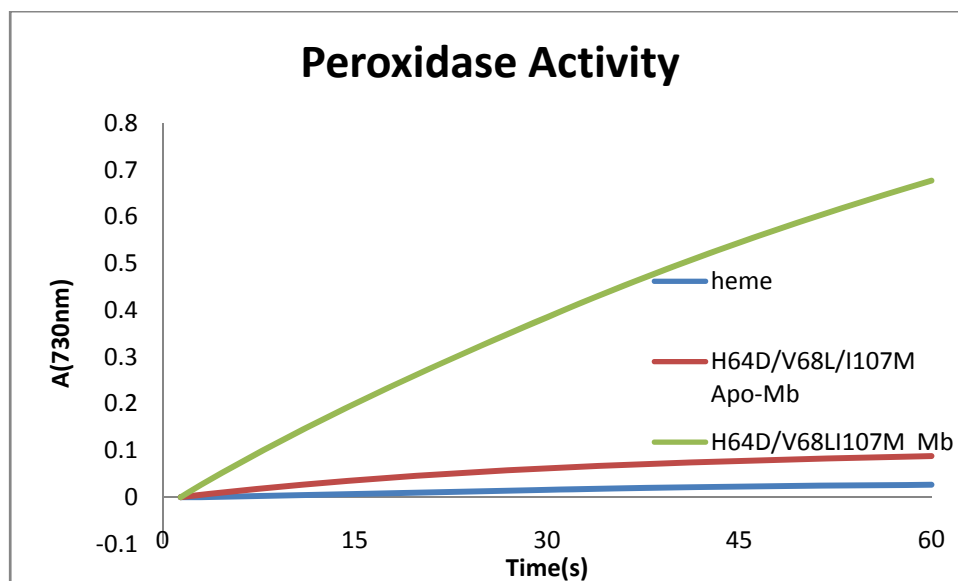


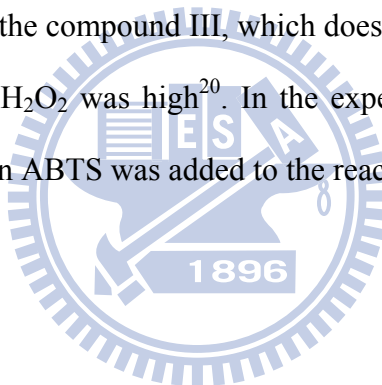
Figure 21. The absorbance change at 730 nm for Mb^{H64D/V68LI107M}, Apo-Mb^{H64D/V68L/I107M}, and heme in 100 mM potassium phosphate buffer at pH 7.0

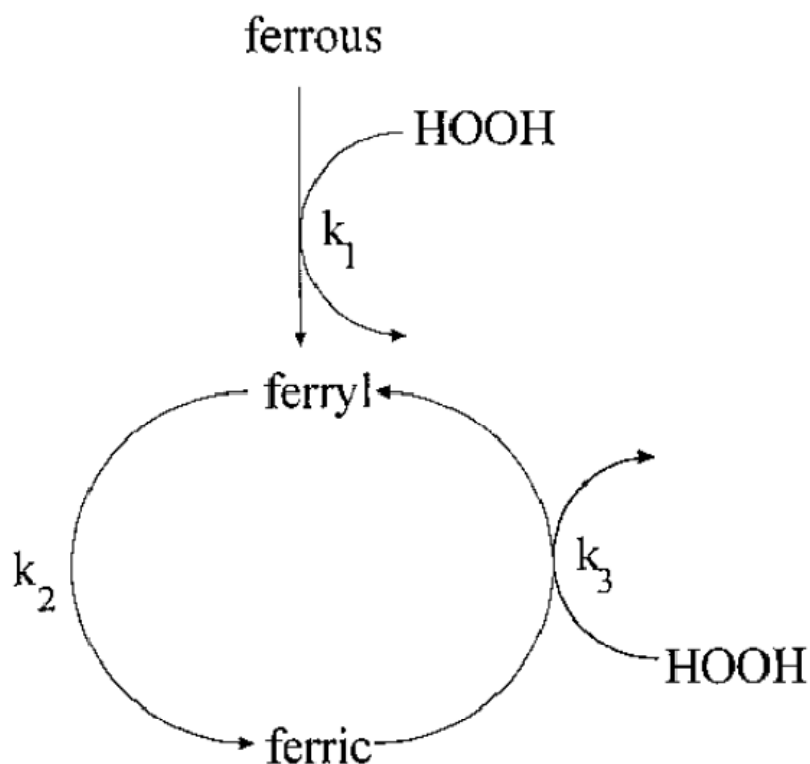
3-6 Enzyme kinetics measurements

Enzyme kinetics is an older approach used to understand enzymatic mechanisms and remains to be the most important aspect. The purified Mb^{L29C/H64D/V68L/I107M}, Mb^{L29F/H64D/V68L/I107M}, Mb^{L29I/H64D/V68L/I107M}, Mb^{L29M/H64D/V68L/I107M}, and Mb^{V17W} were subjected to enzyme kinetics assay. First, we analyzed the enzyme catalytic velocity of ABTS based on altering the concentration of ABTS. Mb variants were mixed with 7.5 mM of H₂O₂ and 0.01 to 5 mM of ABTS. The final concentration of Mb mutants was 0.01 μM. The results of the enzyme kinetics assay were analyzed by using Michaelis-Menten plots. The initial reaction rate v_0 was used as Y axis and the substrate concentration [ABTS] was used as X axis. For enzymes that obey the Michaelis-Menten relationship, we used $1/v_0$ as Y axis versus $1/[ABTS]$ as X axis to draw the Lineweaver-Burk plots. Also, we analyzed the enzyme catalytic velocity of H₂O₂ based on altering the concentration of H₂O₂. Next, Mb variants were mixed with 0.05 to 15 mM H₂O₂ and 1mM ABTS. The [H₂O₂]Michaelis-Menten and Lineweaver-Burk plots were then analyzed. The Michaelis-Menten and

Lineweaver-Burk plots of Mb^{L29C/H64D/V68L/I107M}, Mb^{L29F/H64D/V68L/I107M}, Mb^{L29I/H64D/V68L/I107}, Mb^{L29M/H64D/V68L/I107M}, Mb^{H64D/V68L/I107M}, Mb^{H64D/V68L}, and Mb^{V17W} have been shown in showed Appendix figure 30 and 31.

These two substrates are subject to substrate inhibition, especially H₂O₂. Alayash *et al.* had detailed the reactions of Mb with hydrogen peroxide in previous reports^{10,12,13,19}. In their research, Mb reacted with H₂O₂ but not with ABTS. The ferryl iron species (compound I) changed to the ferric state via auto-reduction (Scheme 6). The mechanism of this process is not well understood, and the identity of the electron donor remains unknown. It may produce the compound III (superoxide radical anion), and it has been shown to slowly reduce to the ferric state. The peroxidase enzyme formed the compound III, which does not have peroxidase activity, when the concentration of H₂O₂ was high²⁰. In the experiment, the enzyme did not form the compound III when ABTS was added to the reaction.





Scheme 7. The rates of the slow kinetic processes were made based on a simple reaction scheme.¹⁰

The steps of the peroxidase reaction are shown in equation 3 below. First, the enzyme is reacted with H_2O_2 to form compound I. The rate constant is represented by k_1 . Second, the ABTS reduced the complex to compound II. Finally, the ABTS continued to reduce the compound II until it reached the resting state and the iron of heme became ferric (Fig. 21). The constants for these reactions are represented by k_2 and k_3 , respectively. Consequently, by changing the concentration of H_2O_2 we were able to measure the catalytic rate of H_2O_2 .

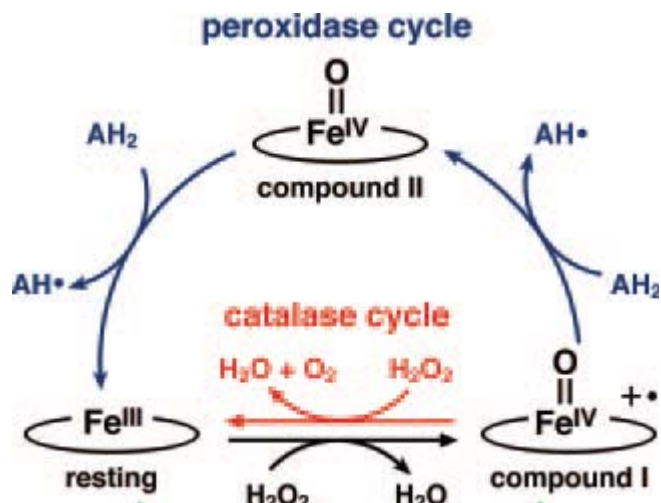


Figure 22. General reaction cycles of heme proteins with peroxide⁹



Equation 3. The equations of peroxidase catalysis

Mb^{H64D/V68L}, Mb^{H64D/V68L/I107M}, Mb^{L29I/H64D/V68L/I107M}, Mb^{L29F/H64D/V68L/I107M}, Mb^{L29C/H64D/V68L/I107M}, Mb^{L29M/H64D/V68L/I107M}, and Mb^{V17W} exhibited better peroxidase activity in crude extract analysis. We purified and reconstituted heme with these mutants; afterward, we finished the kinetic measurements. We have summarized the results in the table below and calculated the turnover number and catalytic efficiency.

ABTS				
Mutated Mb	apparent V'max	apparent K'm	turnover number(<i>k</i> cat)	catalytic efficiency (<i>k</i> cat/ <i>K</i> m)
[Enzyme]=1.00E-05	(mM/min)	(mM)	(min ⁻¹)	(mM ⁻¹ min ⁻¹)
H64D/V68L	0.099	0.389	9893	25448
H64D/V68L/I107M	0.116	0.324	11567	35765
L29I/H64D/V68L/I107M	0.052	0.211	5213	24737
L29F/H64D/V68L/I107M	0.026	0.153	2584	16913
L29C/H64D/V68L/I107M	0.017	0.102	1681	16542
L29M/H64D/V68L/I107M	0.057	0.196	5679	28954
V17W	0.010	0.063	994	15784

Table 9. Kinetic data of ABTS by mutated Mb

H ₂ O ₂				
Mutated Mb	apparent V'max	apparent K'm	turnover number(<i>k</i> cat)	catalytic efficiency (<i>k</i> cat/ <i>K</i> m)
[Enzyme]=1.00E-05	(mM/min)	(mM)	(min ⁻¹)	(mM ⁻¹ min ⁻¹)
H64D/V68L	0.113	1.723	11294	6556
H64D/V68L/I107M	0.121	1.586	12146	7705
L29I/H64D/V68L/I107M	0.009	0.113	868	7645
L29F/H64D/V68L/I107M	0.010	0.117	1008	8585
L29C/H64D/V68L/I107M	0.010	0.200	970	4840
L29M/H64D/V68L/I107M	0.071	1.039	7118	6853
V17W	0.008	0.168	765	4546

Table 10. Kinetic data of H₂O₂ by mutated Mb

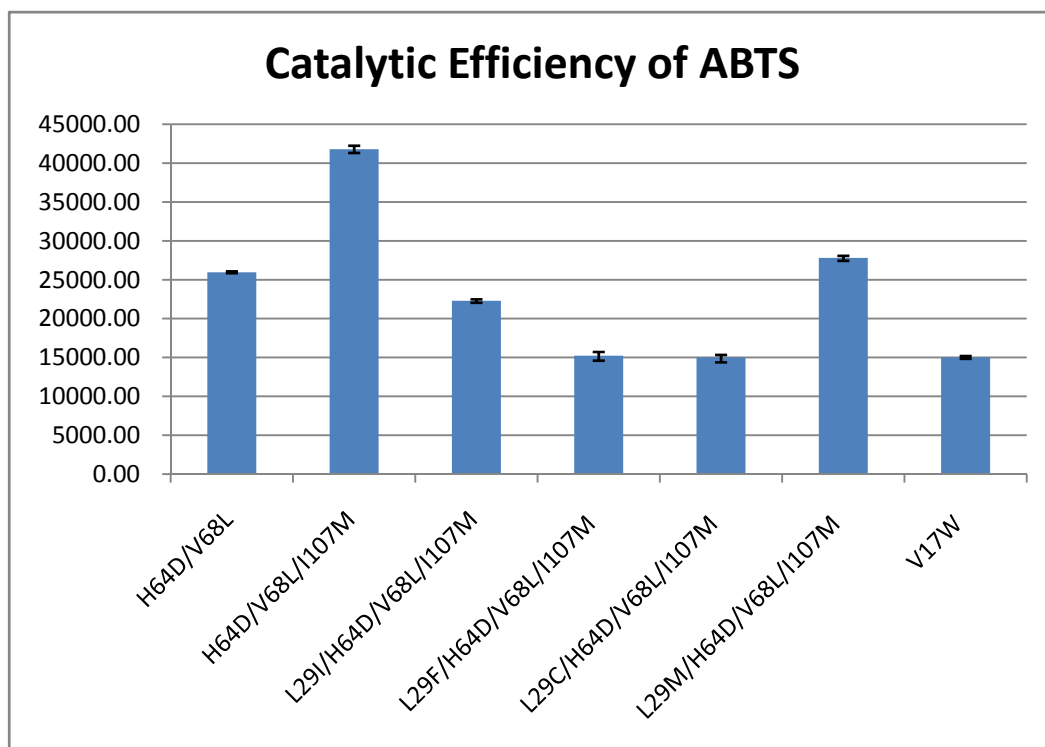


Figure 23. The catalytic efficiency of ABTS

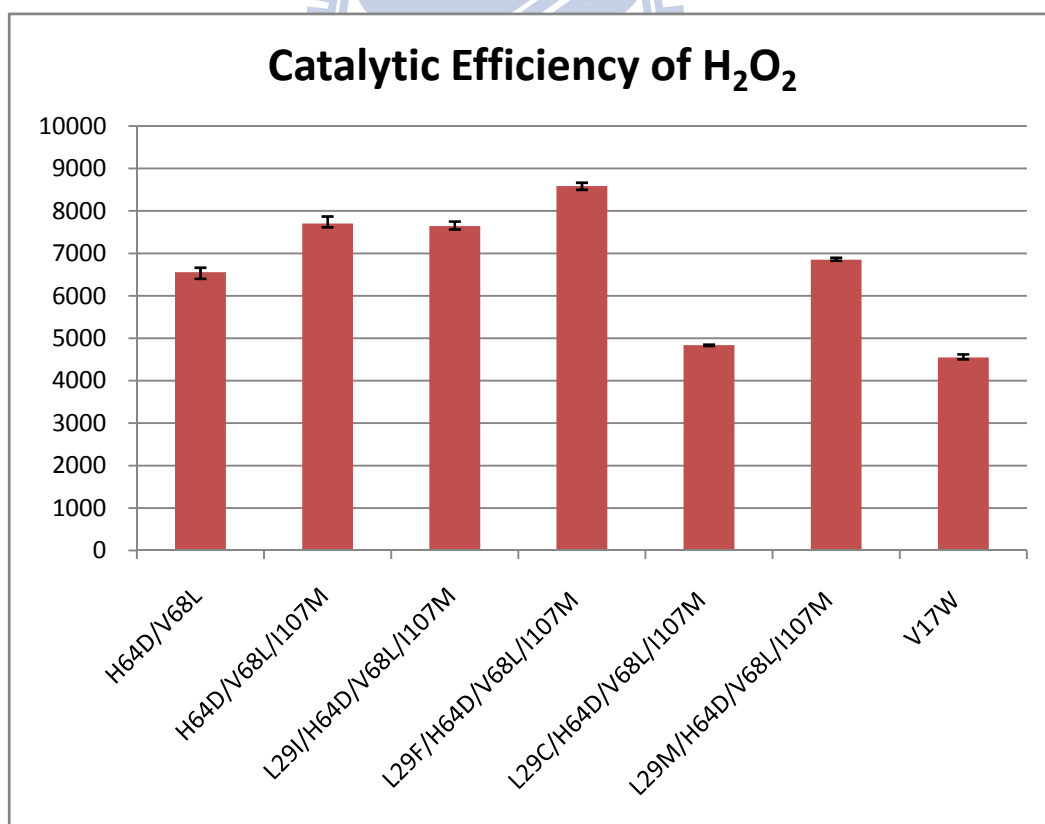


Figure 24. The catalytic efficiency of H₂O₂

Turnover number (also termed k_{cat}) is defined as the maximum number of substrate molecules that an enzyme can convert to product per catalytic site per unit of time and can be calculated as follows: $k_{\text{cat}} = V_{\text{max}}/[E]_0$. The catalytic efficiency allowed for comparison of peroxidase activities of the different mutants.

The activities of the quadruple mutants were worse than that of Mb^{H64D/V68L/I107M}. The result was determined by obtaining the k_{cat} of ABTS and H₂O₂. The catalytic efficiency of H₂O₂ obtained for the quadruple mutants was a little worse than Mb^{H64D/V68L/I107M}. The catalytic efficiency of ABTS was the determining factor of activity. Every quadruple mutant was found to be worse than the triple mutant, which had an obvious difference when compared to other quadruple mutants. We supposed that the phenomenon was the steric effect of R group for amino residues.

The Leu-29 → Ile mutation decreased catalytic efficiency of ABTS by 1.4-fold. This observation suggested that rotation of the substituted side chain about the C α -C β bond was restricted due to branching at the β carbon and prevented ABTS access to the heme center. Such a direct steric interaction could explain the decrease in peroxidase activity by the replacement of Leu-29 with Phe. Yang *et al.* showed the same result in the Leu-68 → Ile¹¹. However, Hiner *et al.* and Brantley *et al.* found that the Leu-29 → Phe mutation decreased the rate of autooxidation 10-fold, but increased oxygen affinity by 15-fold^{21,22}. This data could explain why the Mb^{L29F/H64D/V68L/I107M} catalytic efficiency of H₂O₂ appeared to be as good as Mb^{H64D/V68L/I107M} while the catalytic efficiency of ABTS was worse.

The Leu-29 → Met mutation decreased catalytic efficiency of ABTS by 1.2-fold. This mutation caused a substantially different steric space as a result of Met replacement by Leu than that achieved when Leu is replaced by Ile. On the other hand, Met has a sulfur atom. Met stabilized the oxidation product of ABTS so that the Leu → Met made K_m higher than that of other mutants²³. The stable reactivity of ABTS

follows the order Cys >>> Trp > Tyr > His >>> Cys. The structure of Met is similar to that of Leu. However, Leu and Cys have very different steric spaces even if the Cys has the highest reactivity. The differences between the amino acids affects not only ABTS binding but also H₂O₂ binding.

Val-17 in helix A mediates steric interactions through Leu-69 to Val-68 in helix E. The single mutant, Val-17 → Trp, effectively pushed the E helix closer to the heme iron through the Leu-69. Alayash *et al.* found that Mb^{V68L} had peroxidase activity¹⁰. Their data indicated that the rate constant of H₂O₂ of Mb^{V68L} is better than that of wild type by approximately 1.5 fold. The V17W, like Mb^{V68L}, had peroxidase activity, but it was worse than that of the double mutant, Mb^{H64D/V68L}.

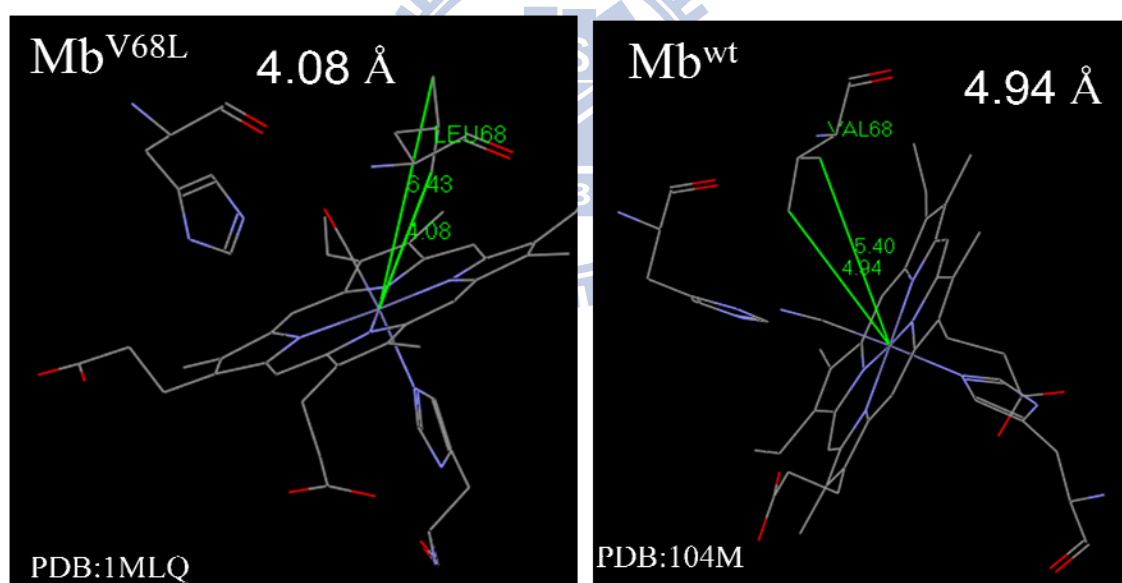


Figure 25. The shortest distance of Leu-68 and Val-68 to iron atom by crystal of Mb^{V68L}(PDB: 1MLQ) and Mb^{WT}(PDB: 104M)

4 Conclusion and Future Perspective

The Leu-29 in Mb is located 7.64Å away from the iron center of heme. We supposed that this amino residue was a key point of subtractive protonation, for example ABTS. After replacing 19 amino acids with Leu-29 to construct Mb^{L29X/H64D/V68L/I107M}, we compared the peroxidase activity of Mb^{L29X/H64D/V68L/I107M} with the peroxidase activity of Mb^{H64D/V68L/I107M}. The activity of H₂O₂ of the quadruple mutants was as good as the triple mutant, but the activity of ABTS was less than that of the triple mutant. The entrance of ABTS to the active site was seriously affected by the steric position of Leu-29. We plan to use a different kind of electron donor in future experiments, to create a different steric stabilization. This experiment will likely provide evidence that Leu-29 may particularly affect the activity of peroxidase.

The His-93 bound with heme could affect the position of iron. We, therefore, sought to determine whether the Mb peroxidase activity was due to the distal heme environment having been altered by amino acid mutation near the heme. In our research, there were no apparent differences between the 20 mutants of Mb^{H93X}. This result was quite similar to the results presented by Xiong *et al*²⁴. The protein backbone of Mb is known to fold and form a hydrophobic pocket that holds the heme in place. The mutated Mb peroxidase activity correlated with the environment around heme. The environment itself was dependent on the amino residue. For this reason, we believe the His-93 mutants did not support an environment for a functional peroxidase active site.

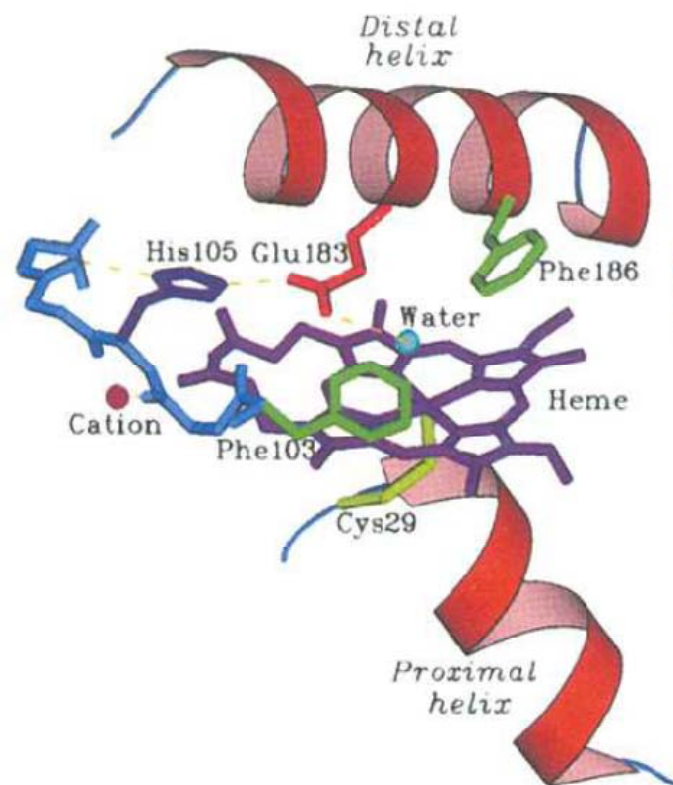
The single mutant, Val-17 → Trp, exhibited good catalytic efficiency. We found that V17W pushed the E helix close to the heme iron through Leu-69. It caused the

Val-68, which was on the E helix, to be nearer the heme iron. In the future, we can mutant the V17W with His-64 → Asp to test the peroxidase activity of Mb^{V17W/H64D}, and we can compare the peroxidase activity of Mb^{H64D/V68L} and Mb^{V17W/H64D}. In addition, we can compare the three-dimensional structure of Mb^{H64D/V68L} and Mb^{V17W/H64D} using an x-ray based approach. Ultimately, we may be able to prove whether the Mb^{V68L} and Mb^{V17W} exert similar effects.

The other single mutants, Phe-43 → Tyr and Phe-46 → Tyr, did not have obvious peroxidase activity. However, better activity was observed for Mb^{F43Y} and Mb^{F46Y} in comparison to wild type Mb. The two sites may not be the major site of peroxidase activity. We can mutate the F43Y and F46Y with the major site of peroxidase activity, like His-64 → Asp, and then compare the peroxidase activity of Mb^{H64D}. We anticipate that will aid in defining the influence of Phe-43 and Phe-46 on peroxidase activity.

Chloroperoxidase (CPO) is a heme-thiolate protein. The optimal pH value for its activity is 2 to 7. CPO halogenates organic substrates susceptible to electrophilic attack. It resembles cytochrome P450-dependent monooxygenases, which also belong to the heme-thiolate protein family and can catalyze a multitude of biotechnologically important oxygen transfer reactions²⁵. Mb^{H64D} is a heme-imidazolate protein, but has the same distal heme environment in the activation of peroxide as CPO (Fig. 9 and 26). It is hoped that our understanding of the Mb mutation approach may also be applied to CPO to enhance its activity or to reduce its disadvantage (Table 11). In addition, CPO itself is resistant to acids and organic solvents. Therefore, our mutation approach may be useful for the examination and development of promising enzymes for industrial use.

(a)



(b)

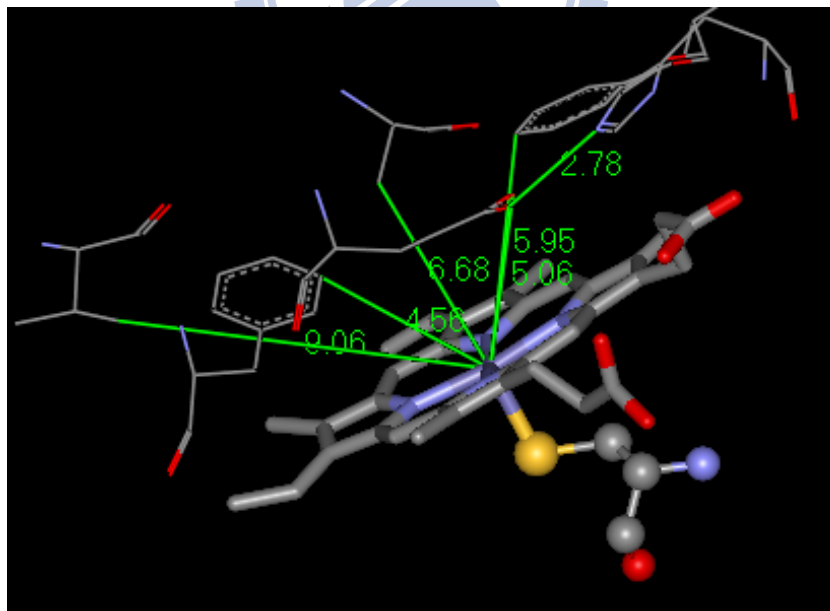


Figure 26. Stereoview of the CPO active site²⁶

CPO				MB
Residue number	Residue name	Nearly atom	Distance (Å)	Possibly homologous residue of Mb
67	Val	CG1	9.06	
71	Ala	CB	6.68	
103	Phe	CZ	5.96	F46
105	His	NE2	----	
183	Glu	OE2	5.06	H64D
186	Phe	CE2	4.56	F43

Table 11. Possibly homologous residues of Mb and CPO



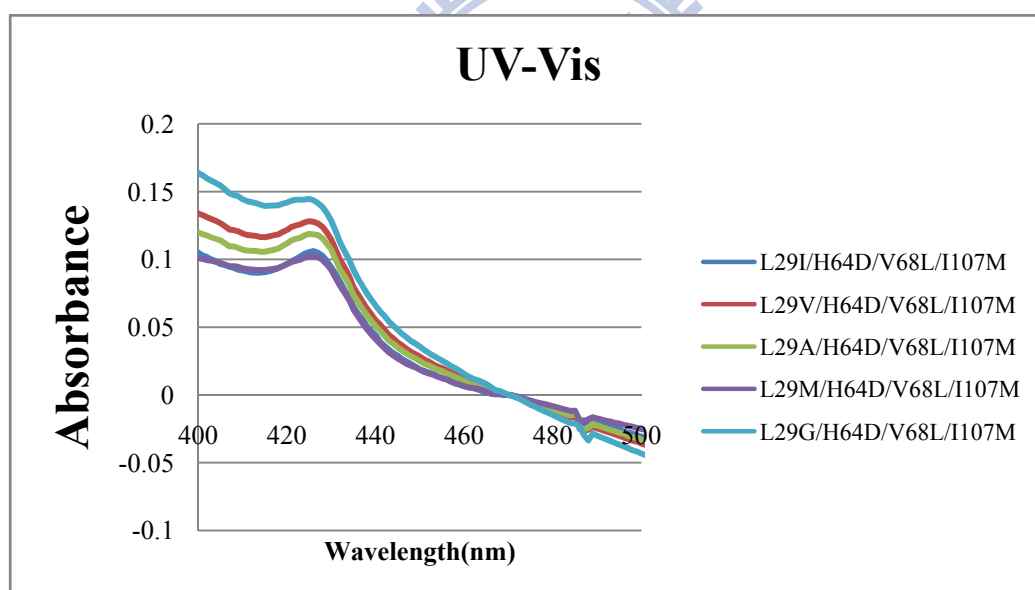
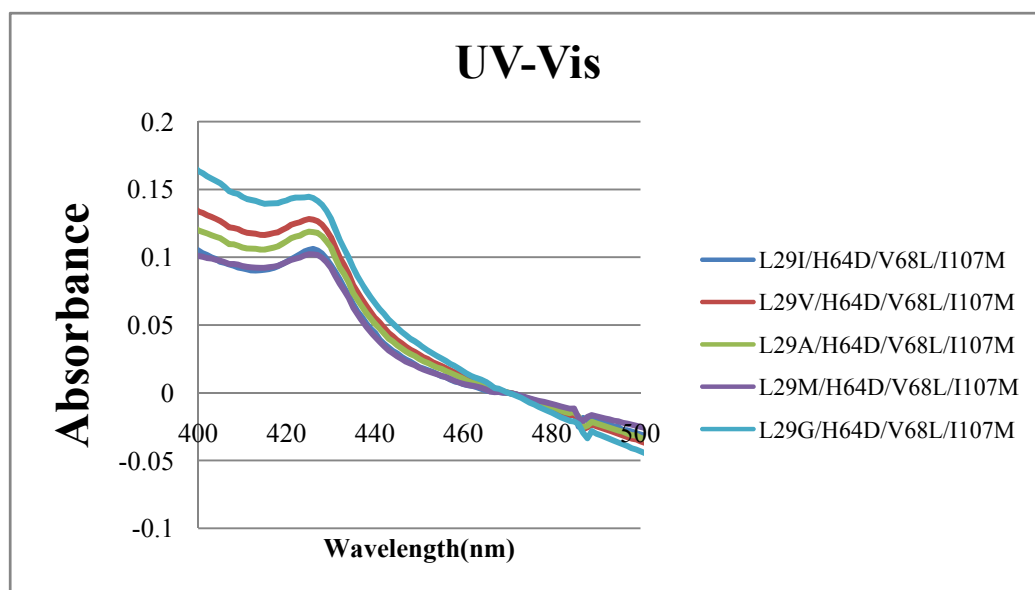
5 References

- (1) Kendrew, J. C. *Science* **1963**, *139*, 1259-66.
- (2) Li, Y.-T.; Hsieh, Y.-L.; Henion, J. D. *J Am Soc Mass Spectrom* **1993**, *4*, 6.
- (3) Lehninger, A. L.; Nelson, D. L.; M, M. **2005**.
- (4) Ozaki, S.; Roach, M. P.; Matsui, T.; Watanabe, Y. *Acc Chem Res* **2001**, *34*, 818-25.
- (5) Chance, B. *the journal of biological chemistry* **1943**, *151*(2), 25.
- (6) George, P. *Biochem J* **1953**, *54*, 267-76.
- (7) Herold, S.; Matsui, T.; Watanabe, Y. *J Am Chem Soc* **2001**, *123*, 4085-6.
- (8) Matsui, T.; Ozaki, S.-i.; Watanabe, Y. *J. Am. Chem. Soc.* **1999**, *121* 9952-9957.
- (9) Pfister, T. D.; Ohki, T.; Ueno, T.; Hara, I.; Adachi, S.; Makino, Y.; Ueyama, N.; Lu, Y.; Watanabe, Y. *J Biol Chem* **2005**, *280*, 12858-66.
- (10) Alayash, A. I.; Ryan, B. A.; Eich, R. F.; Olson, J. S.; Cashon, R. E. *J Biol Chem* **1999**, *274*, 2029-37.
- (11) Yang, H. J.; Matsui, T.; Ozaki, S.; Kato, S.; Ueno, T.; Phillips, G. N., Jr.; Fukuzumi, S.; Watanabe, Y. *Biochemistry* **2003**, *42*, 10174-81.
- (12) Shikama, K. *Chem Rev* **1998**, *98*, 1357-1374.
- (13) Yusa, K.; Shikama, K. *Biochemistry* **1987**, *26*, 6684-8.
- (14) Childs, R. E.; Bardsley, W. G. *Biochem J* **1975**, *145*, 93-103.
- (15) 呂鋒洲; 林仁混 **1991**.
- (16) Lin, H.-M.; Wu, T.-K. *A Thesis Submitted to Department of Biological Science and Technology College of Science National Chiao Tung University* **2006**.
- (17) Guallar, V.; Jarzecki, A. A.; Friesner, R. A.; Spiro, T. G. *J Am Chem Soc* **2006**, *128*, 5427-35.
- (18) Ribeiro, E. A., Jr.; Regis, W. C.; Tasic, L.; Ramos, C. H. *Protein Expr Purif* **2003**, *28*, 202-8.
- (19) Tajima, G.; Shikama, K. *Int J Biochem* **1993**, *25*, 101-5.
- (20) Hiner, A. N.; Hernandez-Ruiz, J.; Arnao, M. B.; Garcia-Canovas, F.; Acosta, M. *Biotechnol Bioeng* **1996**, *50*, 655-62.
- (21) Brantley, R. E., Jr.; Smerdon, S. J.; Wilkinson, A. J.; Singleton, E. W.; Olson, J. S. *J Biol Chem* **1993**, *268*, 6995-7010.
- (22) Olson, J. S.; Eich, R. F.; Smith, L. P.; Warren, J. J.; Knowles, B. C. *Artif Cells Blood Substit Immobil Biotechnol* **1997**, *25*, 227-41.
- (23) Aliaga, C.; Lissi, E. A. *Can. J. Chem.* **2000**, *78*.
- (24) Ye, X.; Demidov, A.; Rosca, F.; Wang, W.; Kumar, A.; Ionascu, D.; Zhu, L.;

- Barrick, D.; Wharton, D.; Champion, P. M. *J. Phys. Chem.* **2003**, *107*, 8156-8165.
- (25) Hofrichter, M.; Ullrich, R. *Appl Microbiol Biotechnol* **2006**, *71*, 276-88.
- (26) Sundaramoorthy, M.; Turner, J.; Poulos, T. L. *Structure* **1995**, *3*, 1367-77.



6 Appendix



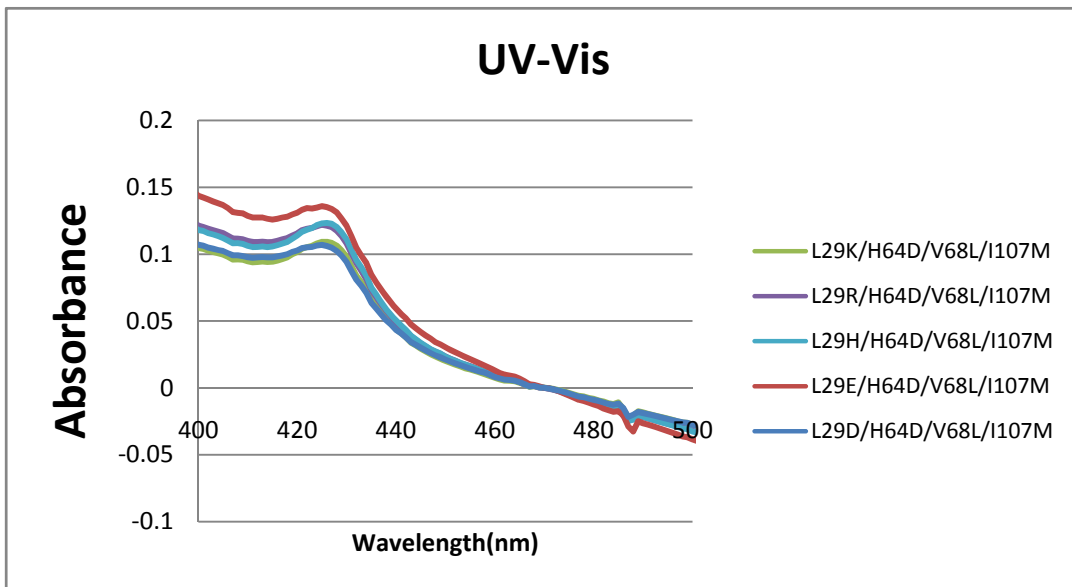
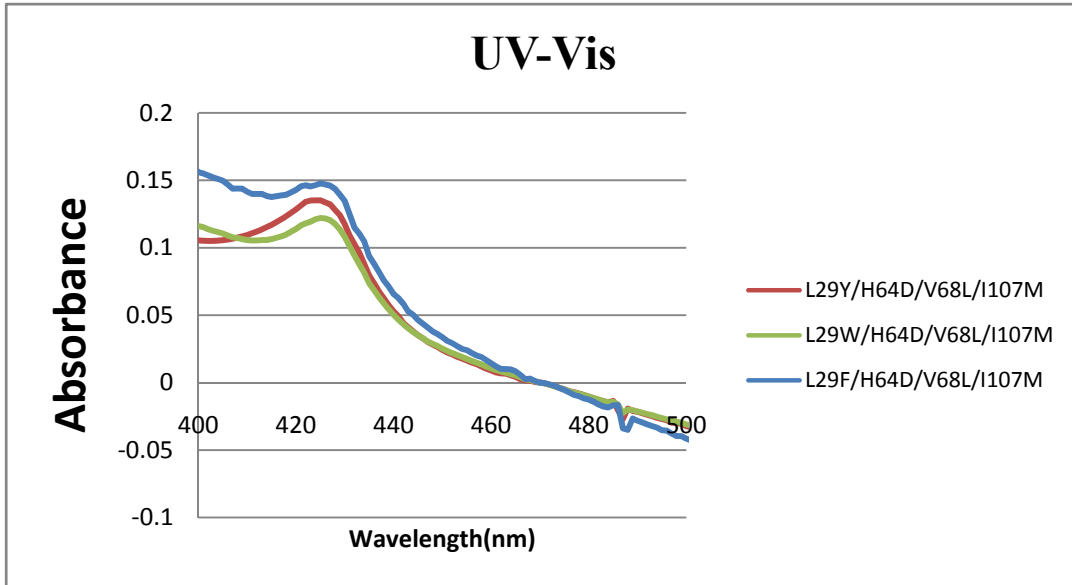
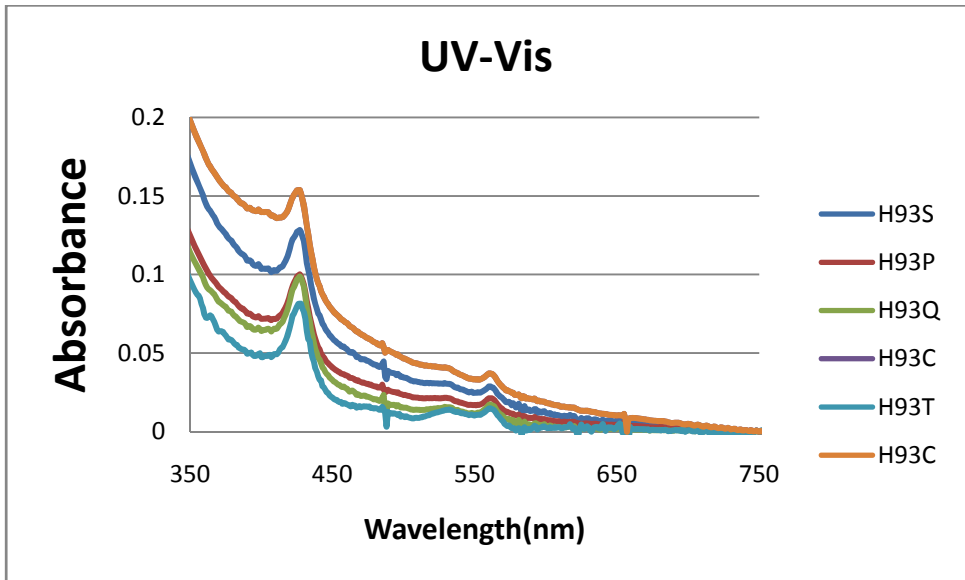
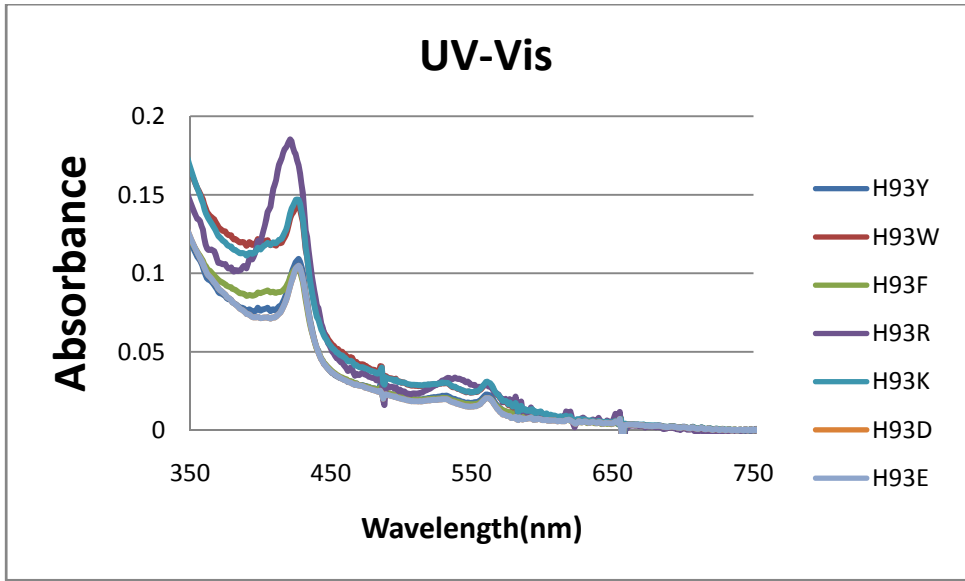


Figure 27. The Soret band of L29X/H64D/V68L/I107M clones



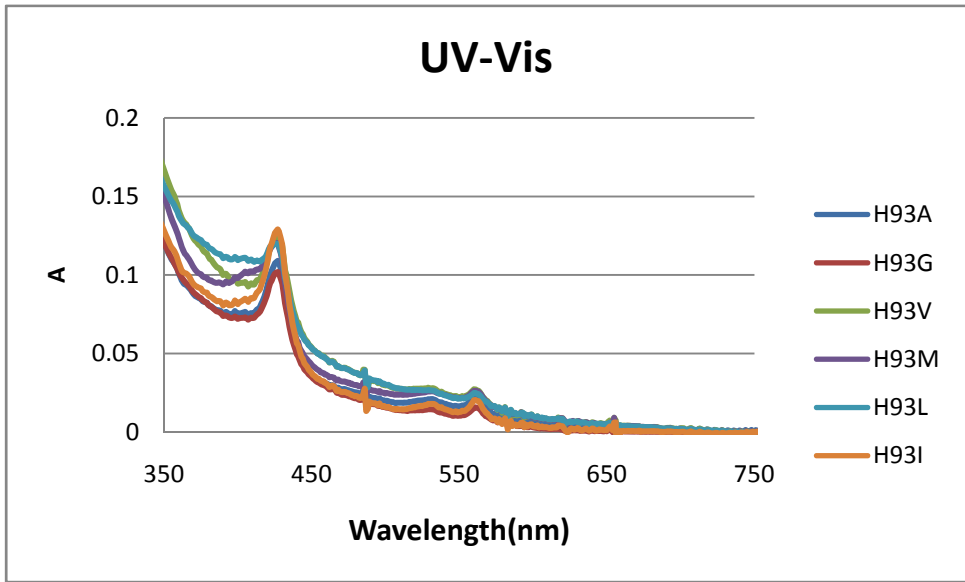
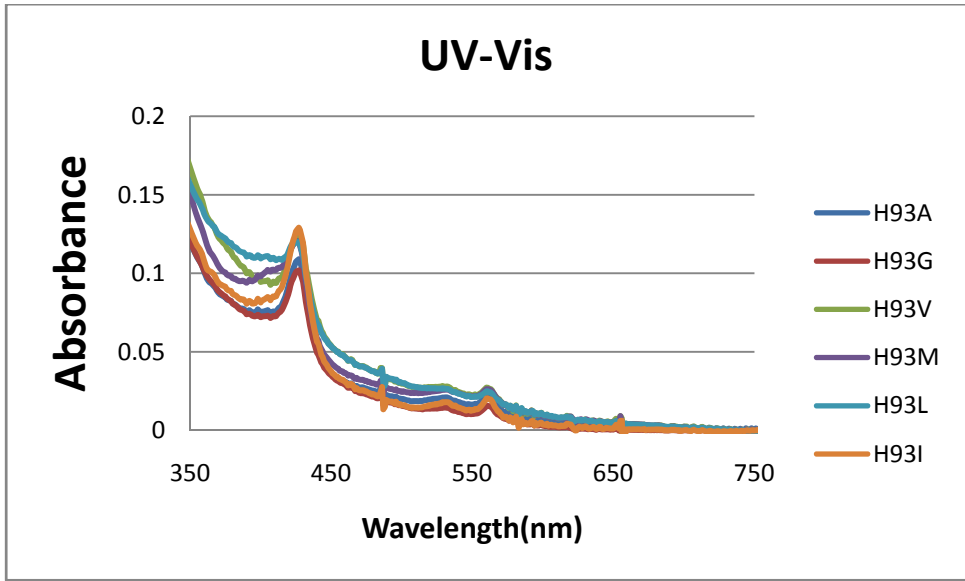


Figure 28. The Soret band of H93X clones

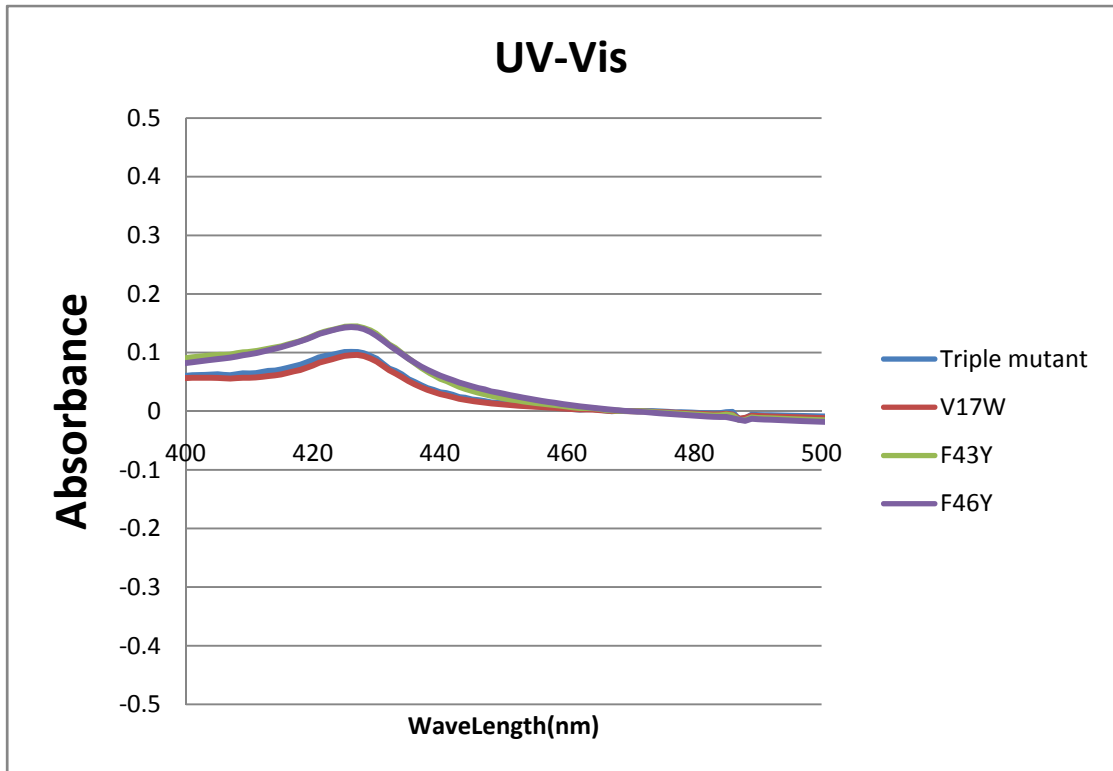
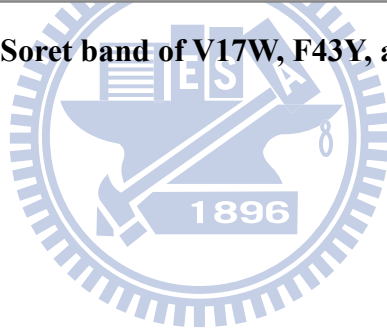
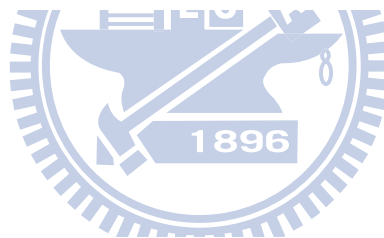
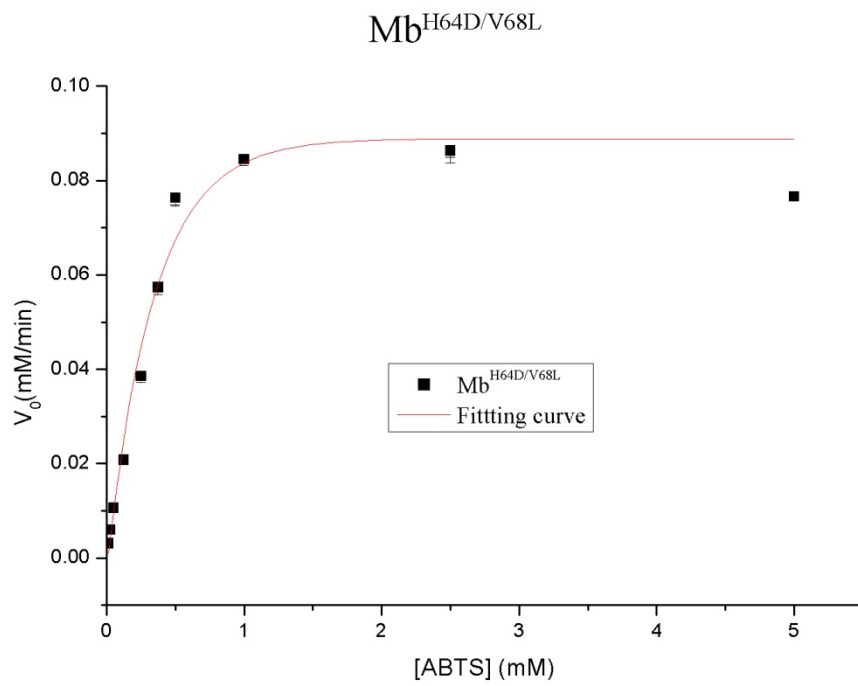


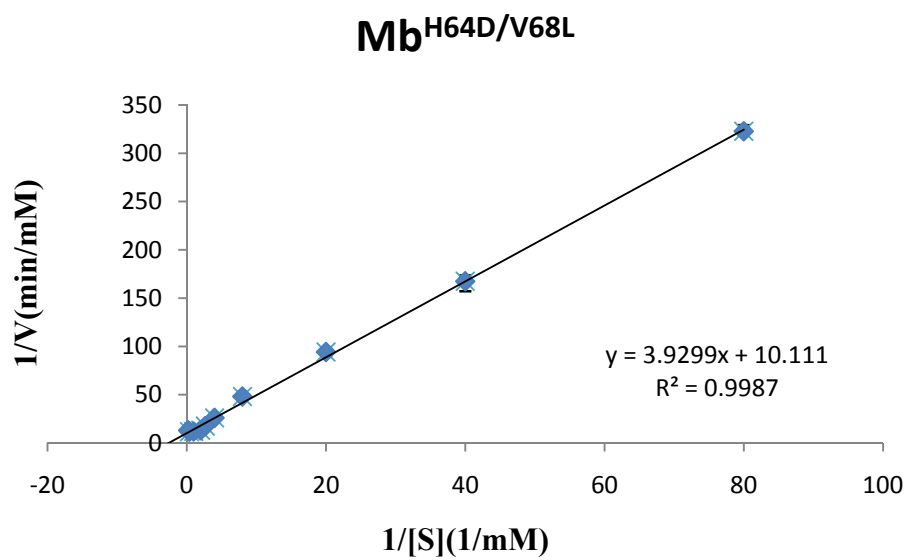
Figure 29. The Soret band of V17W, F43Y, and F46Y clones



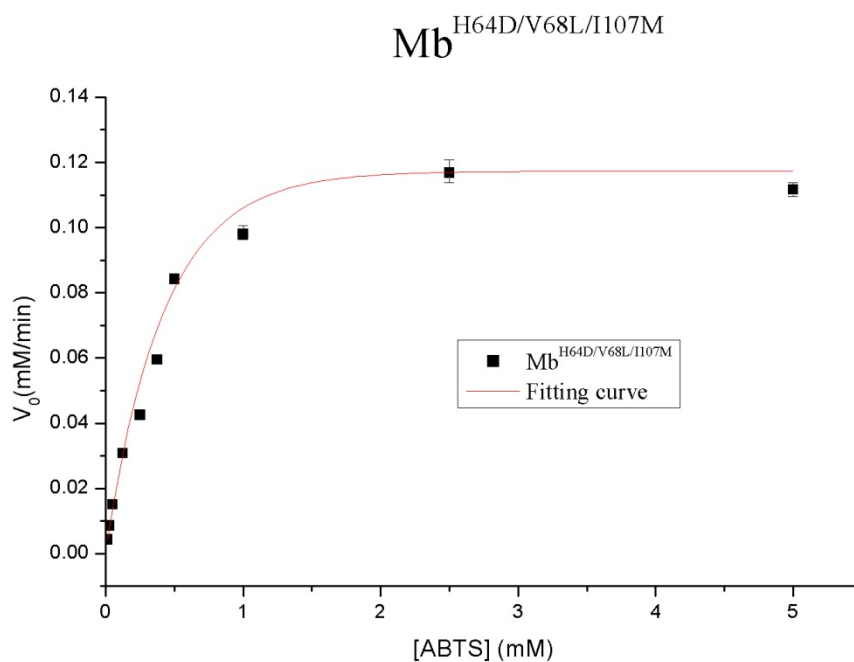
(a1)



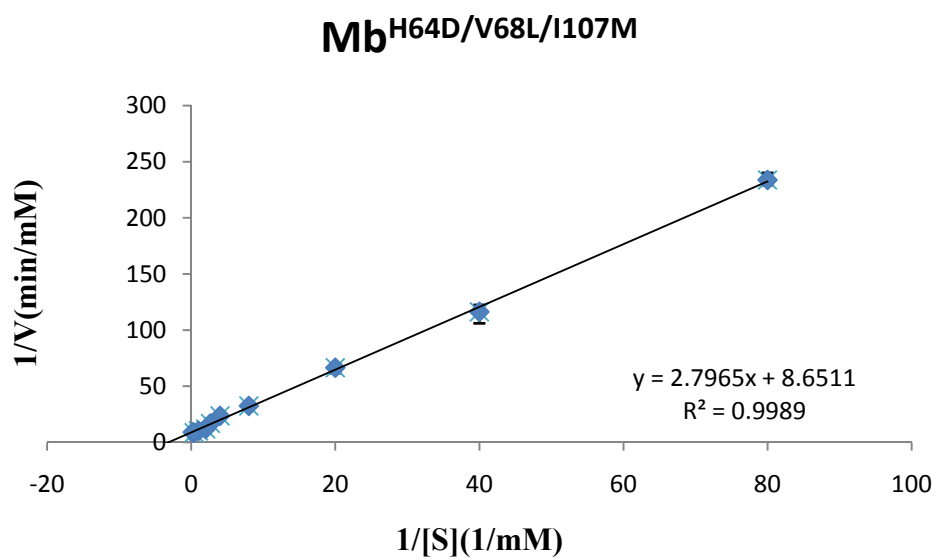
(a2)



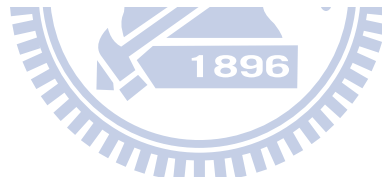
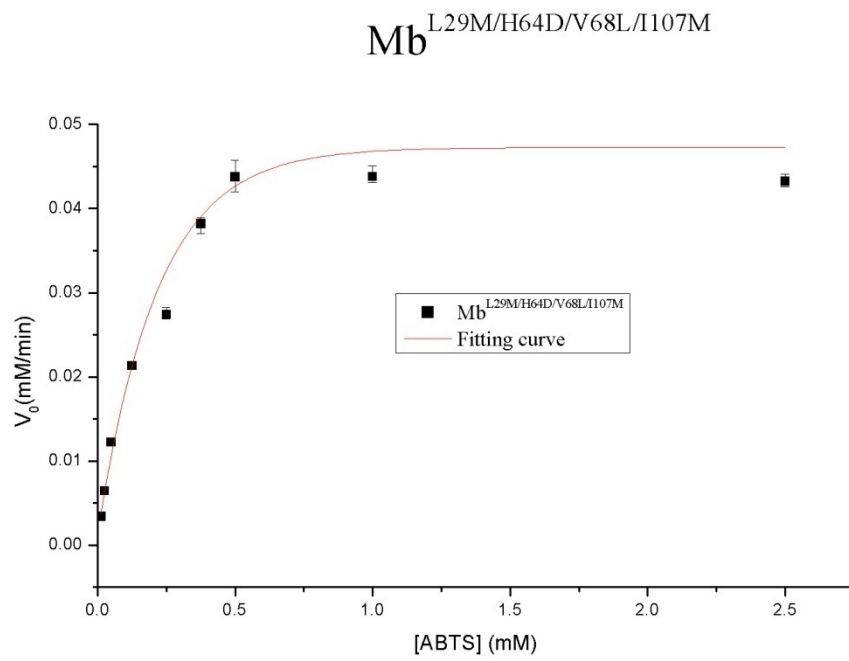
(b1)



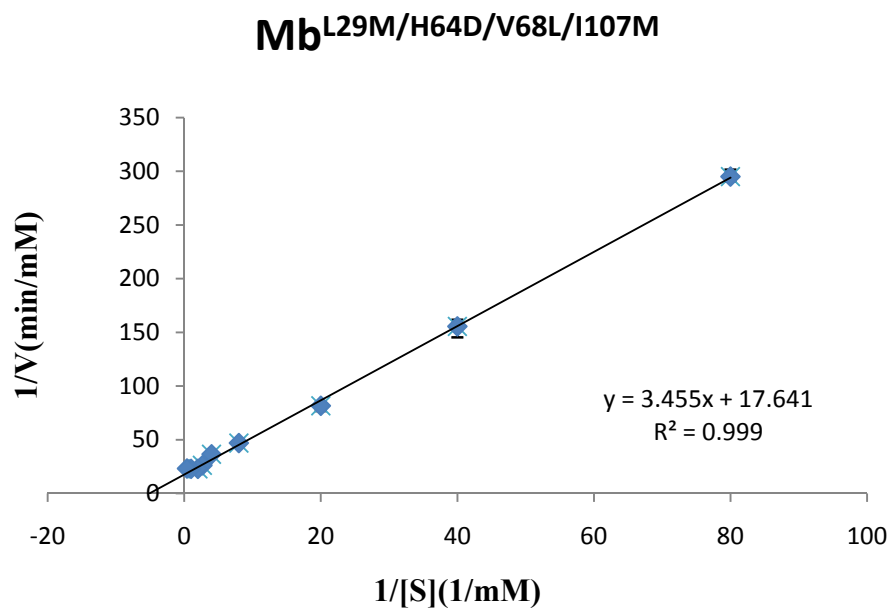
(b2)



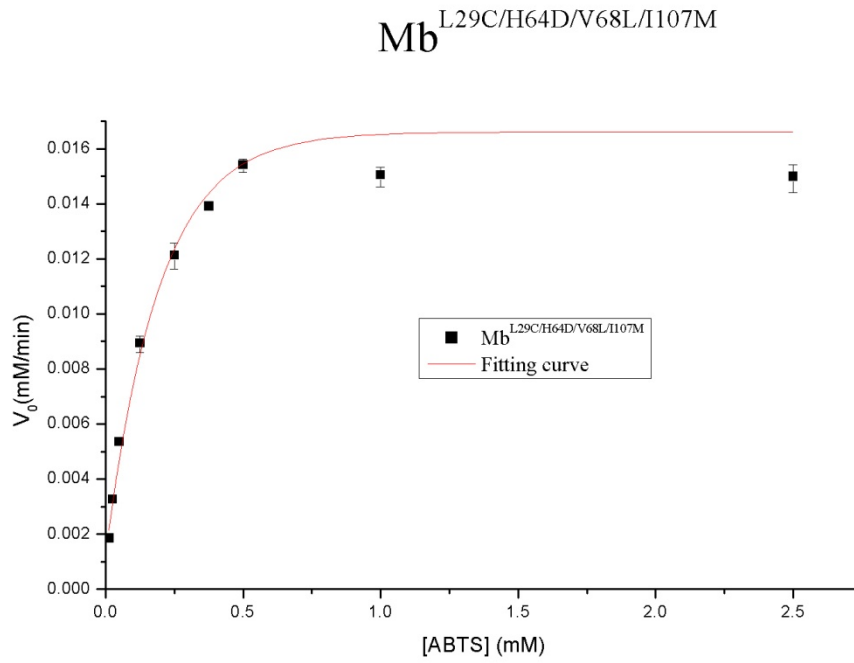
(c1)



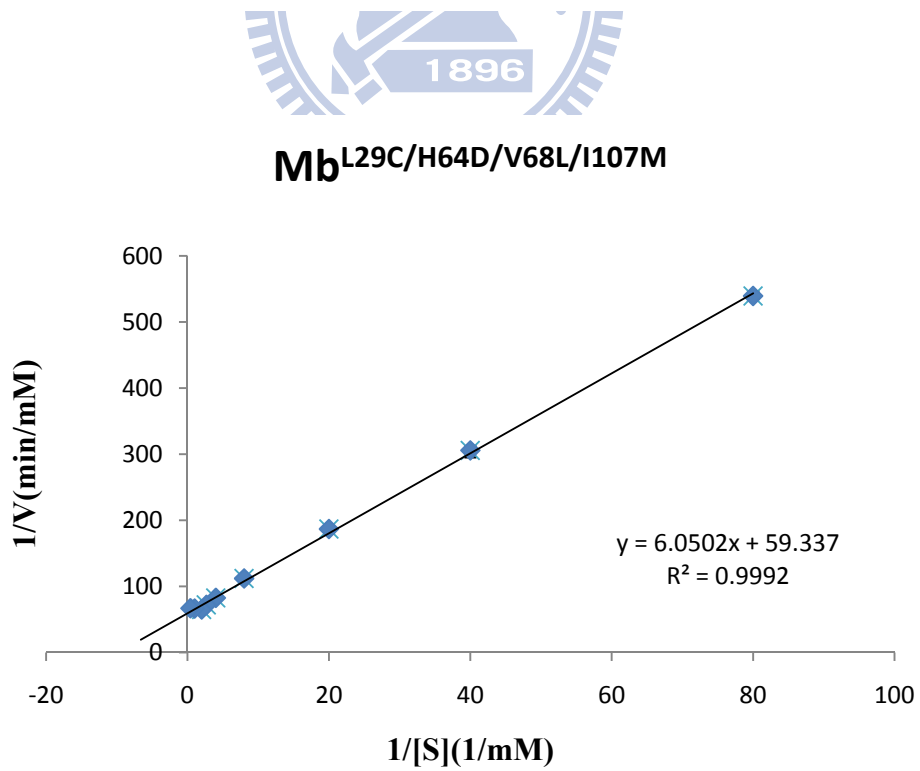
(c2)



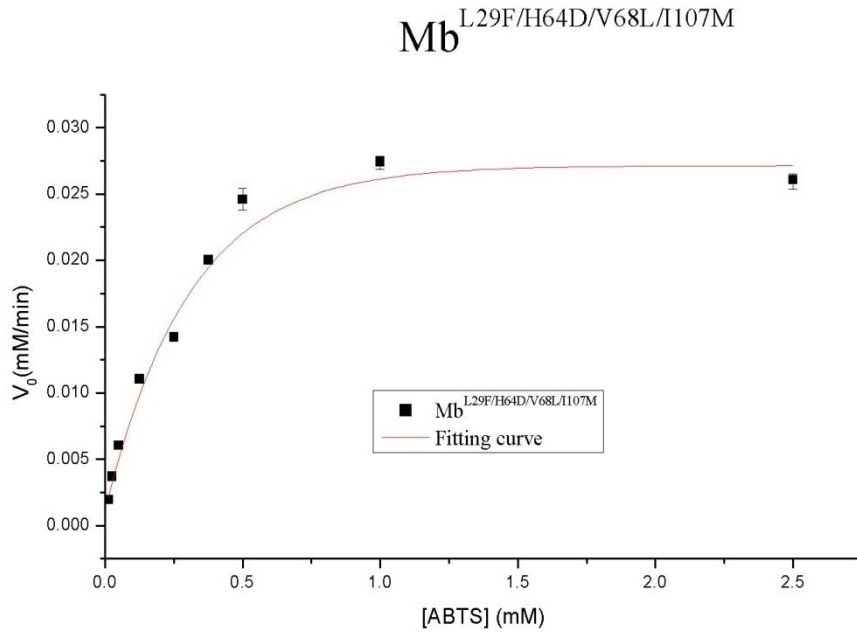
(d1)



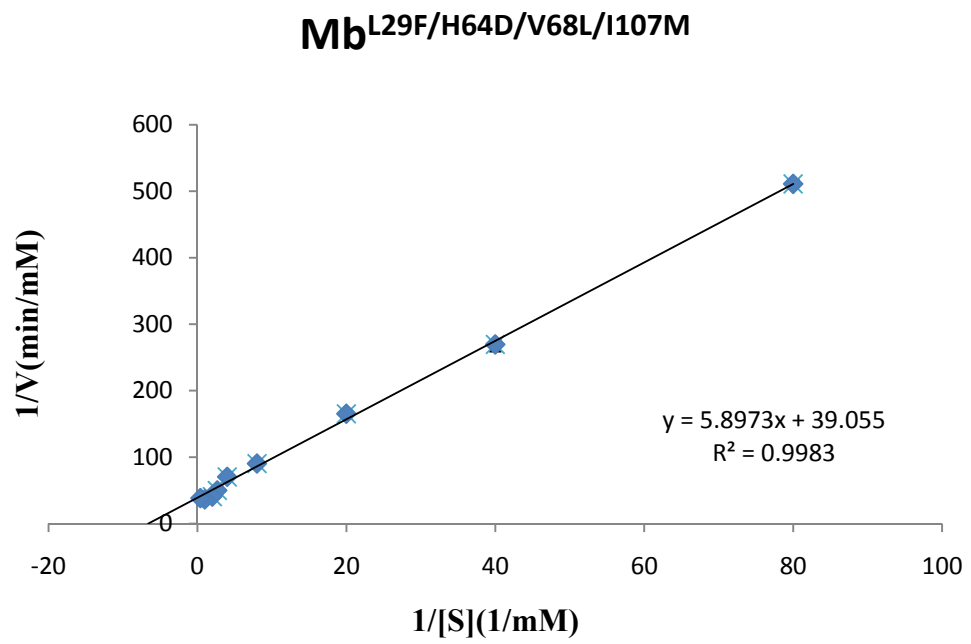
(d2)



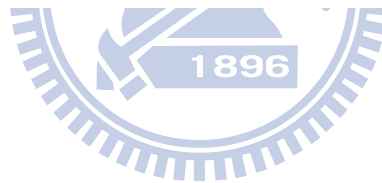
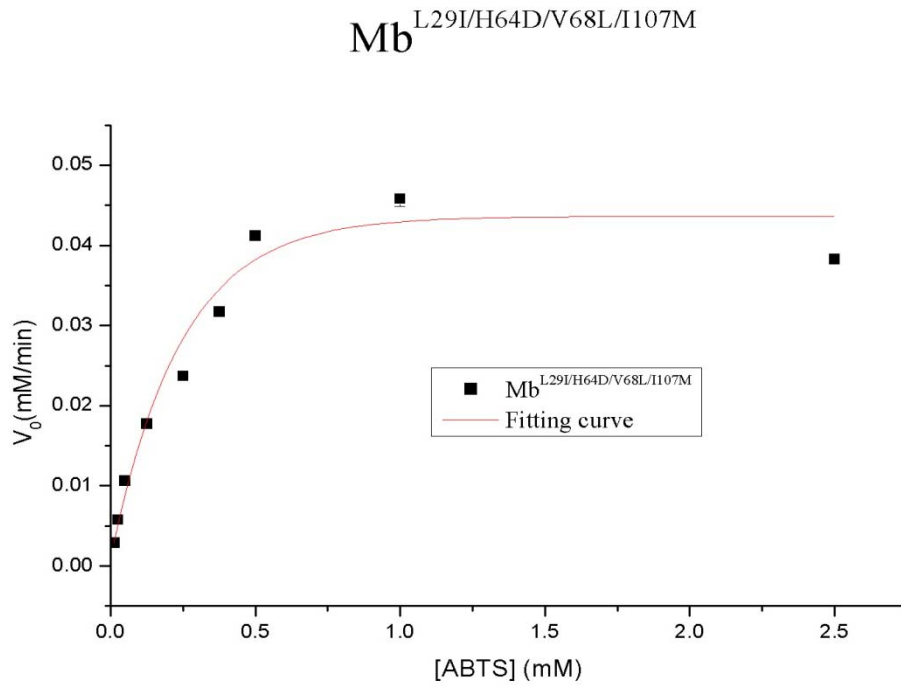
(e1)



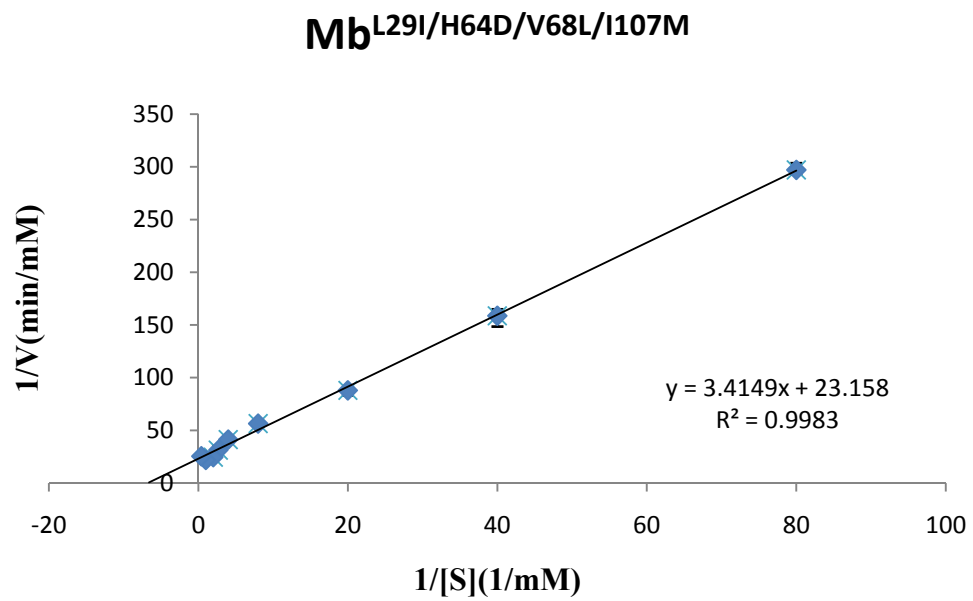
(e2)



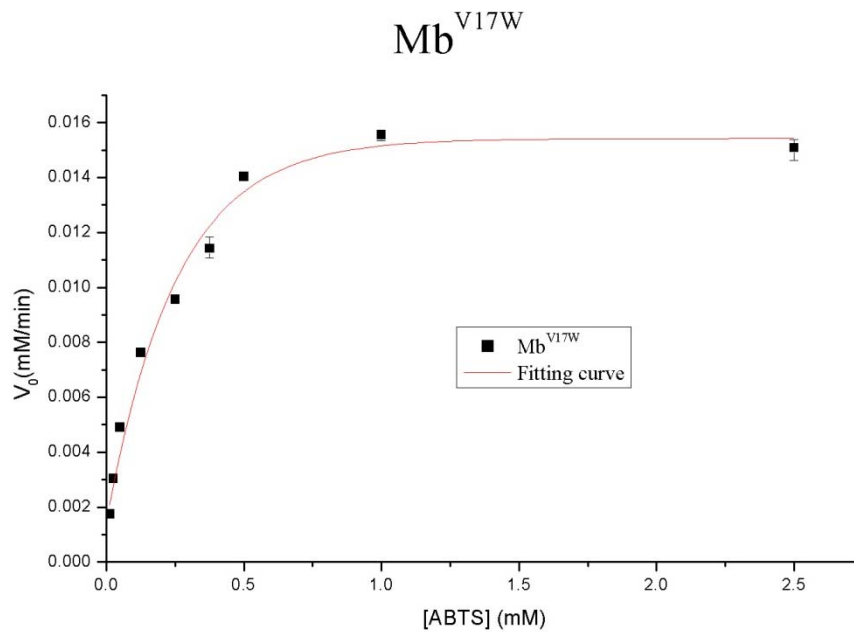
(f1)



(f2)



(g1)



(g2)

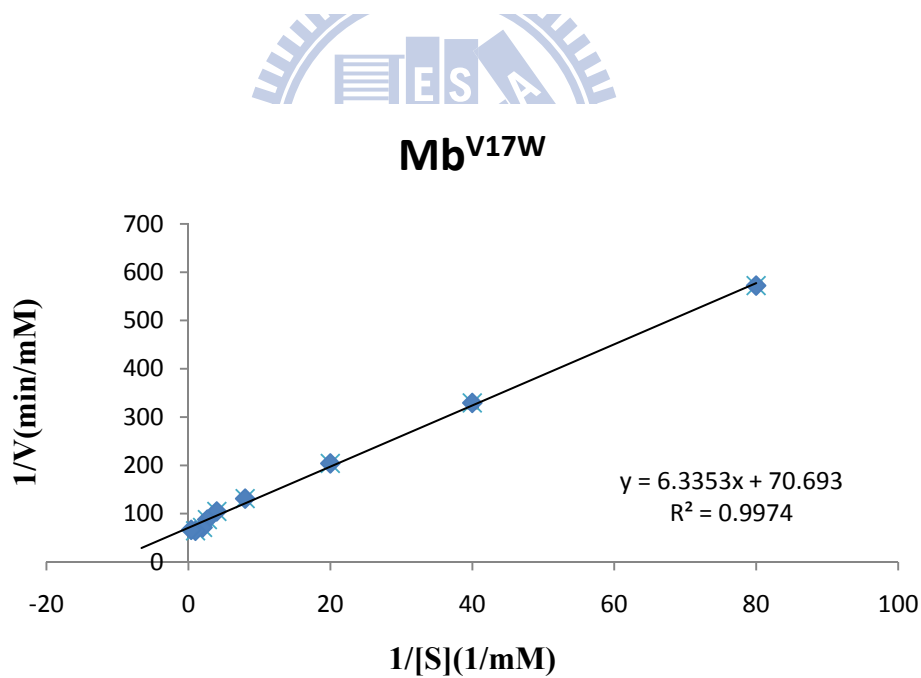
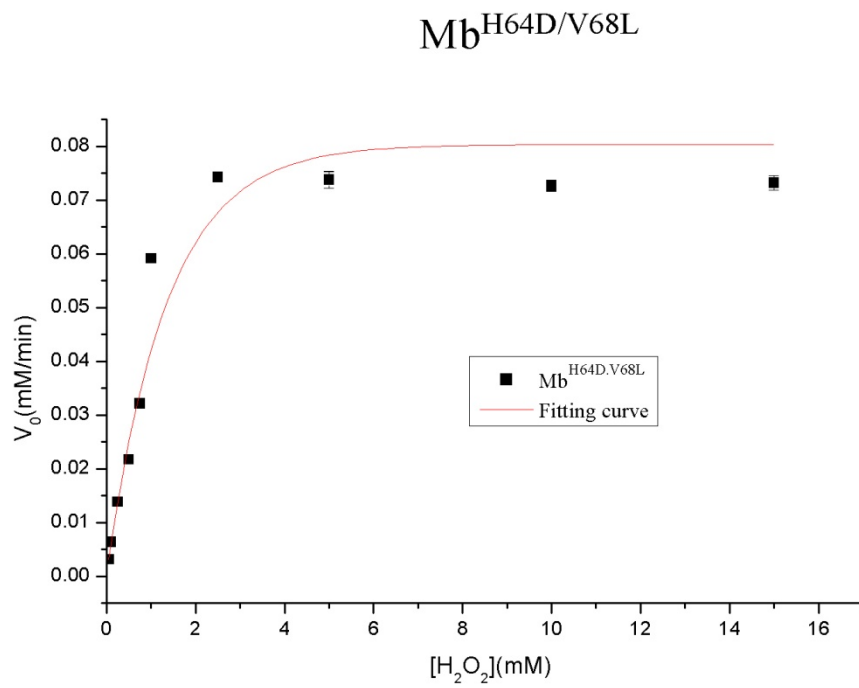


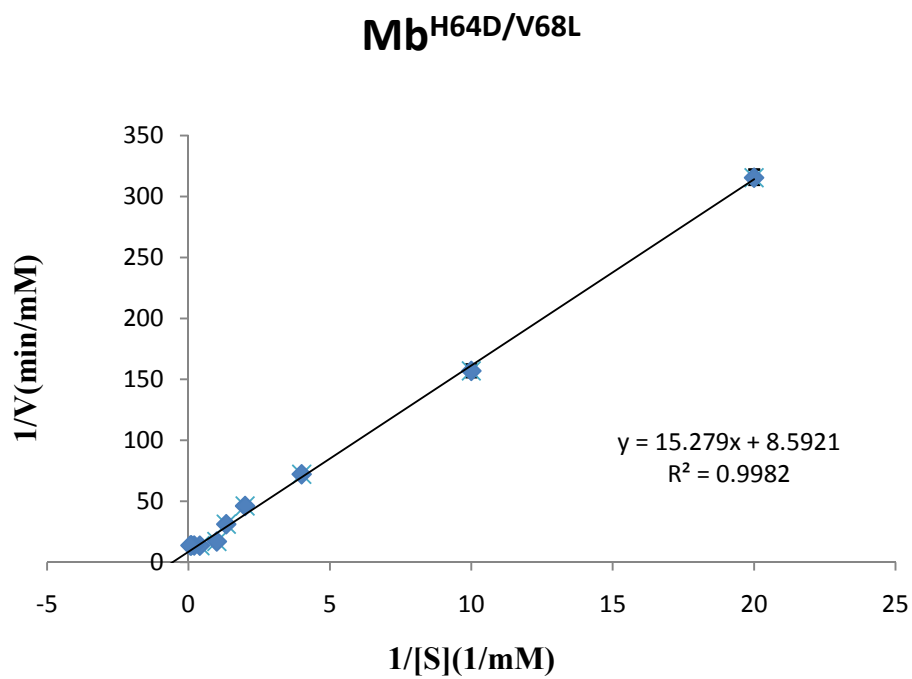
Figure 30. The Michaelies-Menten plot of mutant myoglobin catalyzing different concentration of ABTS, and the Lineweaver-Burk plot of mutant myoglobin for

calculating K[']m and V[']max. (a) Mb^{H64D/V68L} (b) Mb^{H64D/V68L/I107M} (c) Mb^{L29M/H64D/V68L/I107M} (d) Mb^{L29C/H64D/V68L/I107M} (e) Mb^{L29F/H64D/V68L/I107M} (f) Mb^{L29I/H64D/V68L/I107M} (g) Mb^{V17W}

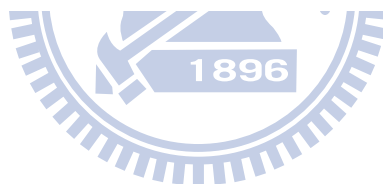
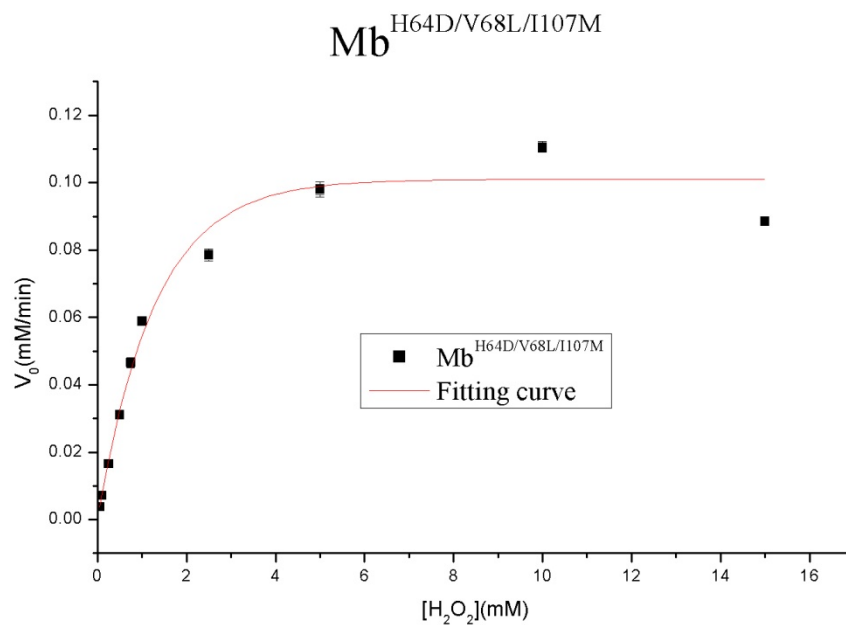
(a1)



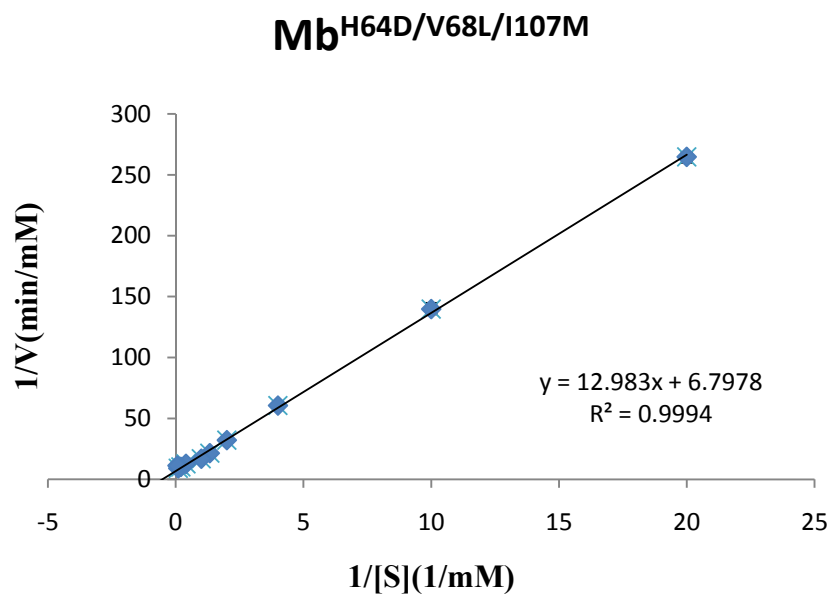
(a2)



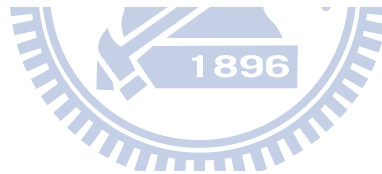
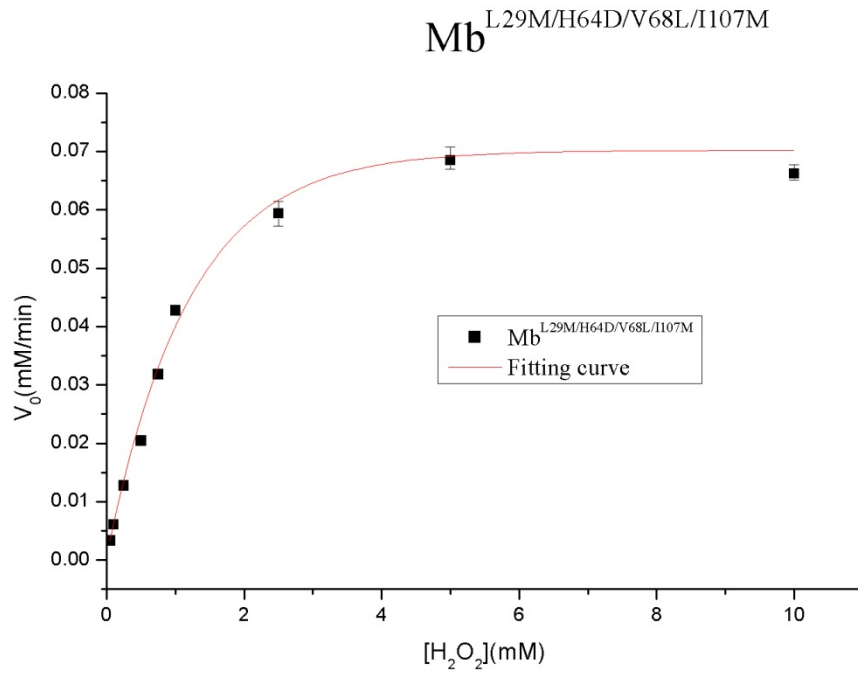
(b1)



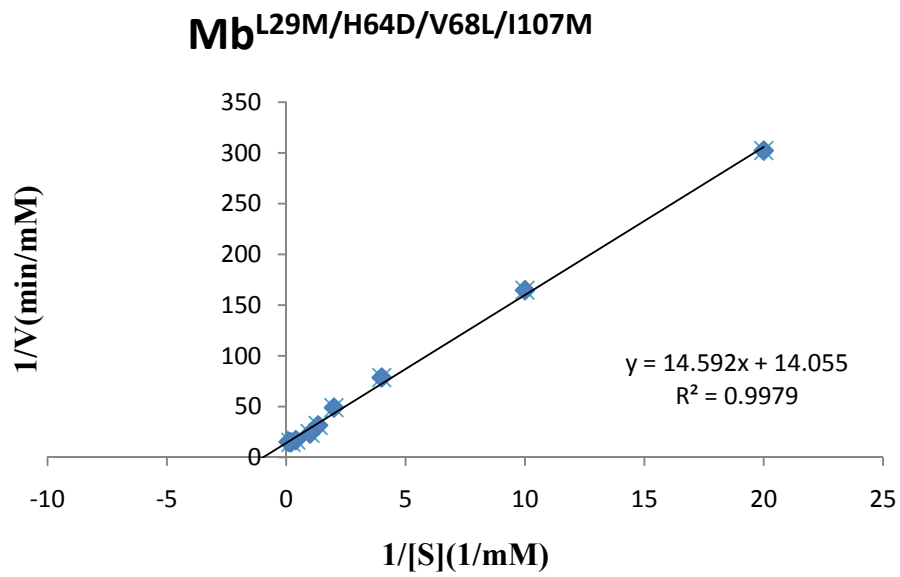
(b2)



(c1)

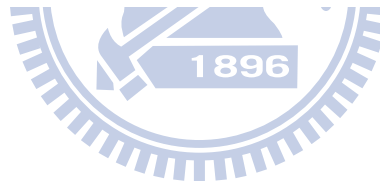
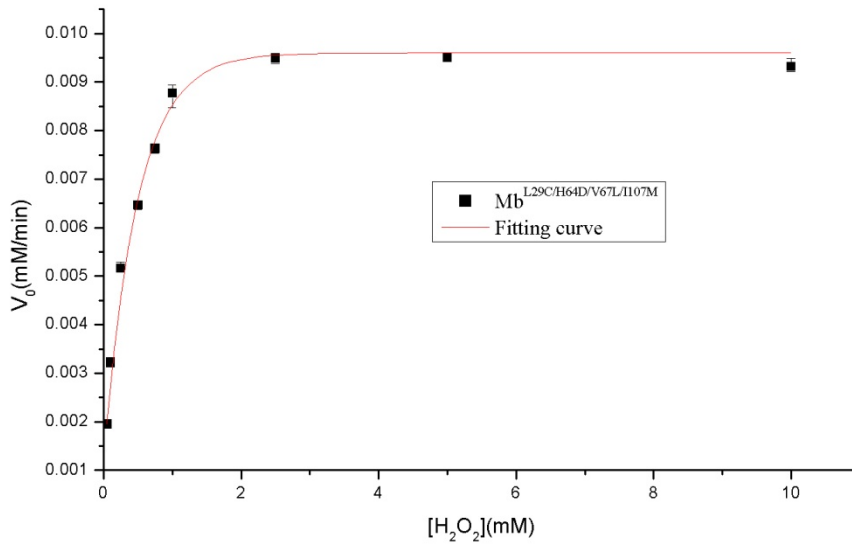


(c2)



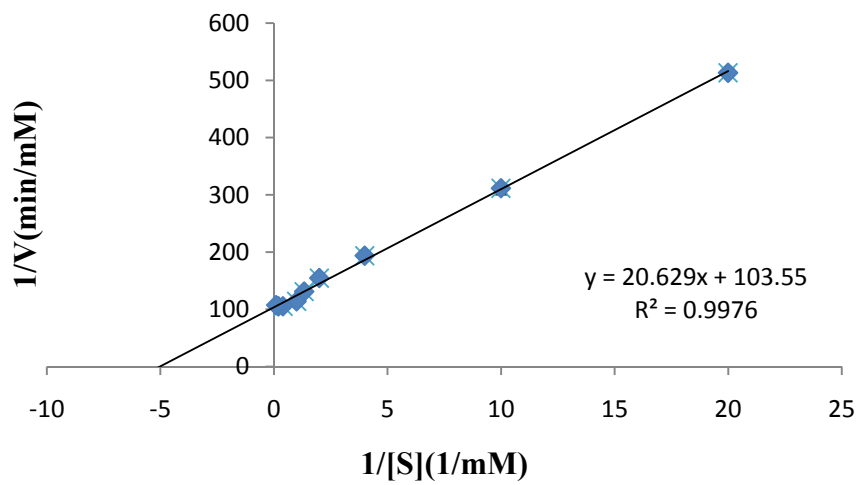
(d1)

Mb^{L29C/H64D/V68L/I107M}

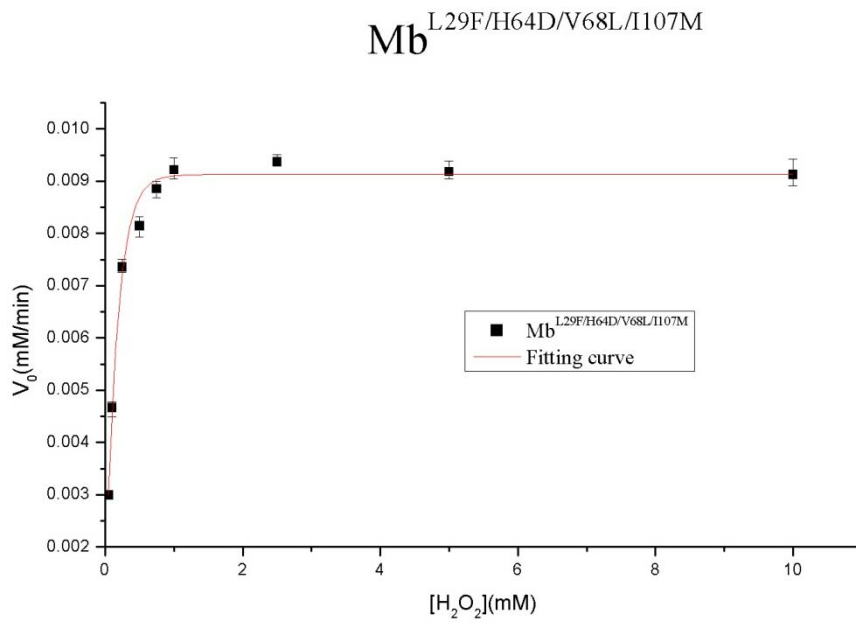


(d2)

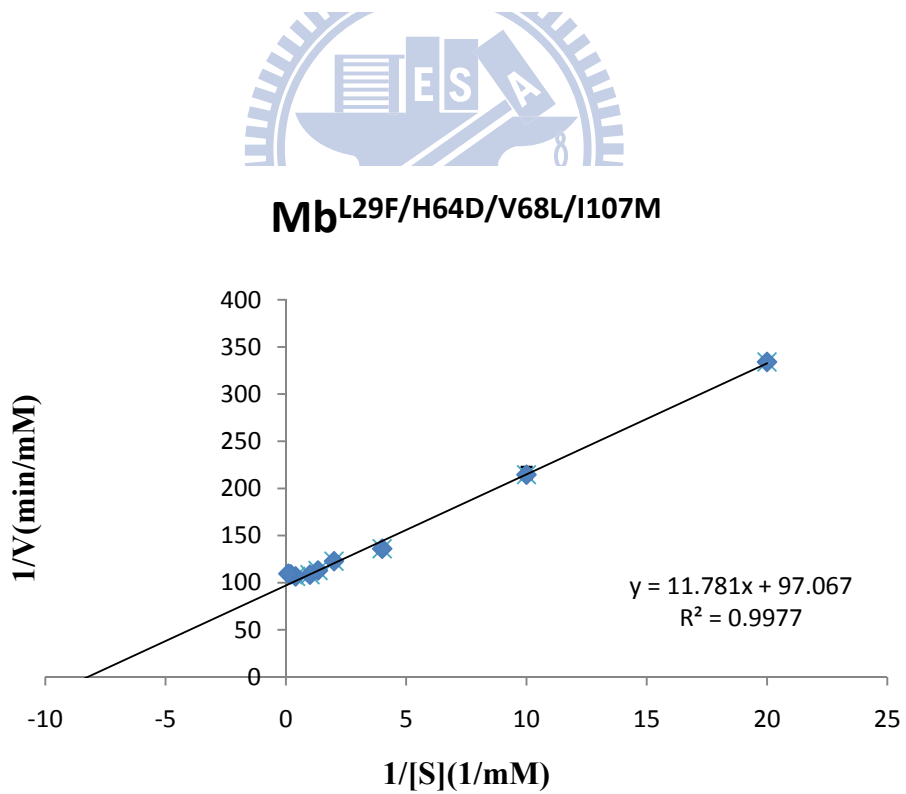
Mb^{L29C/H64D/V68L/I107M}



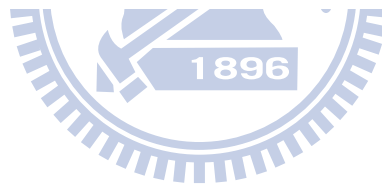
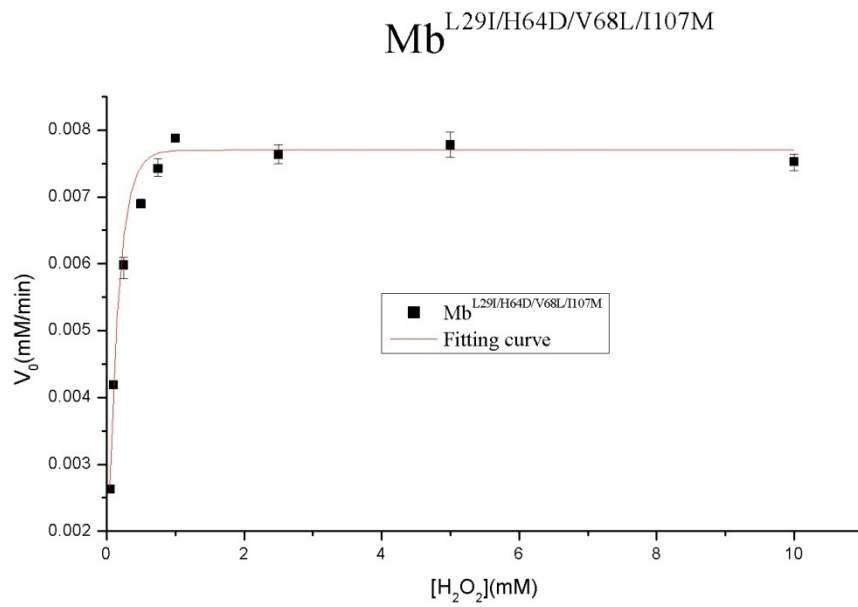
(e1)



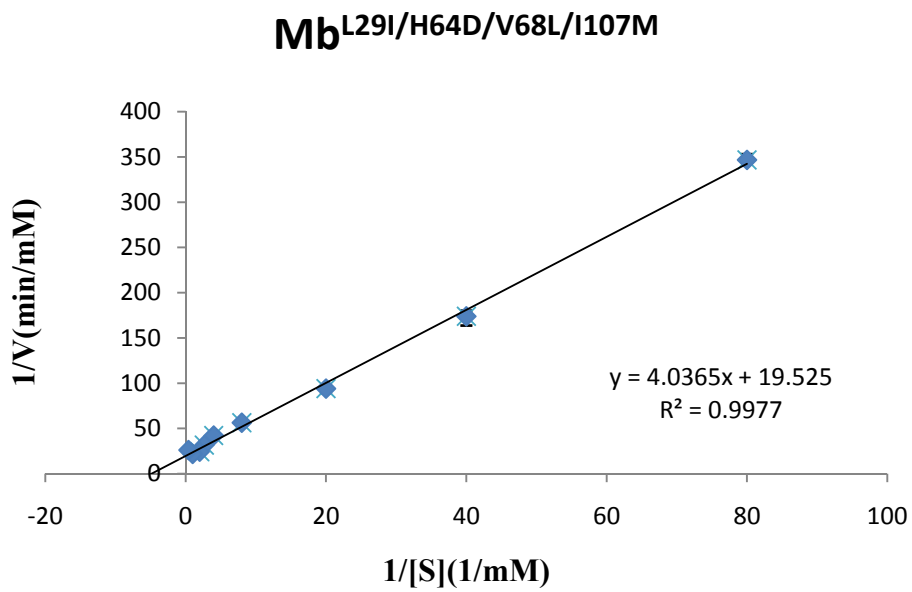
(e2)



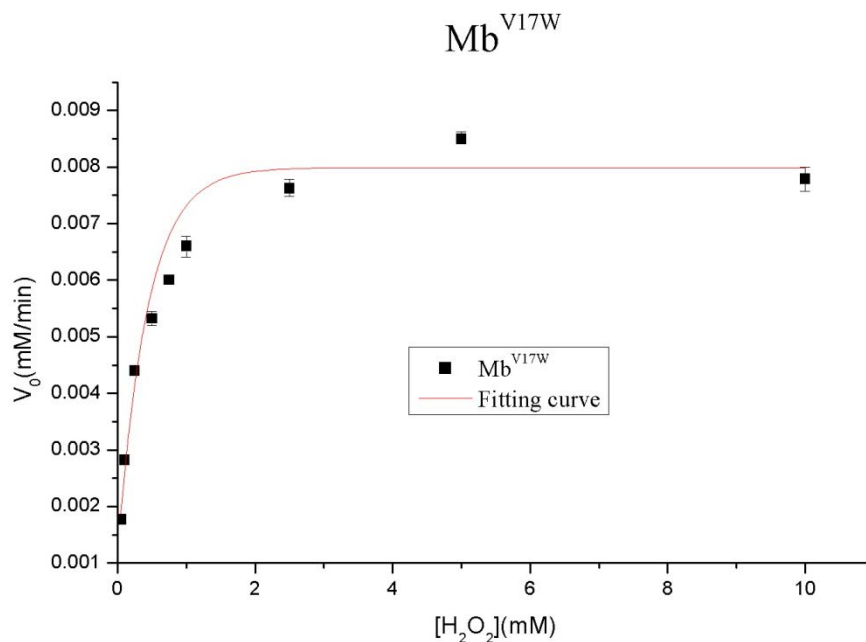
(f1)



(f2)



(g1)



(g2)

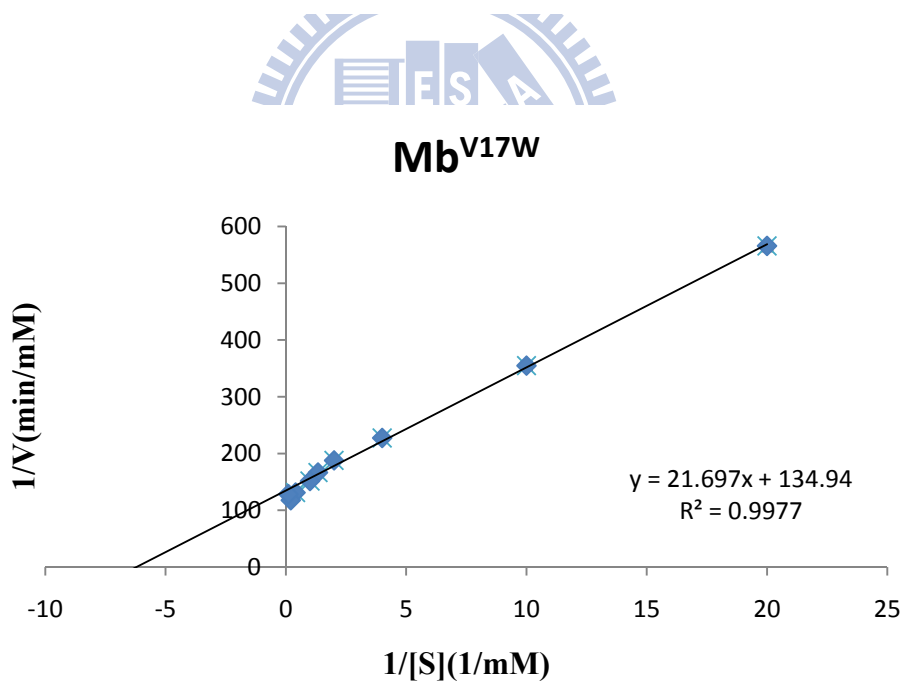


Figure 31. The Michaelies-Menten plot of mutant myoglobin catalyzing different concentration of H_2O_2 , and the Lineweaver-Burk plot of mutant myoglobin for

calculating K_m and V_{max} . (a) $\text{Mb}^{\text{H64D/V68L}}$ (b) $\text{Mb}^{\text{H64D/V68L/I107M}}$ (c)

$\text{Mb}^{\text{L29M/H64D/V68L/I107M}}$ (d) $\text{Mb}^{\text{L29C/H64D/V68L/I107M}}$ (e) $\text{Mb}^{\text{L29F/H64D/V68L/I107M}}$ (f)

$\text{Mb}^{\text{L29I/H64D/V68L/I107M}}$ (g) Mb^{V17W}